

**THE SELECTIVE OXIDATION  
OF N-BUTANE TO  
MALEIC ANHYDRIDE**

By

**MANUJA RAMDEEN**

Submitted in fulfilment of the academic  
requirements for the degree of  
Master of Science  
In the Department of Pure and Applied Chemistry,  
University of Natal,  
Durban

September 2003

---

## Abstract

Industrial catalysts used in commercial processes for the production of maleic anhydride are mainly Vanadium Phosphorous Oxide (VPO) catalysts. The VPO catalyst used is Vanadyl Pyrophosphate  $(VO)_2P_2O_7$  made from its precursor Vanadium Phosphorous Hemi-Hydrate  $VOHPO_4 \cdot 0.5H_2O$  in a non-aqueous medium. In order for the VPO catalyst to perform optimally, a metal promoter, Ru, was selected as the doping agent in this study. Four catalysts of different metal doping concentrations (undoped, 0.2%, 0.6% and 1%) were subjected to the oxidation of n-butane. Promoters are added to facilitate the oxidation of n-butane to maleic anhydride.


n-Butane gas is now being used in many industrial processes, in fixed bed reactors to convert the gas to maleic anhydride. Catalysts were calcined under high temperatures under a nitrogen atmosphere. It was found that with an increase in reaction temperature, there was an increase in conversion of n-butane to maleic anhydride. Selectivity of the product also showed an increase with an increase in temperature at a Gas Hourly Space Velocity (GHSV) of  $1960\text{--}2170\text{hr}^{-1}$ .

Catalysts were characterized using different techniques such as Electron Dispersive X-Ray Spectroscopy, Inductively Coupled Plasma-Atomic Emission Spectroscopy, Fourier Transform – Infra Red, Average Oxidation State, Brunauer Emmett and Teller (surface area), X-Ray Diffraction and Scanning Electron Microscopy. The 0.6% Ru promoted VPO catalyst showed to be most effective in terms of conversion, selectivity and yield, at a temperature of  $450^\circ\text{C}$  as compared to the other catalysts studied. The catalysts degenerated after being subjected to higher temperatures. The selectivity obtained by this catalyst was at 70.2% and the yield obtained was 37%. This study showed that with an increase in Ru up to a certain concentration (0.6%), an increase in selectivity and yield was observed, thereafter, with additional Ru doping, a decrease in selectivity and yield was obtained.

## Preface

The experimental work described in the dissertation was carried out in the Department of Pure and Applied Chemistry, University of Natal, Durban, from January 2001 to December 2003, under the supervision of Dr Holger B. Friedrich.

These studies represent original work by the author and have not otherwise been submitted in any form for any degree or diploma to any tertiary institution. Where use has been made of the work of others, it is duly acknowledged in the text.



---

Manuja Ramdeen  
B.Sc (Hons)

## Table of Contents

<b>Abstract .....</b>	<b>ii</b>
<b>Preface .....</b>	<b>iii</b>
<b>Table of Contents.....</b>	<b>iv</b>
<b>List of Figures .....</b>	<b>viii</b>
<b>Acknowledgements.....</b>	<b>xii</b>
<b>List of Symbols.....</b>	<b>xiii</b>
<b>1. Introduction .....</b>	<b>1</b>
1.1 Maleic Anhydride .....	2
1.1.1 Background.....	2
1.1.2 Uses of Maleic Anhydride.....	3
1.2 Catalyst Manufacture.....	3
1.2.1 Precipitation.....	3
1.2.1.1 Physico-Chemical Considerations.....	5
1.2.2 Impregnated Catalysts .....	6
1.2.3 Calcination.....	6
1.2.4 Formation of Final Catalysts .....	7
1.2.5 The Concept of Oxide Monolayers .....	7
1.2.5 (i) Impregnation.....	8
1.2.5 (ii) Adsorption .....	8
1.2.5 (iii) Chemical Vapour Deposition .....	8
1.2.5 (iv) Co-precipitation .....	8
1.2.6 Influencing Properties of the Final Product.....	8
1.3 Structure of Catalyst .....	9
1.3.1 Crystalline VPO phases:.....	9
1.3.1.1 Dihydrated Vanadyl Othophosphates ( $\text{VOPO}_4 \cdot 2\text{H}_2\text{O}$ ).....	10
1.3.1.2 $\alpha$ - $\text{VOPO}_4$ .....	10
1.3.1.3 $\beta$ - $\text{VOPO}_4$ .....	10
1.3.2 The Structure of Vanadyl Pyrophosphate.....	11
1.3.3 The Orthorhombic Structure of Vanadyl Pyrophosphate .....	12
1.3.3.1 Structure of V-P-O phases .....	15
1.4 Catalyst Performance.....	16
1.5 Reaction Mechanisms.....	16



1.5.1 Uptake of electrons.....	17
1.5.2 Uptake of Hydrocarbons.....	18
1.5.3 Reaction Mechanism: The olefinic route.....	18
1.5.4 Reaction Mechanism: The Alkoxide Route.....	19
1.6 Promoters.....	20
1.6.1 Promotional effects for VPO Catalysts .....	20
1.6.2 Effect of Promoters on $(VO)_2P_2O_7$ .....	21
1.6.3 Effect of Promoter on other VPO Catalysts .....	21
1.6.4 Catalytic Performance of Unpromoted Catalysts .....	22
1.6.5 Catalytic Performance of Promoted Catalysts Prepared by Standard Non-Aqueous HCl Method.....	23
1.6.6 Role of Catalyst Promoters.....	25
1.7 The Effects of Oxidation State .....	25
1.8 Mole Balance .....	26
1.8.1 The General Mole Balance Equation.....	26
1.9 Reactors .....	28
1.9.1 Batch Reactors.....	28
1.9.2 Continuous Flow Reactors .....	29
1.9.2 (i) Continuous Stirred Tank Reactor .....	29
1.9.3 Tubular Reactor .....	30
1.9.4 Packed Bed Reactors .....	31
1.9.5 Fixed Bed Catalytic Reactors .....	32
1.9.5 (i) The importance and scale of fixed bed catalytic processes: .....	32
1.9.5 (ii) Modelling of Fixed Bed Reactors.....	32
1.9.5 (iii) Classification of fixed bed reactor models .....	33
1.10 Catalytic Reactors.....	34
1.10.1 Small Particle size .....	34
1.10.2 Large Particle Size.....	35
1.11 Industrial Catalysts .....	36
1.11.1 Catalysts in an Industrial Reactor.....	37
1.12 Kinetics.....	38
1.12.1 Heterogeneous Catalytic Reactions.....	41
1.13 Characterisation Techniques.....	43
1.13.1 Brunauer Emmett Teller Isotherm.....	43

1.13.1 (i) Significance of Pore Structure and Surface Area in Heterogeneous Catalysis.....	43
1.13.2 X-Ray Diffraction.....	46
<b>2. Experimental.....</b>	<b>50</b>
2.1 Experimental methods of catalyst synthesis.....	50
2.1.1 Synthesis 1 (a): Vanadium phosphorus oxide catalyst ( $\text{VO}_2\text{P}_2\text{O}_7$ ) prepared by the reduction of $\text{VOPO}_4 \cdot 2\text{H}_2\text{O}$ .....	50
2.1.2 Synthesis 2: Vanadium Phosphate Catalyst ( $\text{VO}_2\text{P}_2\text{O}_7$ ) prepared by the Reduction of $\text{VOPO}_4 \cdot 2\text{H}_2\text{O}$ .....	51
2.1.3 Synthesis 3: Preparation of undoped VPO Precursors .....	51
2.1.4 Synthesis 4: Preparation of doped Fe VPO precursors .....	51
2.1.5 Synthesis 5: VPO Catalysts for oxidation of Butane to Maleic Anhydride, Influence of $(\text{VO})_2\text{H}_4\text{P}_2\text{O}_9$ Precursor morphology .....	52
2.1.6 Synthesis 6: VPO Catalysts for Oxidation of Butane to Maleic Anhydride .....	52
2.1.7 Synthesis 7: Iron Doped VPO Catalysts for Oxidation of Butane to Maleic Anhydride .....	52
2.1.8 Synthesis 8: Ruthenium Doped VPO Catalysts for Oxidation of Butane to Maleic Anhydride (1% Ru promoted catalysts) .....	53
2.1.9 Synthesis 9: The Study of the oxidation of Butane over Vanadyl Pyrophosphate .....	53
2.1.10 Synthesis 10: 3% Fe Promoted VPO Catalyst for oxidation of Butane to Maleic Anhydride .....	53
2.1.11 Synthesis 11: 1% Fe Promoted Catalyst.....	53
2.1.12 Synthesis 12: 0.6% Ru Promoted Catalyst .....	54
2.1.13 Synthesis 13: 0.2% Ru Promoted Catalyst.....	54
2.2 Characterization Techniques .....	54
2.2.1 Average Oxidation State.....	54
2.2.2 X-Ray Diffraction (XRD).....	55
2.2.3 Fourier Transform Infrared (FTIR) .....	55
2.2.4 Scanning Electron Microscopy (SEM) and Electron Dispersive X-Ray Spectroscopy (EDX).....	55
2.2.5 Microwave Digestion .....	56
2.2.6 Inductively Coupled Plasma-Atomic Emission Spectroscopy (ICP-AES )	56

2.2.7 Brunauer Emmett and Teller (Surface Area Analysis).....	57
2.2.8 Grain Size Distribution (GSD) using a Laser Beam.....	58
2.3 On Line sample Analysis.....	58
Flame Ionisation Detector Settings (FID) and Thermal Conductivity Settings (TCD) can be seen in the table below.....	59
2.3.1 Reactor Design and Setup.....	59
<b>3. Results and Discussion .....</b>	<b>64</b>
3.1. Results from the synthesis of catalysts that have been tested.....	64
3.2 Catalyst Characterization.....	65
3.2.1 Average Oxidation State (Av) .....	65
3.2.2 Inductively Coupled Plasma-Atomic Emission Spectroscopy (ICP-AES) .....	66
3.2.3 Electron Dispersive X-Ray Spectroscopy (EDX) .....	67
3.2.4 Brunauer Emmett and Teller (BET) .....	67
3.2.5 Scanning Electron Microscopy (SEM).....	69
3.2.6 Fourier Transform Infra-Red Spectroscopy (FT-IR).....	70
3.2.7 X-Ray Diffraction (XRD).....	72
3.3 Reactor studies.....	75
3.3.1 The Gas Hourly Space Velocities (GHSV) .....	75
3.3.2 Catalyst Degradation .....	75
3.4 Catalyst Testing .....	75
3.4.1 Undoped Catalyst .....	75
3.4.2 Catalyst testing of 0.2% Ru Promoted Catalyst .....	77
3.4.3 Catalyst Testing of 0.6% Ru Promoted Catalyst .....	78
3.4.4 Catalyst Testing of 1% Ru Promoted Catalyst .....	79
3.4.5 Comparison of Conversions, Selectivity and Yield for all Catalysts at Varying Temperatures .....	81
<b>4. Conclusion .....</b>	<b>87</b>
<b>Appendix 1.....</b>	<b>88</b>

## List of Figures

Figure 1.1: Preparation scheme for precipitated catalysts. Optional preparation steps are indicated by square brackets. ....	4
Figure 1.2: Simplified scheme for the formation of a solid product from solution. ....	6
Figure 1.3: The figure summarizes the parameters which can be adjusted in precipitation process and the properties which are mainly influenced by these parameters. ....	9
Figure 1.4: Dimeric vanadium-oxygen clusters: (a) trans-bipyramidal unit and (b) cis-bipyramidal unit. ....	12
Figure 1.5: The close packed oxygen basal planes for the unit cell of vanadyl pyrophosphate. ....	13
Figure 1.6: The relationship between the coordination spheres of vanadium octahedra and phosphorus tetrahedra. ....	13
Figure 1.7: (a) Basal oxygen close-packing pattern (10), ....	14
Figure 1.8: Bond lengths for (a) the vanadium coordination sphere, and (b) the phosphorous atoms in the idealized model of vanadium pyrophosphate. ....	15
Figure 1.9: The Mars Van Krevelan Mechanism .....	17
Figure 1.10: Proposed reaction scheme for the oxidehydrogenation of n-butane to 2-butene (a) and 2-butene to butadiene (b) and the oxidation of butadiene to maleic anhydride (c). The final intermediate (c) is represented in Figure 1.12. ....	18
Figure 1.11: The olefinic route .....	19
Figure 1.12: Proposal for a reaction scheme for the oxidation of n-butane to maleic anhydride which implies the alkoxide route (16). ....	20
Figure 1.13: Dependence of rate constant for butane oxidation on final catalyst surface area. ....	24
Figure 1.14: Dependence of rate constant for butane oxidation on final catalyst surface area. ....	24
Figure 1.15: A system volume $Gj$ .....	27
Figure 1.16: Continuous stirred tank reactor .....	29
Figure 1.17: Tubular reactor (PFR) .....	31
Figure 1.18: Common reactor types with moving catalyst beds: (a) fluid bed reactor, (b) bubble column with suspended catalyst, (c) sparged stirred tank with suspended catalyst (30). ....	35

Figure 1.19: Examples of reactors with fixed catalysts beds: (a) adiabatic packed bed, (b) cooled tubular reactor, (c) co current trickle bed reactor, (d) packed bubble column (30).....	36
Figure 1.20: Reaction (R) rate vs. temperature(T) for a reversible reaction. ....	40
Figure 1.21: The five types of adsorption isotherms in the Brunauer classification ...	45
Figure 1.22: Apparatus for the volumetric determination of surface area.....	47
Figure 2.1: The design of the fixed bed reactor showing feed gas and product streams .....	60
Figure: 2.2: Diagram of the Gas Sampling Valve Box.....	61
Figure 2.3: Diagram showing reactors and control panels.....	63
Figure 3.1: Graph showing the average conversions of butane at increasing temperatures for the undoped catalyst .....	76
Figure 3.2: Graph showing selectivity for maleic anhydride for varying temperatures for the undoped catalyst.....	76
Figure 3.3: Graph showing yield of maleic anhydride at varying temperatures for the undoped catalyst .....	76
Figure 3.4: Graph showing trends of n-butane conversions with varying times .....	77
Figure 3.5: Showing selectivity of maleic anhydride at varying temperatures .....	77
Figure 3.6: Showing the yield of maleic anhydride at varying temperatures.....	78
Figure 3.7: Showing conversions of n-butane at varying temperatures .....	78
Figure 3.8: Showing selectivity to maleic anhydride at varying temperatures .....	79
Figure 3.9: Yield of maleic anhydride at varying temperatures for the 0.6% Ru catalyst.....	79
Figure 3.10: Showing conversions of n-butane at varying temperatures for the 1% Ru promoted catalyst.....	79
Figure 3.11: Shows the selectivity to maleic anhydride with varying temperature ....	80
Figure 3.12: Shows the Yield of maleic anhydride at varying temperatures .....	80
Figure 3.13: Graph of conversion vs. temperature for all catalysts prepared.....	81
Figure 3.14: Graph showing selectivity to maleic anhydride vs. temperature .....	82
Figure 3.15: Shows a comparison of yield (%) to maleic anhydride for all catalysts tested at constant conversion of 99% .....	82
Figure 3.16: Graph showing comparison of selectivity at constant conversion (80%) for all catalysts studied .....	83

Figure 3.17: Comparison of selectivity at constant conversion of 99% for all catalysts studied.....	83
Figure 3.18: Graph showing comparison of maleic anhydride yield at constant conversion (80%) for all catalysts studied.....	84
Figure 3.19: Graph showing a comparison of yield to maleic anhydride.....	85
Table 5.13 Showing Phases of VPO Catalysts .....	101
Figure 5.1: XRD spectrum of undoped catalyst precursor .....	102
Figure 5.2: XRD spectrum of used undoped catalyst.....	103
Figure 5.3: XRD spectrum of 0.2% Ru promoted catalyst precursor.....	104
Figure 5.4: XRD spectrum of 0.2% Ru promoted used catalyst .....	105
Figure 5.5: XRD spectrum of 0.6% Ru promoted catalyst precursor.....	106
Figure 5.7: XRD spectrum of 1% Ru promoted precursor.....	108
Figure 5.8: XRD spectrum of 1% Ru promoted used catalyst .....	109
Figure 5.9: FTIR spectrum of undoped catalyst of the precalcined stage. ....	110
Figure 5.10: FTIR spectrum of undoped catalyst of the calcined stage. ....	111
Figure 5.11: FTIR spectrum of the undoped catalyst of the used stage .....	112
Figure 5.12: FTIR spectrum of 0.2% Ru promoted catalyst in the precursor stage. .	113
Figure 5.13: FTIR spetrum of the 0.2% Ru promoted catalyst of the calcined stage. .....	114
Figure 5.14: FTIR spectrum of the 0.2% Ru promoted catalyst of the used stage....	115
Figure 5.15: FTIR spectrum of the 0.6% Ru promoted catalyst of the precursor stage. .....	116
Figure 5.16: FTIR spectrum of the 0.6% Ru promoted catalyst of the calcined stage. .....	117
Figure 5.17: FTIR spectrum of the 0.6% Ru promoted catalyst of the used stage....	118
Figure 5.18: FTIR spetrum of the 1% Ru promoted catalyst of the precursor stage.	119
Figure 5.19: FTIR spectrum of the 1% Ru promoted catalyst of the calcined stage.	120
Figure 5.20: FTIR spectrum of the 1% Ru promoted catalyst of the used stage.....	121
Figure 5.21: SEM images of undoped catalyst precursor.....	123
Figure 5.22: SEM images of undoped catalyst calcined .....	124
Figure 5.23: SEM images of used undoped catalyst .....	125
Figure 5.24: SEM images of 0.2% Ru promoted catalysts precursor.....	126
Figure 5.25: SEM images of 0.2% Ru promoted catalysts calcined .....	127
Figure 5.26: SEM images of the used 0.2% Ru promoted catalysts .....	128

Figure 5.27: SEM images of 0.6% Ru promoted catalysts precursor.....	129
Figure 5.28: SEM images of 0.6% Ru promoted catalysts calcined .....	130
Figure 5.29: SEM images of used 0.6% Ru promoted catalyst.....	131
Figure 5.30: SEM images of 1% Ru promoted catalysts precursor.....	132
Figure 5.31: SEM images of 1% Ru promoted catalyst calcined .....	133
Figure 5.32: SEM images of used 1% Ru promoted catalysts. ....	134
Figure 5.33: EDS spectrum of undoped catalyst precursor .....	135
Figure 5.34: Microwave Digestion Parameters .....	136
Figure 5.35: Temperature vs. time for each vessel in the Paar digester.....	137
Figure 5.34: Microwave digestion parameters .....	138



## Acknowledgements

The technical staff, Mrs Anita Naidoo, Mr Gregory Moodley, Mrs Zarina Sayed-Alley, Mrs Saroj Naidoo, Mr Logan Murugas, Mr Alton Blose, Mr Jodi Couling, Mr Rajesh Suchipersadh, Mrs Jay Govender, Mr Kishore Singh and Mr Brett Parel has largely contributed in assisting me in every possible way with technical difficulty that I experienced over the years spent in the department. The little time spent in the department has allowed me the opportunity to work with such helpful assistance offered.

My supervisor Dr H. B. Friedrich offered his expertise in the Inorganic Department and Catalysis Research group that has equipped me with knowledge and skills that I take with me. His intellectual wisdom and professional character has set a great example to me. This MSc would not have been possible without the assistance of Dr Gert Kruger. I would also like to thank Dr Fiona Graham and the Geology department for analysis of my samples on the Scanning Electron Microscope and on the X-Ray Diffraction.

No achievements would have been possible without the kind, ever willing sacrifices made by Dr Martin Onani, Abdul Samad Mahomad, Nishlan Govender, Johnathan Govender, Kirstem Barnes, Thavendran Govender, Neil Koorbanally and Brenda Moodley to assist me in their capacity to ensure my success. The impact these individuals made in my life would not be forgotten. Dr Ronald Otte and Elphus Moropodi have been generous to offer me the resources necessary at Hillside Aluminium and will always be appreciated.

Throughout my entire University career, my family have constantly stood by me every step of the way. My lifetime achievements are largely due to my parents, Marisha and Shameel Ramdeen who have been the pillars of strength with their hard work, encouragement, love and support that has guided me in achieving my goals.

My best friend Lushen Govender has contributed tremendously in assisting me to achieve the best of my potential. Your eternal love and support will carry us forward in the years to come.



## List of Symbols

% = Percent

$\Delta G$  = Total Free Energy Change

$\Pi$  = Pi

$\beta$  = Pre Exponential Term

$\sigma$  = Solid Fluid Interfacial Energy

$\Gamma$  = Solid Molecular Volume

$\alpha$ ,  $\beta$ ,  $\alpha_i$ ,  $\alpha_{ii}$ ,  $\gamma$ ,  $\delta$  = Crystalline and Polymorphic Phases

$\text{\AA}$  = Angstroms

$>$  = Greater Than

m = Meters

g = Gram

$^{\circ}\text{C}$  = Degrees Celcius

$\Sigma$  = Sum of

$\int$  = Intergral

$\mu$  = Micro

$\rho$  = Pressure of gas

$\rho_o$  = Saturated Vapour Pressure

K = Kelvin

$\lambda$  = Wavelength

vs. = Versus

## **Dedication**

This thesis is dedicated to my loving parents, Hira and Prashiella Ramdeen.  
Thank you for all your love and support.

## 1. Introduction

Ever since the 1960s, when Bergman and Frisch (1) disclosed the vanadium phosphorous oxide (VPO) catalysed reaction of n-butane to maleic anhydride there has been considerable interest in this process. Previously benzene was used, however, due to strict control emissions in the USA, together with high costs of benzene and the fact that benzene is a carcinogen, n-butane became the preferred feedstock.

The oxidation of n-butane to maleic anhydride produces fairly low yields, however, with the addition of a catalyst, the yields are considerably increased. The catalyst used here is a vanadium phosphorus oxide catalyst that is prepared via the synthesis of a catalyst precursor  $\text{VOHPO}_4 \cdot 0.5\text{H}_2\text{O}$ , vanadium phosphorus oxide hemi-hydrate. Thereafter, for a considerable increase in yield of product, a promoter is added. Supported VPO catalysts are important in industrial processes (2).

These promoters affect the activity, selectivity and conversion of catalysts. The purpose of this project is the preparation of VPO catalysts from precursors that have been synthesized by various methods. They are then promoted with a metal chloride to form VPO doped catalysts. Catalysts with various concentrations of Ru were studied. The catalysts were then studied in a fixed-bed continuous flow micro-reactor where n-butane (1%) is oxidised in air to form maleic anhydride, CO and  $\text{CO}_2$ .

Industrial importance of maleic anhydride is largely due to it being the base material for unsaturated polyester resins used in the manufacture of plasticizers and modified resins. Maleic anhydride is also used for automotive resins and fibre applications such as in boats, cars and construction purposes.

## 1.1 Maleic Anhydride

### 1.1.1 Background

An important commercial process in the field of chemical engineering, maleic anhydride (MA) was first produced 150 years ago by the dehydration of maleic acid. In 1920 Weiss and Downs described the formation of maleic anhydride by the catalytic partial oxidation of benzene in air (3). There was also considerable interest in the selective oxidation of n-butane to maleic anhydride since Bergman and Frisch reported in 1966 that VPO catalyses this reaction (1).

Until the 1970s benzene was the preferred feedstock for MA production. n-Butane was uncompetitive due to the lower yields that could be produced. However, in the USA and Europe, large-scale exploration brought the ready availability of n-butane as a natural gas liquid. This, together with the imposition of strict pollution control measures on atmospheric benzene emissions in the USA, meant that by the end of the 1970s n-butane became the preferred feedstock. Thus C4 hydrocarbons such as n-butane have replaced benzene because these hydrocarbons are less expensive, more available and less toxic than benzene. Benzene is recognised as a carcinogen and has the ability to cause leukaemia, a potentially fatal cancer of the white cell producing tissue (4). Butane oxidation also produces a cleaner product stream, forming mainly maleic anhydride and carbon oxides (4). Maleic anhydride (2,5 furandione) and its derivatives (maleic and fumaric acids) are produced with a worldwide capacity of 585 000 tons per year.

So far the only really successful industrial alkane oxidation process is the oxidation of n-butane to MA using VPO (5). Fixed bed production of MA indicated molar selectivities from n-butane of around 75% under typical “industrial” conditions, according to a literature survey. These “industrial” conditions include 2 molar percent butane, conversions of 70-85 percent at temperatures between 400-450°C, and space velocities of about 1100-2000hr<sup>-1</sup>

Fluid bed production has been reported and this offers the use of higher butane concentrations (4%) and thus lowers capital costs. However, with higher butane concentrations, a loss in selectivity has been observed.

Transport bed technology operated by Du-pont shows lower conversions per pass with higher selectivity than normally encountered in fixed or fluid bed systems. This may be the most economically favourable route for MA production (4).

#### 1.1.2 Uses of Maleic Anhydride

Some of the uses of maleic anydride include the manufacture of unsaturated polyester resins, agricultural chemicals, food additives, lubricating oil additives and pharmaceuticals. Consumption is expected to grow to 750 000t and continue to grow at 5% pa (6).

Over half of all maleic anhydride produced worldwide is used in unsaturated polyester resins. The resins are used for the production of fibreglass composites for boats, cars and other consumer products. The resins are also used in the construction and electrical industries, and in pipeline and marine construction. Other applications for MA are in the production of fumaric acid, and assorted copolymers, which make thickeners and dispersants. Smaller amounts of MA are used in pesticide and growth inhibitor production.

### 1.2 Catalyst Manufacture

#### 1.2.1 Precipitation

This method gives a solid form of the catalyst from a liquid solution. Initially, two or more solutions are mixed. This causes the precipitation of an amorphous or crystalline precipitate. The wet solid is then converted to the finished catalyst by filtration, washing, drying, forming, calcination and activation (Fig. 1.1).

Precipitates are formed by mixing concentrated solutions of metal salts and produced in a finely divided form with high surface areas. The mixing of the salts is of great importance to achieve a high surface area and small particle sizes. After filtration, the precipitate is washed and dried. After the catalyst is dried, the precursor is activated. The precursor is converted to its active form through physical and chemical changes. The catalyst is generally heated to cause calcination or decomposition.

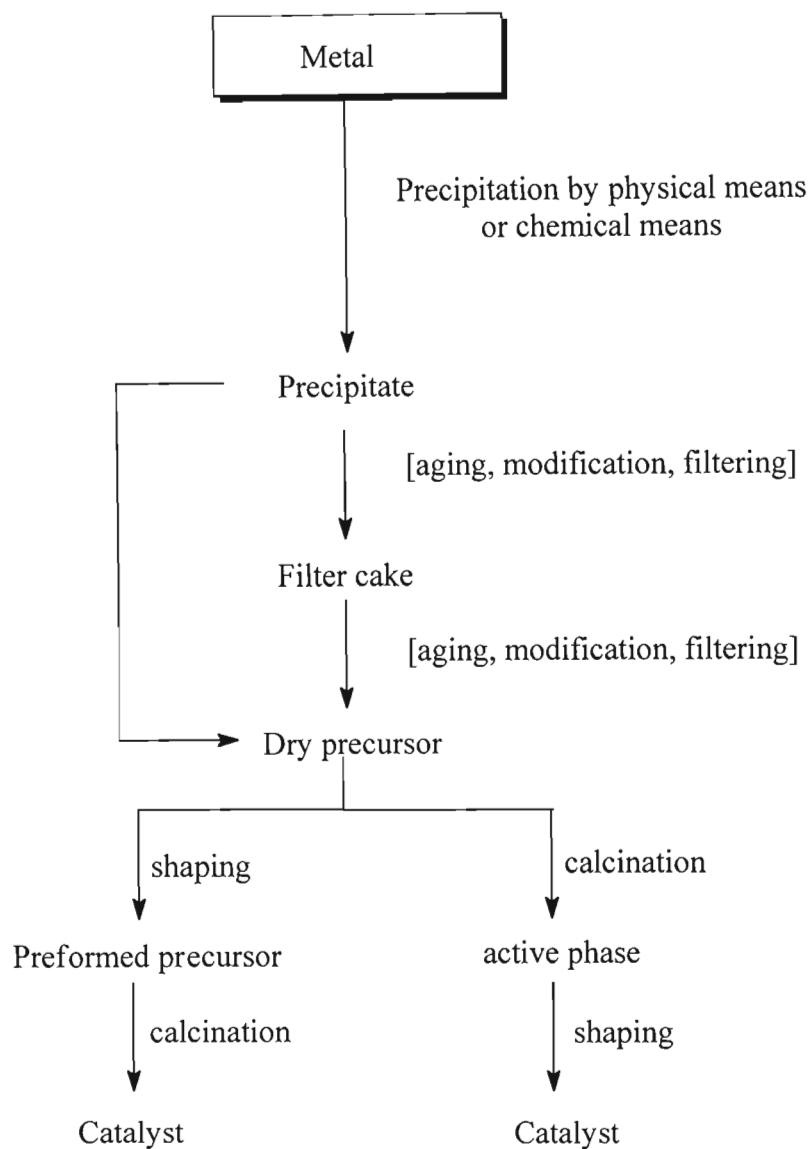


Figure 1.1: Preparation scheme for precipitated catalysts. Optional preparation steps are indicated by square brackets.

Advantages of precipitation are:

1. Greater uniform mixing on a molecular scale.
2. Active species distribution through the final catalyst particle being uniform.
3. Easier to achieve higher concentrations of the catalytically active phase.
4. Better control over pore size and pore size distribution is possible.

### 1.2.1.1 Physico-Chemical Considerations

For a solid to precipitate, from a homogeneous solution, a nucleus has to form. This is governed by the free energy of agglomerates of the constituents of the solution. The total free energy change due to agglomeration,  $\Delta G$ , is determined by:

$$\Delta G = \Delta G_{\text{bulk}} + \Delta G_{\text{interface}} + \Delta G_{\text{others}}$$

Where  $\Delta G_{\text{bulk}}$  is the difference of the free energy between solution species and solid species,

$\Delta G_{\text{interface}}$  is the free energy change related to the formation of the interface, and

$\Delta G_{\text{others}}$  summarizes all other contributions.

At supersaturating conditions  $\Delta G_{\text{bulk}}$  is always negative, but to create an interface, energy is needed,  $\Delta G_{\text{interface}}$  is thus positive. For spherical particles,  $\Delta G_{\text{bulk}}$  increases with  $4\pi r^3/3$  while the interfacial energy only increases with  $4\pi r^2$ . There is thus the critical size  $r$  of the agglomerate, after which  $\Delta G_{\text{bulk}}$  predominates the total free energy change, and the total free energy decreases with the particle size. The critical size is the size of the nucleus (7).

From the Figure 1.2, the most important curve is the nucleation curve, which describes the development of the precursor concentration with time. If the precursor concentration exceeds the critical threshold concentration a nucleus will form and precipitation will begin. The nucleus is defined as the “smallest solid-phase aggregate of atoms, molecules or ions which is formed during a precipitation and which is capable of spontaneous growth”.

The nucleation process is temperature dependent, since the rate constant for homogeneous nucleation usually does not follow an Arrhenius-type law, but is better derived by

$$dN / dt = \beta \exp (-A / \ln^2 s)$$

where  $\beta$  is a pre exponential term,  $A$  the interfacial energy parameter  $16\pi\sigma^3\Gamma^2 / 3(kT)^3$ ,  $\sigma$  the solid fluid interfacial energy,  $\Gamma$  the solid molecular volume, and  $s$  the supersaturation.

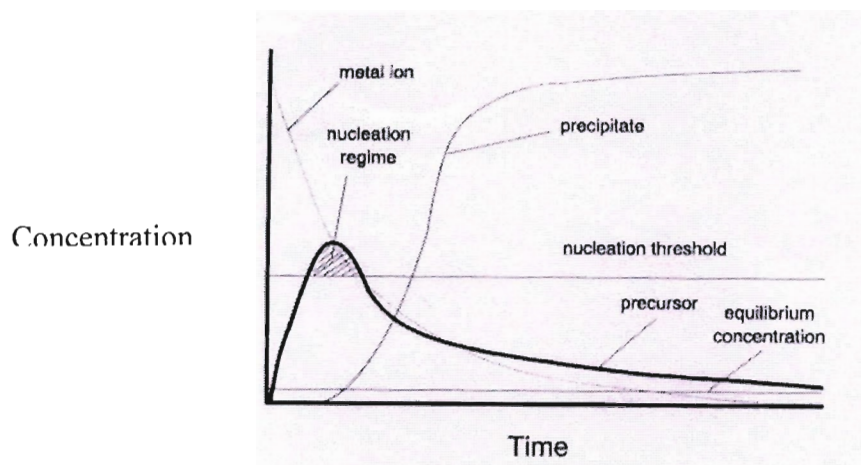


Figure 1.2: Simplified scheme for the formation of a solid product from solution.

A key factor is the supersaturation, which can be reached either by physical means, which is usually cooling down of the mixture, or evaporation of the solvent, or by chemical means i.e. addition of a precipitating agent. The precipitating agent either changes the pH thus leading to condensation of precursors to the hydroxides or the oxides or introduces additional ions into the system by which the solubility product for a certain precipitate is exceeded (7).

### 1.2.2 Impregnated Catalysts

Impregnation of the porous support with a solution of the active component is also generally used in catalysis. A solution is made up with the component to be put on the support. The support is dipped into this solution or the solution is sprayed onto the support. The degree of uniformity varies with the absorptive properties of the carrier and the method of manufacture. The use of an alcoholic solution may lead to a substantially different concentration distribution than with an aqueous solution.

### 1.2.3 Calcination

Calcination involves heating the catalyst precursor in an oxidising atmosphere at a temperature above the operating temperature of the catalyst. The purpose of calcining the catalyst is to stabilise the physical, chemical and catalytic properties of the catalyst. Reactions or processes that occur during calcination are:



- thermally unstable compounds decompose under gaseous vapour and are converted to oxides.
- decomposition of products can form new products
- amorphous regions become crystalline
- various crystalline modifications undergo reversible conversions
- change of pore structure and mechanical strength of precipitated catalyst.

#### 1.2.4 Formation of Final Catalysts

In many cases, prepared solids are not catalytically active. Comparing non supported compounds to compounds dispersed on a carrier, indicates that the kinetics under exactly the same conditions are always altered, and in some cases may lead to different catalytic materials. This is the case when some chemical reaction takes place between the active substance and the support. The reactivity reflects that of the new compound (7). The phenomena taking place during the last stages of the formation of the active phase are calcination, reduction, or sulfidation and are usually called activation. Activation is defined by IUPAC as the transformation of precursor solid to the active phase (8). This is a crucial operation, which determines all the practical properties of catalysts: activity, selectivity, and resistance to ageing.

#### 1.2.5 The Concept of Oxide Monolayers

Supported vanadium oxide catalysts are important in industrial processes. In many cases they are doped with promoters to improve their activity and or selectivity, and supports are used to improve mechanical strength, thermal stability and lifetime. Supports were long believed to be inert in catalytic reactions; it is known now however, that the structure and composition of the materials used as support can influence the activity and selectivity of the active phase to a marked degree (2). Russell and Stokes suggested the concept of an oxide monolayer (9), as being most efficiently used when present as a layer applied as thinly as possible over the surface of a similar support (2). The oxide then exists as a monolayer and is maximally influenced by the support. Use of a supported oxide has several advantages over an unsupported oxide e.g. higher mechanical strength, better thermal stability and larger surface area.

Thermal stability of monolayers has been related to the ratio of the charge on the supported cation to the sum of the cation and oxide ion radii (10).

Catalyst preparation for Vanadium Oxide Monolayer Catalysts requires two techniques: firstly dispersion and this can be achieved by impregnation, adsorption from solution, co-precipitation or deposition and the second stage is calcination.

#### 1.2.5 (i) Impregnation

This term denotes a procedure whereby a certain volume of solution containing a compound of the active element is totally adsorbed into the pores of the support.

#### 1.2.5 (ii) Adsorption

Adsorption is used to describe the removal from solution of a species containing the active element through interaction with the hydroxyl groups on the surface of the support.

#### 1.2.5 (iii) Chemical Vapour Deposition

Deposition is laying down of the active component in the gas phase from a volatile inorganic or organometallic compound to the exterior surface of a support by reaction with its hydroxyl groups.

#### 1.2.5 (iv) Co-precipitation

The active oxides and the supporting oxides or their precursors may be co-precipitated from a solution containing compounds of each element, this usually produces an intimate mixing of catalyst and support, but the active component is dispersed throughout the bulk as well as being at the surface (2).

#### 1.2.6 Influencing Properties of the Final Product

Precipitates with specific properties are generally desired. These properties could be the nature of the phase formed, chemical composition, purity, particle size, surface area, pore sizes, pore volumes, separability from the mother liquor, and many more, including drying, pelletising, or calcination. Figure 1.3 below shows a summary of parameters that can be adjusted in precipitation processes and the properties that are mainly affected by these parameters (7).

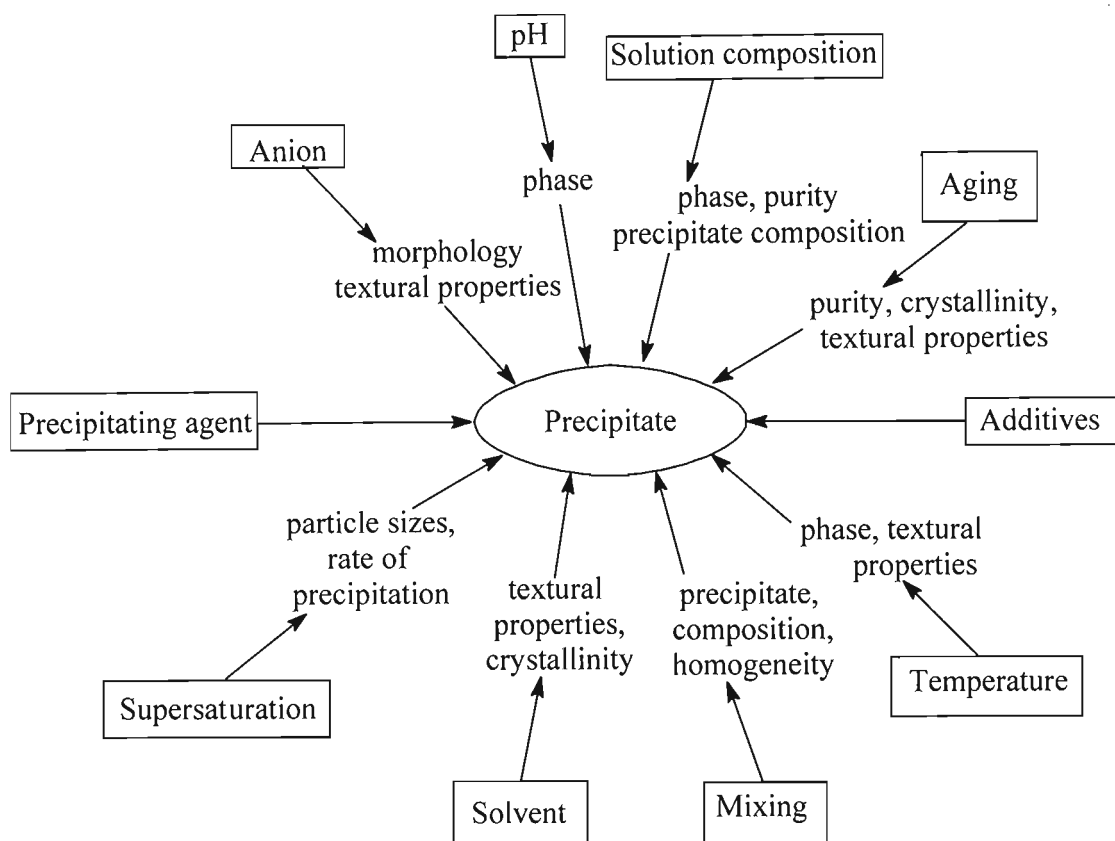


Figure 1.3: The figure summarizes the parameters which can be adjusted in precipitation process and the properties which are mainly influenced by these parameters.

### 1.3 Structure of Catalyst

#### 1.3.1 Crystalline VPO phases:

The VPO system is characterised by a number of crystalline phases containing e.g. vanadium (iv) and vanadium (v). The vanadyl orthophosphate ( $\text{VOPO}_4$ ) crystal structure consists of  $\text{VO}_6$  and  $\text{PO}_4$  groups arranged in layers  $[\text{VOPO}_4]_\infty$  held by long V-O bonds or by hydrogen bonds (4). This leads to rich intercalation chemistry with formation of layered solids consisting of inorganic and organic layers or the formation of solvated inorganic intercalation compounds. The structures of crystalline ( $\alpha$ ,  $\beta$ ) and polymorphic [ $\alpha$ , ( $\alpha_i$ ,  $\alpha_{ii}$ ),  $\gamma$ ,  $\delta$ ] phases of  $\text{VOPO}_4$  will be described. See Appendix for phases encountered in the XRD spectra.

#### 1.3.1.1 Dihydrated Vanadyl Orthophosphates ( $\text{VOPO}_4 \cdot 2\text{H}_2\text{O}$ )

In dihydrated vanadyl orthophosphates ( $\text{VOPO}_4 \cdot 2\text{H}_2\text{O}$ ) the vanadium atom lies on a four fold axis and is surrounded by six oxygen atoms to give a distorted octahedron. Four different tetrahedral phosphates provide the four equatorial oxygens. One of the axial vanadium-oxygen bond distances is very short corresponding to a vanadium-oxygen double bond ( $\text{V}=\text{O}$ ).

#### 1.3.1.2 $\alpha$ – $\text{VOPO}_4$

The  $\alpha$ - $\text{VOPO}_4$  is composed of distorted chains of highly distorted  $\text{VO}_6$  octahedra sharing 4 oxygen atoms with 4 different  $\text{PO}_4$  layers. Along the  $c$ -axis, a distortion of the  $\text{VO}_6$  octahedra occurs, forming a very long V-O bond and a short  $\text{V}=\text{O}$  bond. The oxy vanadium units are therefore approximated as  $\text{VO}_5$  pyramids.

#### 1.3.1.3 $\beta$ - $\text{VOPO}_4$

The  $\beta$ - $\text{VOPO}_4$  phase possesses  $\text{VO}_5$  pyramids and  $\text{PO}_4$  tetrahedra analogous to  $\alpha$ - $\text{VOPO}_4$ , resulting in a network structure. The following transition occurs during thermal treatment.



The crystal structure of  $\delta$ - $\text{VOPO}_4$  and  $\gamma$ - $\text{VOPO}_4$  is similar to the atomic arrangement found in vanadium (iv) hydrogen phosphate [ $\text{VO}(\text{HPO}_4) \cdot 0.5\text{H}_2\text{O}$ ]. Here the pairs of edge sharing octahedra with trans vanadyl oxygens are alternately unshared with  $\text{PO}_4$  tetrahedra (4). It can be obtained from the dihydrated vanadium (v) phosphate by reduction with organic alcohols or from the reduction of  $\text{V}_2\text{O}_5$  followed by  $\text{o-H}_3\text{PO}_4$ .

Hydrogen phosphate (OH) groups are directed into the interlayer space.

Intercalation chemistry is important in structure and catalytic related chemistry of  $\text{VOHPO}_4 \cdot 0.5\text{H}_2\text{O}$ . According to Centi and Trifiro (4) intercalation properties are affected by the preparation of vanadyl hydrogen phosphate hemi-hydrate ( $\text{VOHPO}_4 \cdot 0.5\text{H}_2\text{O}$ ) in the following ways:

1. Nonstoichiometry is easily accommodated as evidenced by the preparation of compounds with 0.9-1.2 P: V atomic ratio without any modification properties.

2. Preparation has an effect on microstructure e.g. morphology and solid-state reactivity.

Reduction of the vanadium (v) compound occurs using either HCl or isobutylalcohol.

The 010 planes of vanadyl hydrogen phosphate ( $\text{VOHPO}_4 \cdot 0.5\text{H}_2\text{O}$ ) are interconnected in a tri-dimensional structure by weak hydrogen bonding of phosphates and water molecules. The organic alcohol competes with this effect, reducing the bonding between the planes and allows the formation of crystals where the (010) planes are found giving rise to the plate-like morphology. This effect, as well as increased surface area, modifies surface properties due to a change in the relative ratio of the (010) crystalline planes (4). The alcohol can remain partially between intercalated layers and induce modifications of the vanadyl hydrogen phosphate structure, which modifies its solid-state reactivity. The transformation of V(iv) to vanadium(v) is an important step in forming the active catalyst  $(\text{VO})_2\text{P}_2\text{O}_7$  from  $\text{VOHPO}_4 \cdot 0.5\text{H}_2\text{O}$ .

The vanadyl pyrophosphate,  $(\text{VO})_2\text{P}_2\text{O}_7$ , crystal structure is built of chains of vanadium polyhedra linked by phosphate groups. The vanadium atoms are linked by the oxygen atoms of the vanadyl in V-O-V chains in the *c*-direction. The vanadium octahedra are linked in pairs through a common edge forming double chains. The vanadyl groups in the paired vanadium octahedra are oriented trans to one another. The conversion of hemihydrate to pyrophosphate can take place without any V-O-P bonds breaking. The structural order of the precursor phase is constant during the transformation to vanadyl pyrophosphate. Terminal vanadyl oxygen atoms in the face shared octahedra and pairs of vanadyl hydrogen phosphate have a syn arrangement in the precursor phase, whereas in vanadyl pyrophosphate, they are in anti positions.

### 1.3.2 The Structure of Vanadyl Pyrophosphate

The VPO system is characterized by the formation of a number of crystalline phases containing compounds of both vanadium(iv) and vanadium(v) (4). The transition of the structure to vanadyl pyrophosphate from its vanadyl hydrogen phosphate precursor demonstrates complicated pathways from precursor to product.

Primary focus has been on the vanadyl pyrophosphate phase,  $(VO)_2P_2O_7$  which demonstrates exceptional selectivity in the 14 electron oxidation of n-butane to maleic anhydride (4).

The catalytic performance has been related to crystal morphology and size, presence of non-stoichiometric phosphorous and variations in the bulk oxidation state of vanadium (11). In order to fully understand structure and performance dependence in this system, a thorough investigation of the crystallography and variation in the structure of vanadyl pyrophosphate has been necessary (11). The transformation of the hydrogen phosphate hemisolvate precursor to the vanadyl pyrophosphate product has been reported to be topotactic with the elimination of two water molecules (12) with an amorphous intermediate phase required to complete the transformation. Point group symmetry around the face showed that the vanadyl dimeric unit in the precursor is  $C_{2v}$ , but the edge shared dimer in the vanadyl pyrophosphate product is  $C_1$  as can be seen in the figure below.

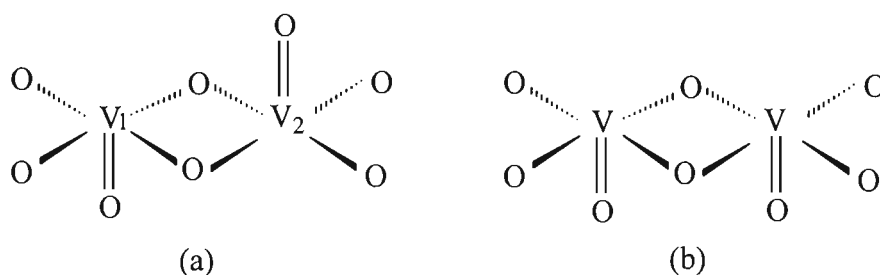


Figure 1.4: Dimeric vanadium-oxygen clusters: (a) trans-bipyramidal unit and (b) cis-bipyramidal unit.

Considerable reorganization occurs during the transition and vanadyl pyrophosphate occurs in two polytypical forms.

### 1.3.3 The Orthorhombic Structure of Vanadyl Pyrophosphate

Vanadyl pyrophosphates, in the orthorhombic form, vary in colour and possess subtle structural differences relative to variation in the symmetry of the vanadium atom sites within the asymmetric unit. The single crystals possess no variation in the

phosphorous (P) atom positions. The structure of  $(VO)_2P_2O_7$  has been determined and is orthorhombic,  $Pca2_1$ , with  $a = 7.725\text{\AA}$ ,  $b = 16.576\text{\AA}$ ,  $c = 9.573\text{\AA}$  and  $Z = 8$  (13). A schematic of the plane packing in the unit cell (Figure 1.5) of  $(VO)_2P_2O_7$  consists of two close-packed layers of oxygen atoms that lie parallel to the  $bc$ -plane at  $\frac{1}{4}$  and  $\frac{3}{4}$  along the  $a$ -axis.

These planes in Figure 1.6 are made up of basal oxygens of vanadium octahedra and phosphate tetrahedra shown below.

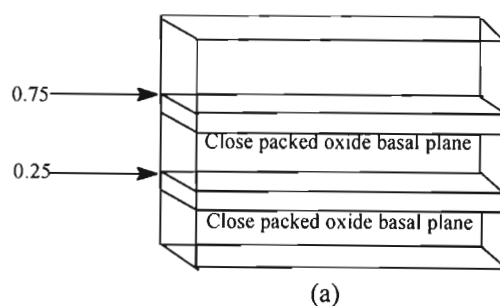


Figure 1.5: The close packed oxygen basal planes for the unit cell of vanadyl pyrophosphate.

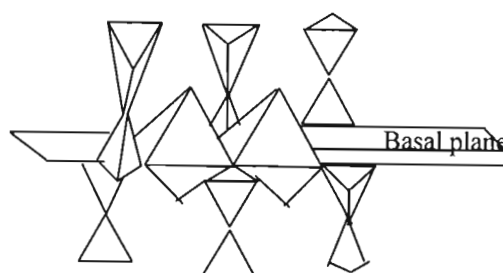


Figure 1.6: The relationship between the coordination spheres of vanadium octahedra and phosphorus tetrahedra.

The structure of  $VOHPO_4 \cdot 0.5H_2O$  is constituted of pairs of  $VO_6$  octahedra sharing a common face (12). Couples of octahedra are connected together, through  $PO_4$  tetrahedra, forming the (001) planes. In one octahedra pair, the  $V=O$  bonds are in cis position. Between the (001) planes,  $H_2O$  molecules are connected through H bonds (4).

$(VO)_2P_2O_7$  presents an orthorhombic structure in which two  $VO_6$  octahedra are edge sharing. Octahedra pairs are connected by  $PO_4$  tetrahedra which gives a layer structure in the (100) plane. In opposition to  $VOHPO_4 \cdot 0.5H_2O$ , the  $V=O$  bonds in octahedra pairs are in trans position, and the layers are connected by pyrophosphate groups.

Figure 1.7 below illustrates the close packed pattern for the basal plane and the relative positions of the vanadium and phosphorus sites.

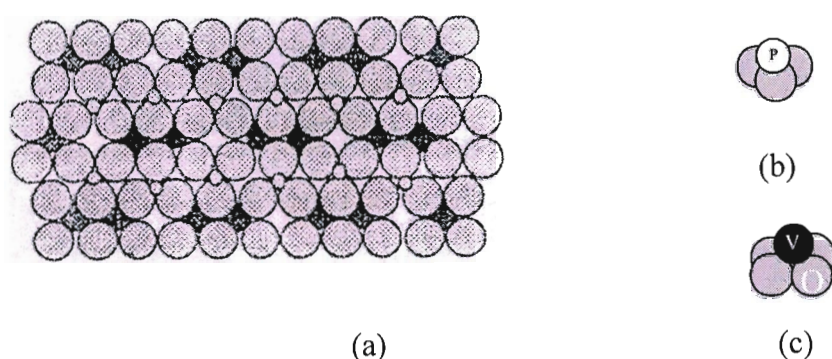


Figure 1.7: (a) Basal oxygen close-packing pattern (10),  
(b) phosphorous tetrahedral interstices and (c) vanadium octahedral interstices.

This model indicates a degree of non-planarity and distortion of the oxygen basal plane. The vanadium atom lies on a four fold axis and is surrounded by six oxygen atoms to give distorted octahedra. The four equatorial oxygens are provided by four different  $PO_4$  tetrahedra. One of the axial  $V-O$  bond distances is very short, corresponding to the vanadium oxygen double bond ( $V=O$ ).

The vanadium octahedra are square pyramidally distorted. The vanadium atoms lie  $0.33\text{\AA}$  out of the basal plane oriented toward the vanadyl oxygen ( $V=O$ ). Figure 1.8 illustrates (a) co-ordination geometry about the vanadium atoms and (b) about the phosphorous atoms, each idealized from the experimental model (10).

There are four classes of oxygen atoms in the  $\gamma$  polymorph namely:

Double bridging oxygen ( $V-O-P$ ), triple bridging oxygen ( $P-O-V_2$ ), vanadyl oxygen ( $V=O$ ) and pyrophosphate oxygen ( $P-O-P$ ). The triple and double bridging oxygens all lie in the basal planes. The coordinates for all the vanadyl oxygens lie within the



unit cell. Two positions are possible for each vanadium atom: above or below the basal plane. If the vanadium atoms lie above the basal planes at  $\frac{1}{4}$  and  $\frac{3}{4}$ , the direction of the vanadyl column will be aligned with the direction of the  $a$ -axis.

If they lie below these planes, then the direction of the column will be anti parallel to the  $a$ -axis. Phosphorus atoms can also lie above / below the basal planes at  $\frac{1}{4}$  and  $\frac{3}{4}$  on the  $a$ -axis. However, both phosphorus atoms of an individual pyrophosphate group must lie between two adjacent basal layers. Altogether, there are 104 atoms contained within the unit cell of vanadyl pyrophosphate: 48 basal oxygen atoms, 16 vanadyl oxygen atoms, 16 vanadium atoms (8 pairs) and 8 pyrophosphates (24 atoms).

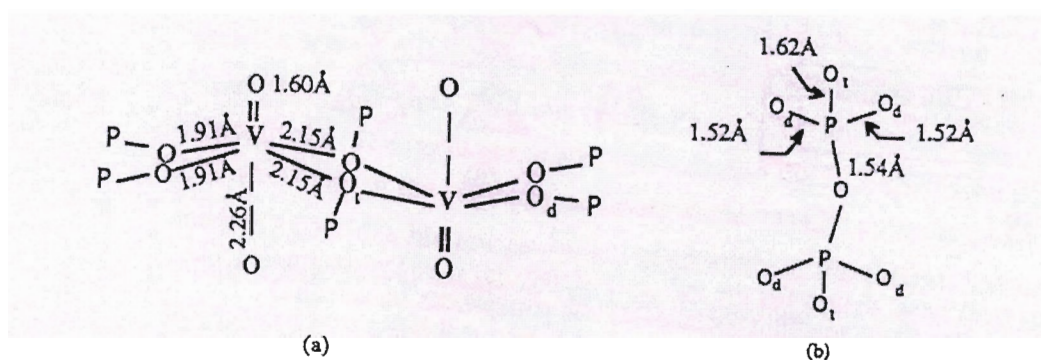


Figure 1.8: Bond lengths for (a) the vanadium coordination sphere, and (b) the phosphorous atoms in the idealized model of vanadium pyrophosphate.

### 1.3.3.1 Structure of V-P-O phases

There are different VPO phases with vanadium in the +5, +4 and +3 oxidation states for which structures have been resolved (14).

- The V(v) phases correspond to hydrates like  $\text{VOPO}_4 \cdot \text{H}_2\text{O}$ ,  $\text{VOPO}_4 \cdot 2\text{H}_2\text{O}$ , and phosphates,  $\text{VOPO}_4$  ( $\alpha_I$ ,  $\alpha_{II}$ ,  $\beta$ ,  $\gamma$  and  $\delta$ ).
- The V(iv) phases correspond to vanadyl hydrogen phosphates like  $\text{VOPO}_4 \cdot 0.5\text{H}_2\text{O}$ ,  $\text{VOPO}_4 \cdot 4\text{H}_2\text{O}$  or  $\text{VO}(\text{H}_2\text{PO}_4)_2$ , to pyrophosphate  $(\text{VO})_2\text{P}_2\text{O}_7$ , and to metaphosphates  $\text{VO}(\text{PO}_3)_2$ .
- The V(iii) phases correspond to  $\text{VPO}_4$  and  $\text{V}(\text{PO}_3)_3$ .

The vanadyl hydrates and hydrogen phosphates are generally considered as catalyst precursors (13).

## 1.4 Catalyst Performance

**Deactivation:** Deactivation is caused by fouling (e.g. Coke formation) or by poisoning.

**Selectivity:** Selectivity is the ratio of the moles of a particular product (usually the desired product) formed to the moles of another (usually the undesired product) produced in a set of reactions:

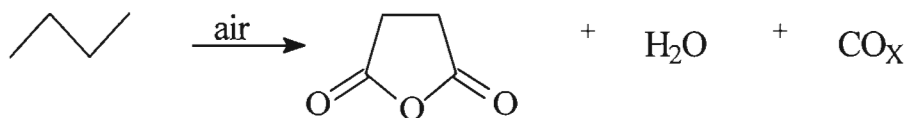
Selectivity = moles of product/ moles of reactant converted.

**Conversion:** the fraction of feed or some component of the feed that is converted to products. Thus % conversion is  $100 \times \text{moles of feed that react} / \text{moles of feed introduced}$ .

**Yield:** The moles of final product divided by the moles of initial reactant consumed.

## 1.5 Reaction Mechanisms

The redox cycle and the acid-base behaviour of the catalyst surface is often described by the Mars Van Krevelen Mechanism. This applies to the selective oxidation of n-butane to maleic anhydride (Equation 1).



Equation 1. The reaction of n-butane to maleic anhydride

In the Mars Van Krevelen Mechanism, Figure 1.9, the reactant hydrocarbon is adsorbed on an  $M_1^{n+}$  site to form a chemisorbed species. The adsorbed species reacts with the lattice oxygen that is associated with the  $M_1^{n+}$  site, to produce a partially oxidized product. To replenish the oxygen lost, the lattice oxygen from a neighbouring site  $M_2^{m+}$  moves to  $M_1^{n+}$ . Electrons produced at  $M_1^{n+}$  are relocated to  $M_2^{m+}$ . Molecular oxygen is adsorbed on the  $M_2^{m+}$  site where it is converted to lattice oxygen. A diagram representing this mechanism is shown in Figure 1.9.

In this process, the catalyst is alternately reduced by the compound to be oxidized and oxidized by the gaseous molecular oxygen. The redox mechanism can be illustrated by the equations 2, 3 and 4.

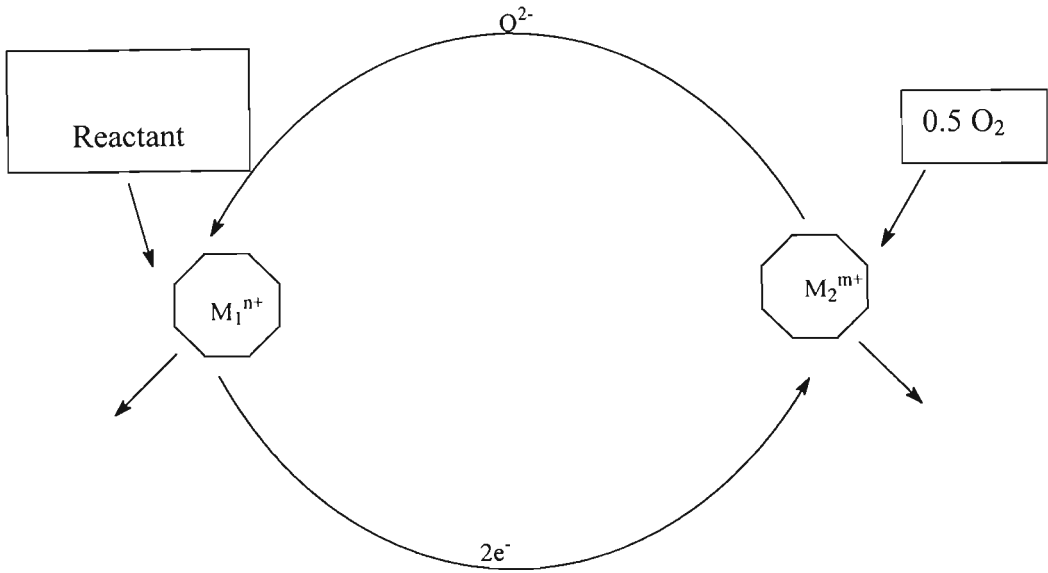
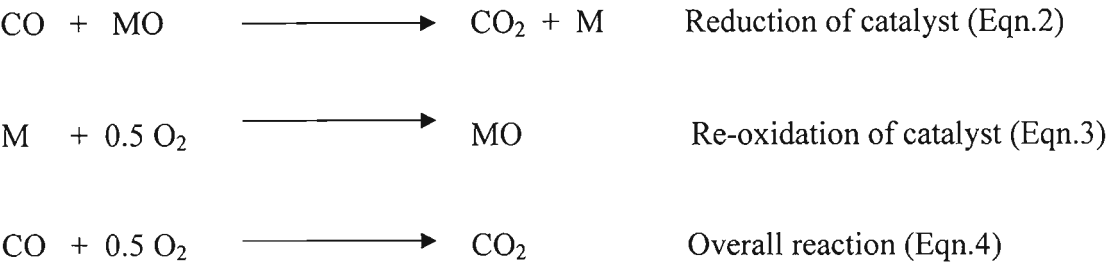


Figure 1.9: The Mars Van Krevelan Mechanism



This redox cycle depends on the availability of catalyst surface sites to accept or donate electrons.

### 1.5.1 Uptake of electrons

The replenishing of lattice oxygen of the catalyst during the selective oxidation of hydrocarbons demands the continuous supply of  $O^{2-}$  in order to maintain an ongoing reaction. The gaseous oxygen ( $O_2$ ) transforms to lattice oxygen ( $2O$ ), which is an

important step in the selective oxidation reaction. The molecular oxygen first adsorbs onto the catalyst surface and thereafter the molecule gains electrons and forms  $O^{2-}$  ions.

### 1.5.2 Uptake of Hydrocarbons

The hydrocarbon adsorption and activation on the surface of the oxidation catalyst is as important as the adsorption and activation of the oxygen molecule. Complexities of hydrocarbons do not allow the complete process to be shown clearly, however, olefin species shall be shown in Figure 1.10.

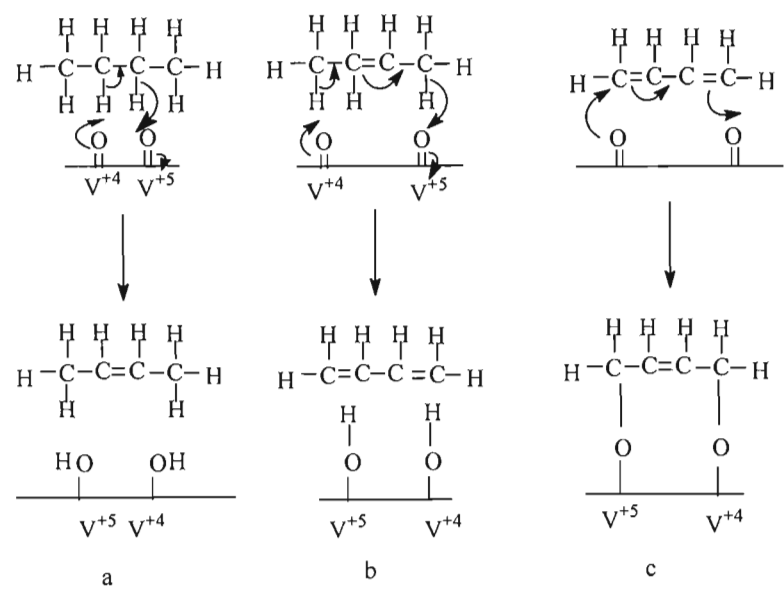


Figure 1.10: Proposed reaction scheme for the oxidehydrogenation of n-butane to 2-butene (a) and 2-butene to butadiene (b) and the oxidation of butadiene to maleic anhydride (c). The final intermediate (c) is represented in Figure 1.12.

### 1.5.3 Reaction Mechanism: The olefinic route

The complex selective oxidation reaction involves the abstraction of eight H atoms and three O insertions. The conversion of n-butane to maleic anhydride over the VPO catalyst is commonly used in industry as mentioned previously.

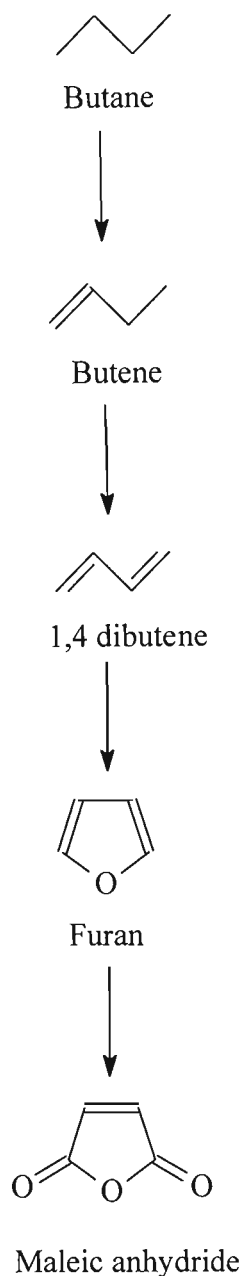


Figure 1.11: The olefinic route

The reaction could either follow the olefinic route (Figure 1.11) (15) or alkoxide route (Figure 1.12). All of the intermediates react on the VPO catalyst faster than n-butane does; therefore it is difficult to observe these intermediates.

#### 1.5.4 Reaction Mechanism: The Alkoxide Route

The alkoxide route involves a static model and a local site of a small size with a specific number of vanadium atoms and a precise  $V^{4+}/V^{5+}$  distribution.

EPR studies have shown that under reaction on  $VOPO_4$  phases,  $V^{4+}$  ensembles are created while isolated  $V^{4+}$  cations disappear probably by oxidation (16).

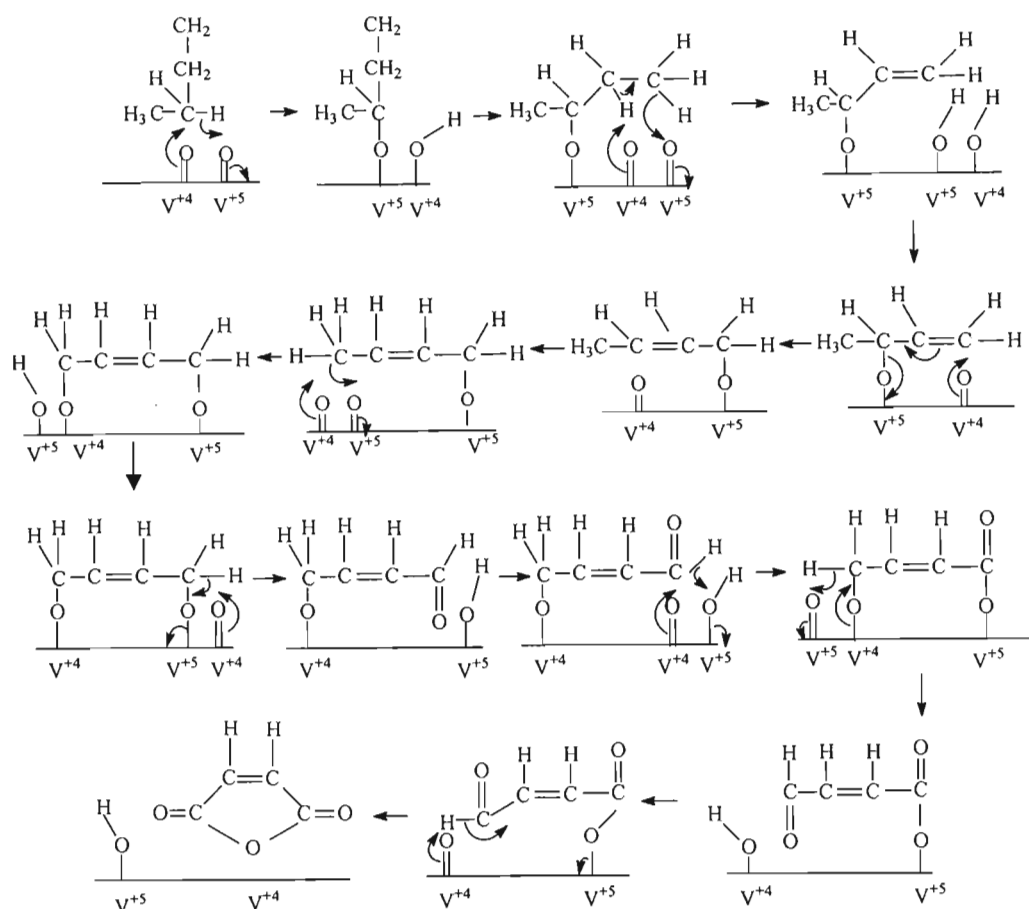


Figure 1.12: Proposal for a reaction scheme for the oxidation of n-butane to maleic anhydride which implies the alkoxide route (16).

## 1.6 Promoters

Promoters refer to a substance that, when added in relatively small amounts in the preparation of a catalyst, imparts better activity, selectivity or stability. The promoter may be added to the reactants in small amounts and it acts by being adsorbed onto the catalyst. Promoters can be classified as textural promoters or structural promoters. A textural promoter (stabiliser) acts by a physical effect; a structural promoter acts by a chemical effect (3).

### 1.6.1 Promotional effects for VPO Catalysts

Promoter compounds can be added either:

- Together with vanadium and phosphorus compounds prior to preparation of the catalyst precursor or,

(b) By impregnation of the catalyst precursor prior to formation of the final catalyst by heat treatment.

The way promoters are added is of crucial importance (17).

#### 1.6.2 Effect of Promoters on $(VO)_2P_2O_7$

Several promoters have been used by the HCl addition method (18) as stated by C. J. Kiely, *et al.* Usually the HCl method gives superior catalytic performance and is the preferred method for most promoted catalysts (17).

However, more recently it was shown that benzyl alcohol and HCl, as reductants, yield catalysts of similar efficacy (19). The main precursor compound prepared for both aqueous and non-aqueous solvents has been shown to be  $VOHPO_4 \cdot 0.5H_2O$ , which becomes  $(VO)_2P_2O_7$ , the active form, on heating.

The role of solvents was crucial in obtaining the best catalytic performance, and non-aqueous solvents were preferred. The catalysts showed high surface areas ( $> 20m^2g^{-1}$ ) compared to aqueous preparation ( $2-3m^2g^{-1}$ ). Non-aqueous preparation can reliably give higher surface area catalysts (17).

The catalysts can be divided into:

1. Type one formulations containing P:V atomic ratios  $>1$  with high promoter: V atomic ratios i.e. excess P: promoter ratio is approximately unity.
2. Type two promoted formulations containing lower promoter: V atomic ratios.

#### 1.6.3 Effect of Promoter on other VPO Catalysts

Hodnett and Delmon, (20) showed that the addition of cobalt up to  $Co/V = 0.05$  increased specific activity, but the surface area decreased with increasing Co content, and the highest conversion was observed with the unpromoted catalysts. An optimum level of selectivity to maleic anhydride occurs at  $Co/V$  in the range of 0.01-0.02 (20).

Cheng concluded that promoters drastically decrease both the thickness of platelets in the layered morphology, and their crystallite sizes (21).

Hutchings and Higgens used a simple kinetic analysis to gauge their effect upon the catalytic performance (22). Mo and Co showed a promotional effect, increasing the product yield per unit surface area. These cations have an electronic effect that induces the fast adsorption of Maleic Anhydride limiting its over oxidation and it was suggested that Co and Mo may induce defect formation in the active phase. The pure  $\text{VOPO}_4$  vanadium phosphate phases ( $\alpha$ ,  $\beta$  &  $\gamma$ ) were found to be extrinsic n-type semiconductors with the presence of substitutional  $\text{V}^{4+}$  ions acting as acceptor centres.

The addition of silica at levels of up to 5.3% was studied and optimum performance was found for 1.5% Si. Promotion of both catalyst activity and selectivity was observed with these Si promoted catalysts.

A number of promoters e.g. Ce, Co, Cr, Cu, Fe, Hf, La, Mo, Nb, Ni, Ti and Zr have been shown to be effective at very low concentrations.

As noted by Hodnett and Delmon (20) additional levels of promoters usually lead to a distinct decrease in maleic anhydride yield. This is due to additional promoters forming separate phases, which under the oxidising conditions would be expected to be oxides that would promote only total oxidation.

#### 1.6.4 Catalytic Performance of Unpromoted Catalysts

Hutchings and Higgens (22) prepared catalysts using HCl as the reducing agent with water or isobutanol as the solvent. The P: V ratio of the two precursors were the same ( $\text{P: V} = 1.20 \pm 0.01$ ) and analysis by XRD showed that they comprised mainly  $\text{VOHPO}_4 \cdot 0.5\text{H}_2\text{O}$  and  $(\text{VO})_2\text{P}_2\text{O}_7$  respectively. The difference between catalysts prepared using water and isobutanol was that the surface area of catalyst containing isobutanol was significantly higher. The activity of the catalyst prepared using HCl as the reducing agent with isobutanol as a solvent is significantly better than that prepared using water as a solvent. The catalyst prepared using isobutanol can be used at lower temperatures, and as maleic anhydride selectivity is a function of temperature, improved pass yields are obtained. The optimum pass yield of maleic



anhydride for the isobutanol catalyst is 60% at 385°C, 1000h<sup>-1</sup>, whereas pass yield for the aqueous catalysts is 50% at 500°C, 1000h<sup>-1</sup>.

#### 1.6.5 Catalytic Performance of Promoted Catalysts Prepared by Standard Non-Aqueous HCl Method

Hutchings and Higgins (22) prepared catalysts containing a range of additives together with V<sub>2</sub>O<sub>5</sub> at the start of the standard non-aqueous HCl precursor preparation. Cr, Nb, Pd, Sb, Ru, Th, Zn, and Zr were found to have little effect on the specific activity, although Cr, Zn and Zr showed a significant increase in surface area. Fe, Cs and Ag were found to decrease the specific activity.

Significant decreases in the primary selectivity were observed with Cs, Pd, Ru, Zn and Zr. The Figure 1.13 below shows a plot of the rate constant for butane conversion ( $k_1 + k_2$ ) versus the final surface area.

The magnitude of  $k_3^*$  (Fig. 1.14) indicates the extent to which consecutive oxidation of maleic anhydride is occurring and  $k_3$  generally increases with increasing surface area. However,  $k_3$  for Cs, Pd, Ru, Th, Zn and Zr is markedly higher than suggested by the general trend. The value of  $k_3$  for Fe is lower than the trend and indicates that the relative rates of maleic anhydride and butane oxidation can be determined by the ratio  $k_3 / (k_1 + k_2)$ . Due to this Ag, Cs, Pd, Ru, Zn & Zr all promote the over oxidation of maleic anhydride but, significantly, Mo acts as a poison for the overoxidation.

Using specific activity  $(k_1 + k_2) / sa^{**}$  and the relative oxidation rate  $k_3 / (k_1 + k_2)$  as performance indicators for the effectiveness of the additives, it is apparent that only Co and Mo can be considered to act as promoters.

\* The rate constant  $K_3$  can be obtained from the slope of the plot of  $[k_1x + (k_1 + k_2) Sx]$  versus  $[k_1/GHSV - Sx]$  where  $x$  is the fractional conversion of butane,  $S$  is the fractional selectivity to maleic anhydride and GHSV is the Gas Hourly Space Velocity.

\*\* surface area

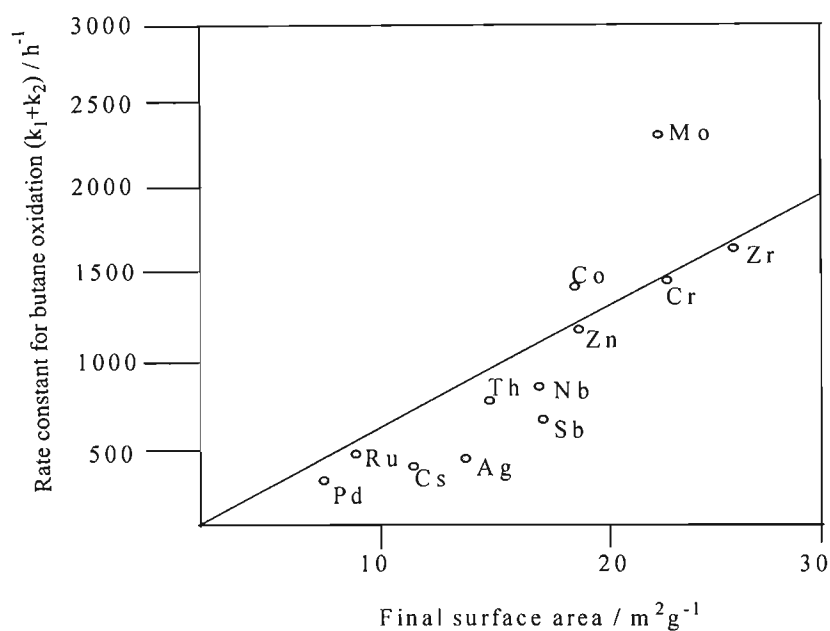


Figure 1.13: Dependence of rate constant for butane oxidation on final catalyst surface area.

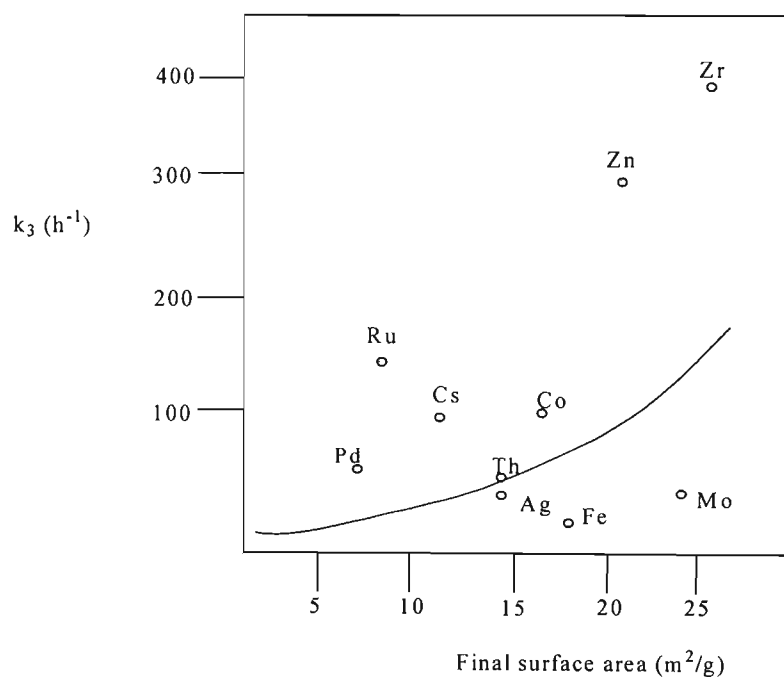


Figure 1.14: Dependence of rate constant for butane oxidation on final catalyst surface area.

### 1.6.6 Role of Catalyst Promoters

The role of many promoter compounds is mainly to control the final catalyst surface area of  $(VO)_2P_2O_7$ . The promoter metal cation is observed to be present in a phase other than  $(VO)_2P_2O_7$ . The role of the metal cation is to act as a P scavenger, since in the absence of the metal cation  $VO(H_2PO_4)_2 \cdot xH_3PO_4$  would be formed, which when present would lead to the formation of a low surface area catalyst. With the above catalysts, there is a small effect on specific activity and the main effect is due to an increase in surface area. The selectivity to maleic anhydride is significantly decreased, as is observed with Ag, Cs, Pd, Ru, Zn, & Zr. Naumann and Behan (23) showed that additives such as Ag, Pd and Ru increase the reduction of  $V_2O_5$  and therefore decrease the vanadium oxidation state and this then adversely affects the selectivity.

Low levels of Ce, Cr, Cu, Fe and Hf are also effective promoters. The synthesis of modified vanadium phosphorous catalysts for the oxidation of C4 hydrocarbons to maleic anhydride showed that added iron acts as a promoter (24). In general, promoters only constitute a small part of the overall composition of VPO catalysts (17).

Promoters may be classified in two groups:

1. where the promoter is added to the bulk of the catalyst,
2. cases where the promoter is added in such a way as to favour its being located finally at the surface.

### 1.7 The Effects of Oxidation State

The valence state of vanadium in the active surface, the  $V^{4+}/V^{5+}$  equilibrium on the surface of a vanadyl pyrophosphate during n-butane oxidation has been demonstrated, which is dependent on time activation (4). The best results were associated with a  $(VO)_2P_2O_7$  structure in which P atoms were associated with  $V^{4+}$  in a crystalline matrix and with  $V^{4+}$  in a disordered matrix together with  $V^{5+}$ , implying the importance of  $V^{4+}$ - $V^{5+}$  mixed valencies together with the  $(VO)_2P_2O_7$  structure (25).

The activated VPO catalyst was prepared by adding  $V_2O_5$  (11.8g) to isobutanol (250ml).  $H_3PO_4$  (16.49g 85%) was then added into the solution and refluxed for

16hrs. The VPO catalyst was then doped with Co and Fe which lead to the formation of  $(VO)_2P_2O_7$  a poorly crystallized structure, which strongly improves the catalytic performance. The activated VPD, prepared via  $VOHPO_4 \cdot 2H_2O$ , was prepared from  $V_2O_5$  (12g) and  $H_3PO_4$  (115.5g 85%) which were refluxed in  $H_2O$  (24ml  $H_2O/g$  solid) for 8 hrs. This was then doped with Fe and in this precursor catalyst  $(VOHPO_4 \cdot 0.5H_2O)$  (26), Fe causes the  $(VO)_2P_2O_7$  to exist as a poorly crystalline  $(VO)_2P_2O_7$  structure and this explains the poor performance of this catalyst. However, Co generates significantly crystalline  $(VO)_2P_2O_7$  together with a poorly crystalline  $(VO)_2P_2O_7$  structure, a combination that gives enhanced catalytic performance. The best catalytic performances can be correlated with the presence of these two structures with  $V^{4+}$  cations and  $V^{4+} - V^{5+}$  dimers (26). These dimers control the catalytic activity for n- butane oxidation to maleic anhydride. The specific activity of the catalyst increases with increasing concentration of  $V^{4+} - V^{5+}$  dimers.

$(VO)_2P_2O_7$  alone is not the active phase for selective oxidation of n-butane to maleic anhydride, but a suitable  $V^{4+}/V^{5+}$  balance is required for best performance on this matrix. Nakamura et. al. (1974) (27) claimed a correlation between the yield of maleic anhydride and the degree of aggregation of vanadium ions which resulted from preparations using different hydroxycarboxylic acids as reducing agents. Yield increases as a function of degree of aggregation. The optimum average vanadium value for all catalysts was close to 4+. There was an indication that  $V^{5+}$  ions were present for maleic anhydride formation and this involved a redox cycle between  $V^{4+}$  and  $V^{5+}$ . Catalysts with metal-oxygen double bonds were active in maleic anhydride formation and  $V = O$  were active sites. Facile movement of electrons through the aggregated reduced structures facilitated dissociation of  $O_2$  (g) and formation of the necessary surface  $V = O$  active sites with vanadium in the 5+ oxidation state.

## 1.8 Mole Balance

### 1.8.1 The General Mole Balance Equation

A mole balance of species j will be considered in a system volume, where species j represents the particular chemical species of interest such as water (28). Refer to Figure 1.15.

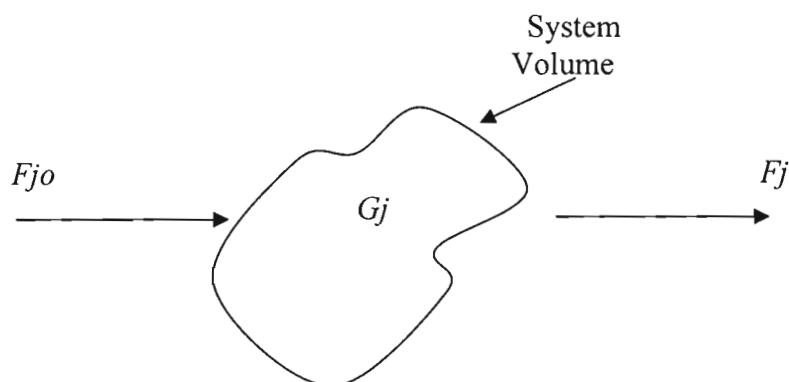


Figure 1.15: A system volume  $G_j$

Where  $F_{jo}$  = rate of flow of  $j$  into the system (moles/time),

$G_j$  = rate of generation of  $j$  by a chemical reaction within the system (moles/time),

$F_j$  = rate of flow of  $j$  out of the system (moles/time).

A mole balance on species  $j$  at any instance in time  $t$ , yields the following equation

rate of flow of $j$ into the system (moles/time)	+	rate of generation of $j$ by a chemical reaction within the system (moles/time)	-	rate of flow of $j$ out of the system (moles/time)	=	rate of accumulation of $j$ within the sys. (moles/time)
---	---	--	---	---	---	--

$$\text{Mole balance: in} + \text{generation} - \text{out} = \text{accumulation}$$

$$F_{jo} + G_j - F_j = \frac{dN_j}{dt} \quad (5)$$

Where  $N_j$  represents the number of moles of species  $j$  in the system at time  $t$ .

$$G_j = r_j \cdot V \quad (\text{system variables are constant})$$

Where  $r_j$  = rate of formation of species  $j$ .

$$\frac{\text{moles}}{\text{time}} = \frac{\text{moles}}{\text{time} \cdot \text{volume}} \cdot \text{volume}$$

Suppose the rate of formation of species  $j$  for the reaction varies with the position in the system volume. It has the value  $r_{j1}$  at location 1 which is surrounded by a small volume  $\Delta V$ , within which the rate is uniform, similarly, the reaction rate has a value  $r_j$  at location 2 and the associated volume  $\Delta V_2$ .

The rate of generation,  $\Delta G_{j1} = r_{j1} \Delta V_1$ .

The total rate of generation within the system volume

$$G_j = \sum_{i=1}^m \Delta G_{ji} = \sum_{i=1}^m r_{ji} \Delta V_i \quad (6)$$

where  $m$  = subvolumes

For the appropriate limits (ie. Let  $m \rightarrow \infty$  and  $\Delta V \rightarrow 0$ ) and making use of the definition of an integral, we rewrite

$$G_j = \int_V r_j dV \quad (7)$$

$r_j$  will be an indirect function of position since properties of reacting material can have different values.

Replacing  $G_j$  :

$$F_{jo} - F_j + G_j = \frac{dN_j}{dt} \quad (8)$$

By its integral form the general mole balance equation for any chemical species  $j$  that is entering, leaving, reacting and or accumulating within any system volume  $V$ :

$$F_{jo} - F_j + \int_V r_j dV = \frac{dN_j}{dt} \quad (9)$$

## 1.9 Reactors

### 1.9.1 Batch Reactors

A batch reactor has no inflow or outflow of reactants or products,  $F_{jo} = F_j = 0$ . The

general mole balance on species  $j$  is  $\frac{dN_j}{dt} = \int_V r_j dV$ .

If the reaction mixture is perfectly mixed so that there is no variation in the rate of reaction, we can take  $r_j$  out of the equation and we get the mole balance in the form:

$$\frac{dN_j}{dt} = r_j V \quad (10)$$

### 1.9.2 Continuous Flow Reactors

#### 1.9.2 (i) Continuous Stirred Tank Reactor

The figure below illustrates a commonly used stirred tank operated continuously. This continuous stirred tank reactor (CSTR) is normally run at steady state and is usually operated to be quite well mixed. Hence there are no spatial variations in concentration, temperature, or reaction rate throughout the vessel. The concentration and temperature are constant throughout the vessel and it is therefore the same at the exit stream. Certain systems have non-ideal mixing therefore the CSTR model will be inadequate and other techniques have to be looked at. The general mole balance equation

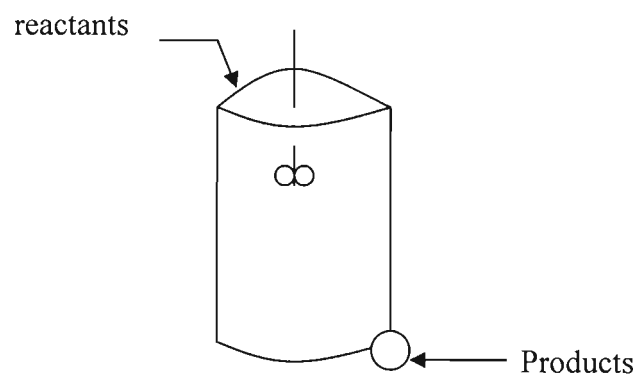


Figure 1.16: Continuous stirred tank reactor

$$F_{j0} - F_j + \int_V r_j dV = \frac{dN_j}{dt} \quad (11)$$

At steady state  $\frac{dN_j}{dt} = 0$

If the rate of reaction remains the same,  $\int_V r_j dV = V r_j$  (12)

For a CSTR a familiar form of the design equation is shown:

$$V = F_{j0} - F_j / r_j \quad (13)$$

The molar flow rate  $F_j$  is just the product of the concentration of the species  $j$  and the volumetric flow rate  $V$  :

$$F_j / C_j V \quad (14)$$

$$\frac{\text{moles}}{\text{time}} = \frac{\text{moles}}{\text{volume}} \cdot \frac{\text{volume}}{\text{time}}$$

### 1.9.3 Tubular Reactor

A tubular reactor consists of a cylindrical pipe and is normally operated at steady state, as is the CSTR. We consider systems in which the flow is highly turbulent and that of plug flow may model the flow field. There is no radiation variation in concentration and the reactor is referred to as plug flow reactor (PFR), see Figure 1.17.

The reactants are continually consumed as they flow down the length of the reactor and the concentration varies continuously in the axial direction through the reactor. The reaction rate will also vary. The general mole balance equation

$$F_{j0} - F_j + \int_V r_j dV = \frac{dN_j}{dt} \quad (15)$$

The reactor is divided into a number of subvolumes so that within each subvolume  $\Delta V$ , the reaction rate may be considered spatially uniform.

Assume a subvolume is located a distance  $y$  from the entrance of the reactor, we let  $F_j(y)$  represent the molar flow rate of species  $j$  into volume  $\Delta V$  at  $y$  and  $F_j(y + \Delta y)$  the molar flow of species  $j$  out of the volume at the location  $(y + \Delta y)$ . In a spatially uniform subvolume  $\Delta V$ ,

$$\int_{\Delta V} r_j dV = r_j \Delta V \quad (16)$$

For a tubular reactor operated at steady state

$$\frac{dN_j}{dt} = 0 \quad (17)$$

$$\text{Equation 1.4 becomes } F_j(y) - F_j(y + \Delta y) + r_j \Delta V = 0 \quad (18)$$

$r_j$  is a function of reactant concentration which is a function of the position  $y$  down the reactor. The volume  $\Delta V$  is the product of the cross sectional area  $A$  of the reactor length  $\Delta y$ .

$$\Delta V = A \Delta y$$

Substitute in equation (18) for  $\Delta V$  and divide by  $\Delta y$  to obtain



$$-\left[ F_j(y + \Delta y) - F_j(y) \right] / \Delta y = -Ar \quad (19)$$

The definition of the derivative:

$$\lim_{\Delta x \rightarrow 0} \left[ f(x + \Delta x) - f(x) \right] / \Delta x = df/dx \quad (20)$$

Taking the limit as  $\Delta y$  approaches zero, we obtain  $-dF_j/dy = -Ar$

Divide by  $-1$ , we get  $dF_j/dy = Ar_j \quad (21)$

If  $dV = A dy$ , one form of the design equation for a tubular reactor  $dF_j/dV = r_j \quad (22)$

The same equation can be applied if the cross-sectional area varies along the length of the reactor.

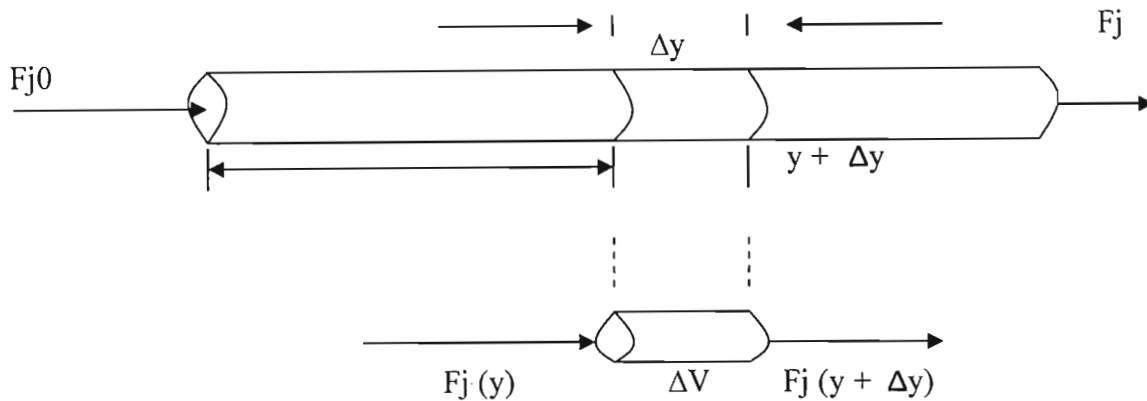


Figure 1.17: Tubular reactor (PFR)

#### 1.9.4 Packed Bed Reactors

The principal difference between reactor design calculations involving homogeneous reactions and those involving fluid solid heterogeneous reactions is that the reaction rate depends on the mass of the solid catalyst,  $W$ , rather than on reactor volume,  $V$ .

The reaction rate of a substance A, for a fluid-solid heterogeneous system is defined as

$$-r_A = \frac{\text{g.mole A (reacted)}}{\text{s.g (catalyst)}}$$

The mass of the catalyst is important to the rate of the reaction. Reactor volume is of secondary importance. For the design equation, we replace the volume co-ordinate in equation 18 as previously mentioned with the catalyst weight co-ordinate W. The PBR has no radial gradients in concentration, temperature or reaction rate.

The general mole balance equation on species A over catalyst weight  $\Delta W$ :

$$\text{In} - \text{out} + \text{generated} = \text{accumulated.} \quad (23)$$

$$F_A(W) - F_A(W + \Delta W) + r'_A \Delta W = 0 \quad (24)$$

Dimensions of the general term in Equation 23 are

$$r'_A \Delta W = \frac{\text{moles A}}{(\text{time.mass of catalyst})} \cdot (\text{mass of catalyst})$$

Which is the same as molar flow rate for a PBR

$$\frac{dF_A}{dW} = r'_A \quad (25)$$

When pressure drop and catalyst decay are neglected, the integral form of the packed catalyst bed design equation can be used to calculate catalyst weight (23).

$$W = \int_{F_{AQ}}^{F_A} \frac{dF_A}{r'_A} \quad (26)$$

### 1.9.5 Fixed Bed Catalytic Reactors

#### 1.9.5 (i) The importance and scale of fixed bed catalytic processes:

Solid catalysts have led the chemical industry to grow in a spectacular way through the development of new or the rejuvenation of established processes. These major catalytic processes are carried out in fixed bed reactors. Some of the main processes are listed in Table 1.1 below.

#### 1.9.5 (ii) Modelling of Fixed Bed Reactors

General models of fixed bed reactors now range from the very simple to the very sophisticated ones presented in the last 2-3 years. Reactor design, due to the degree of sophistication, in the first place depends on the process. Equally important is the degree of accuracy with which the kinetic and transport parameters are known.

Table 1.1: Main Fixed Bed Catalytic Processes

Basic Chemical Industry		Petrochemical Industry	Petroleum Refining
Steam	primary	Ethylene oxide	Catalytic reforming
Reforming	secondary	Ethylene dichloride	Isomerization
CO conversion		Vinylacetate	Polymerization
CO methanation		Butadiene	(Hydro)desulfurization
Ammonia	} synthesis	Maleic anhydride	Hydrocracking (fluidized bed)
Sulfuric acid		Pthalic anhydride	
Methanol		Cyclohexane	
Oxo		Styrene	

1.9.5 (iii) Classification of fixed bed reactor models

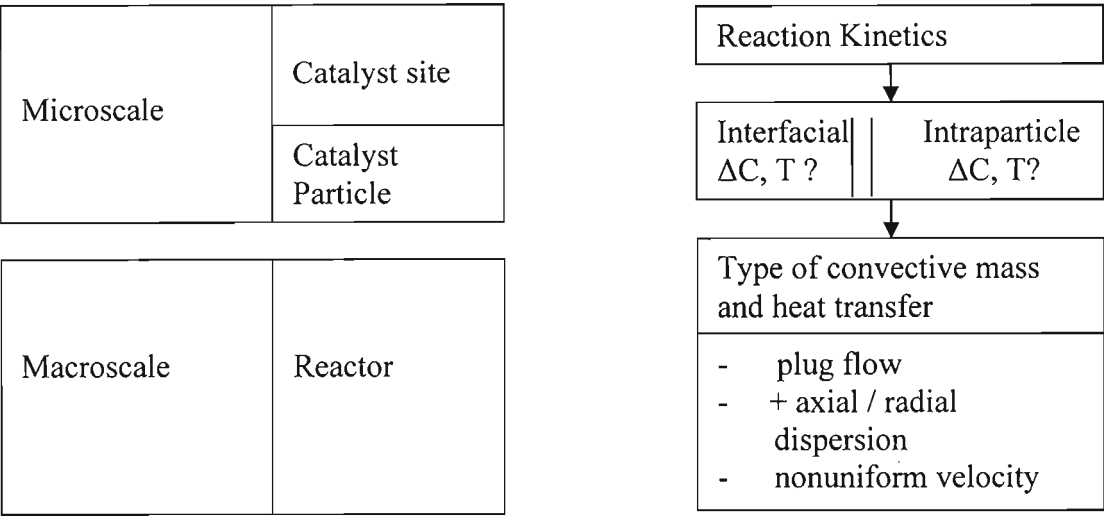
The models have been grouped in two main categories viz.: Pseudohomogeneous and heterogeneous as Table 1.2a shows. Pseudohomogeneous models do not account for the presence of catalyst, in contrast with heterogeneous models, which lead to separate conservation equations for fluid and catalyst.

Table 1.2a: Aspects to be dealt with in the modelling of fixed bed reactors

	A-Pseudohomogeneous Models Models $T=T_s$ , $C=C_s$		B-Heterogeneous $T \neq T_s$ , $C \neq C_s$
One-dimensional	(i)	basic, ideal gradients	+ interfacial
Two-dimensional	(ii)	+ axial mixing	+ intraparticle gradients
	(iii)	+ radial mixing	radial mixing

Table 1.2b below shows the problems that have to be faced in fixed bed reactor modelling and design. It relates the aspects on microscale and macroscale. The modelling of the macroscale (reactor) is mainly determined by the hydrodynamics.

Table 1.2b: Problems faced with fixed bed reactors modelling and design.



The models are then classified in order of growing complexity. The basic model is the pseudohomogeneous one-dimensional model, which considers transport by plug flow in the axial direction. Some mixing in the axial direction may be superimposed on the plug flow so as to account for nonideal flow conditions.

The model becomes two-dimensional if radial mixing occurs. The basic model considers transport by plug flow but distinguishes between conditions in the fluid and on the solid (29).

1.10 Catalytic Reactors

Large and small catalyst particles determine the type of heterogeneous catalytic reactor to be used.

1.10.1 Small Particle size

The small catalyst particles are separated at the reactor exit or are carried along with the fluid. Particle sizes are from 10µm to 1mm. Figure 1.18 below shows common reactor types. Figure 1.18(a) shows the fluid bed reactor, where the gaseous feed keeps the small catalyst particle in suspension. The catalyst carried over in the exit stream is separated. Fluid bed reactors are also used for feed mixtures of a liquid and gas.

If the feed stream is a liquid, which requires long residence times, the suspension bubble column or an agitated tank reactor is used, [Figure 1.18(b) and (c)]. Elaborate filtering systems at the reactor exit are required to remove the catalyst from the liquid stream. Gases are generally used in this type of system because the suspension reactors are mostly used for hydrogenation and oxidation.

### 1.10.2 Large Particle Size

In a packed bed reactor, large particle catalysts can be kept stationary so that the reaction mixture passes through the bed of particles. The aim is to keep the catalyst charge for as long as possible to avoid the trouble of eliminating the catalyst from the product stream coming out of the reactor. Particle size is usually  $> 2\text{mm}$ .

Figure 1.19 (a), shows the adiabatic packed bed reactor which is used for single-phase

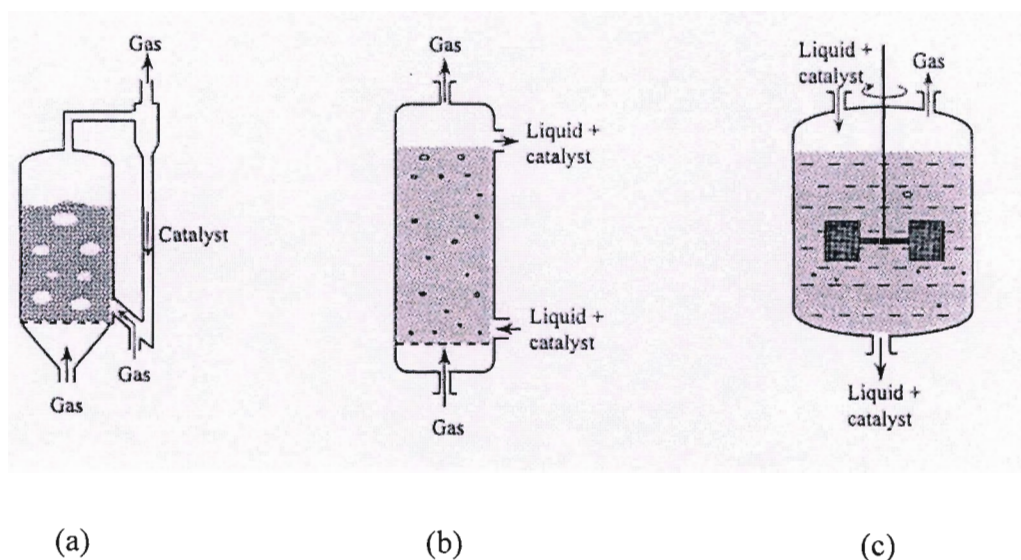


Figure 1.18: Common reactor types with moving catalyst beds: (a) fluid bed reactor, (b) bubble column with suspended catalyst, (c) sparged stirred tank with suspended catalyst (30).

reaction mixtures, either liquids or gases with moderate heat effects. This reactor consists of a large number of parallel tubes, which are cooled with liquid flowing around the outside of the tubes. Adiabatic packed bed and cooled tubular reactors can be used both for gaseous and liquid reactor feeds.

When a mixture of gas and liquid is to be fed to a packed bed reactor, then for shorter residence times, the trickle flow reactor (shown in Fig. 1.19(c)) is used. The liquid and gas are fed concurrently at the top and the liquid wets the catalyst particles and slowly trickles to the bottom through the bed. The gas dissolves in the liquid and is transported to the catalyst surface, where reactions take place with reactants coming from the liquid phase.

For larger residence times, the packed bed bubble column reactor (d) is used. The reactor is filled with liquid through which the gas bubbles slowly upwards. Residence times of the order of hours can be achieved and the catalyst is fully exposed to the liquid phase.

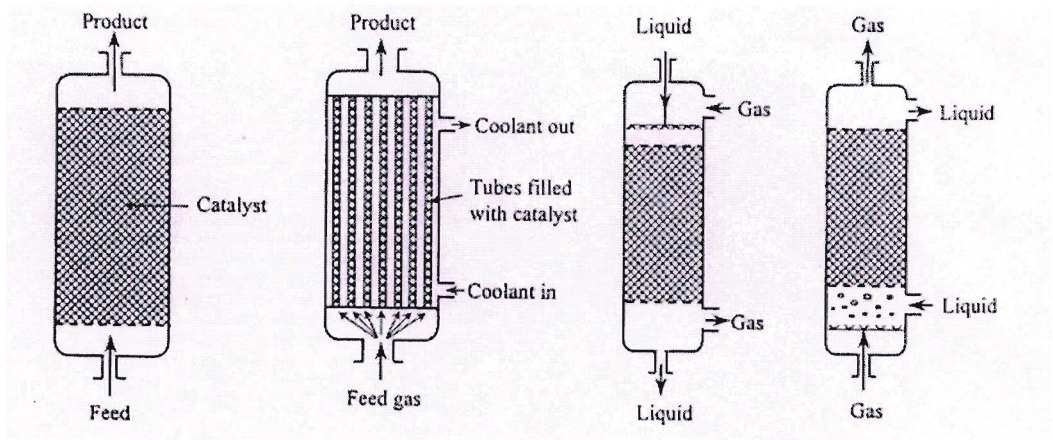


Figure 1.19: Examples of reactors with fixed catalysts beds: (a) adiabatic packed bed, (b) cooled tubular reactor, (c) co current trickle bed reactor, (d) packed bubble column (30).

### 1.11 Industrial Catalysts

Catalysis is the acceleration of a chemical reaction by a substance, which may take part in the reaction, but is not changed by the reaction. This substance may be mixed with the reaction mixture to form one single phase with it. This implies a



HOMOGENEOUS catalyst. The substance can also be a HETEROGENEOUS catalyst if it forms its own separate phase.

This thesis focuses on HETEROGENEOUS catalysis where the catalyst is a solid particle / powder itself known as the VPO catalyst.

The reactants (butane in air) have to pass over the VPO catalyst that enhances the reaction rate. Resistance plays a role when the reactants are transported to the catalyst and the products moved away from it. Heat is applied to the product lines at 160°C to prevent any condensation occurring in the product lines. These solid catalysts display specificity for particular reactions and selectivity for desired products. The uses of solid catalysts are therefore essential (30).

#### 1.11.1 Catalysts in an Industrial Reactor

A fixed bed continuous flow micro-reactor was used as a model for the industrial reactor for this project. The butane air mixture flows into the reactor from one end. The rate of flow of the butane gas is a prime factor, as are temperature and catalyst properties, in determining the amount of conversion. Velocity and turbulence determine how rapidly molecules are carried from the fluid to the exterior surface of the catalyst powder. Rapid transfer from fluid to solid outer surface is obtained with highly turbulent flow, which means a highly irregular flow pattern with velocities deviating from the desired main flow. Great turbulence is obtained with high flow velocities, large particles than low velocities. Turbulence also has a strong influence on the rate of heat transfer between the catalyst powder and the butane gas and also to the wall of the cylinder.

Variable residence times do occur and have to be taken into account in the design and operation of large industrial reactors.

The molecule in the reactor reacts once it has arrived at the exterior boundary of the solid catalyst. For porous catalysts, the interior surface greatly exceeds the exterior surface. For example, a 3mm-diameter pellet has an interior surface area 100000 times larger than the exterior surface of the pellets. Some catalysts of a non-porous nature, that are active and are of a convenient size, can also achieve useful reaction rates. These catalysts are useful in that they prevent any diffusion effects. If diffusion

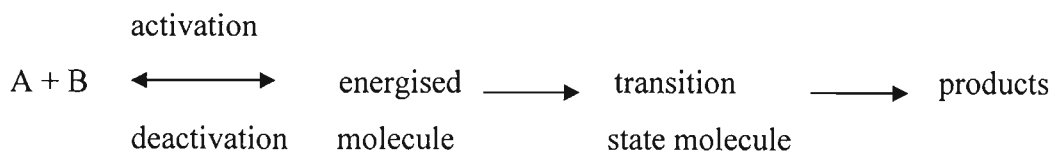
is fast relative to the rate of reaction, then the catalyst interior is bathed in the fluid of the same composition. The composition will depend on the position of the pellet in the reactor (distance from inlet). If the diffusion rate is of the same order of magnitude as the reaction rate, the concentration of reactants and products vary within the pores.

The effects of diffusion limitations are:

1. The activity of the catalyst is lower
2. The order of reaction may be changed
3. A drastic change in selectivity
4. The temperature gradient may become large.

## 1.12 Kinetics

Elementary reactions consist of an activation of the reactants, followed by a transition state and decomposition of the transition state into reaction products.



The reaction rate constant  $k$ , represents the influence of temperature. The reaction rate constant does not depend on the composition of the reaction mixture.

$$k = k\alpha \exp\left\{-\frac{Ea}{RT}\right\} \quad (27)$$

Where  $\frac{Ea}{R}$  = activation energy of the reaction

$Ea/R$  = activation temperature

The chemical activity or fugacity (gases) influences the rate. This is expressed as:

$$a_J = \gamma_J \rho_J / RT$$

where  $a_J$  = chemical activity

$\gamma_J$  = activity coefficient

$\rho_J$  = partial pressure of component J

$\gamma_J \rho_J$  = fugacity

For ideal reaction mixtures  $\gamma_J = 1$ .



For elementary reactions and ideal reaction mixtures, the reaction rate is proportional to the concentration of each of the reactants, since the number of molecular collisions per unit time is proportional to it. For a bimolecular elementary reaction:



$$|R| = -dC_A/dt = -dC_B/dt = kC_AC_B$$

A conventional notation is shown above for the reactions carried out in liquids. For gases:

$$|R| = k'P_AP_B$$

$$\text{with } k' = k/(RT)^2$$

$$\begin{aligned} \text{and } |R| &= -1/RT \cdot dP_A/dt \\ &= -1/V_B RT \cdot dP_A/dt \\ &= k'P_AP_B \end{aligned}$$

For nonideal elementary reaction mixtures, the chemical reaction rate can be approximated in some range of concentration by a power law equation.

$$|R| = kC_A^n \quad (28)$$

With the equation above the reaction is said to be of the order  $n$  with respect to A.

For a bimolecular overall reaction, power laws can also be used:



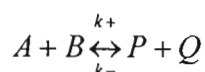
the following equation can also be applied:

$$|R| = kC_A^n C_B^m \quad (29)$$

The reaction is of order  $n$  with respect to A and of order  $m$  with respect to B. The total order of reaction is  $(n + m)$ .

These overall reactions discussed below will apply to kinetic schemes of catalysis.

Reactions in practise are often reversible.



The chemical reaction for an elementary and ideal reaction is:

$$|R| = k + C_A C_B - k - C_P C_Q \quad (30)$$

The activation energies are shown by

$$E_+ = E_- - \Delta H_r$$

where  $E_+$  = forward reaction

$E_-$  = reverse reaction

$\Delta H_r$  = reaction enthalpy

For exothermic reactions,  $|R|$  in Equation 30, decreases with increasing temperature.

At a constant reaction mixture composition,  $|R|$  can pass through a maximum as a function of temperature. It will become zero for the temperature at  $|R|$  equilibrium (i.e.  $k + C_A C_B - k - C_P C_Q$ ).

For endothermic reactions as can be seen in Figure 1.20,  $k_+$  increases with an increase in temperature. Therefore

$|R|$  increases with increasing temperature.

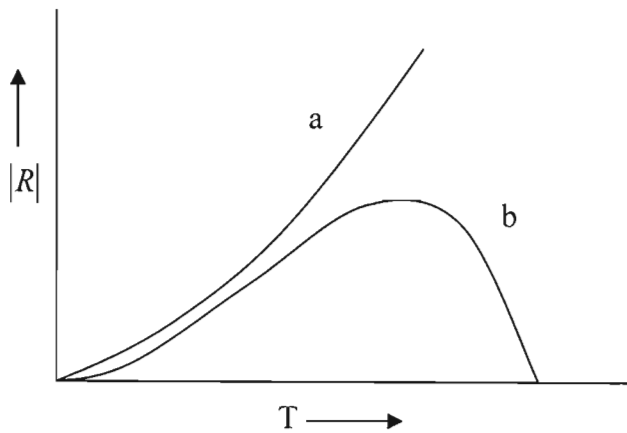


Figure 1.20: Reaction (R) rate vs. temperature(T) for a reversible reaction.

(a) endothermic reaction

(b) exothermic reaction.

The maximum rate for exothermic reactions for a specific temperature can be found from:

$$T_{\max} = \Delta H_r / R \cdot \left\{ \ln \frac{C_P C_Q k - E_-}{C_A C_B k + E_+} \right\}^{-1}$$

Temperature therefore depends on the reaction mixture. If a chemical equilibrium is reached, the reaction rate becomes zero and reaction mixture composition must fulfil the equilibrium condition (31).

$$\frac{C_P C_Q}{C_A C_B} = K$$

Where  $K$  = equilibrium constant

Since  $|R| = 0$  at equilibrium

$$\text{Therefore } K = \frac{k_+}{k_-}$$

### 1.12.1 Heterogeneous Catalytic Reactions

These reactions take place on the surface of solid catalysts. The following three phenomena are essential in determining the micro kinetics of these reactions:

1. Adsorption of the reactants
2. Reaction of the adsorbed reactants
3. Desorption of the products.

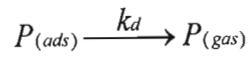
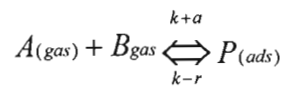
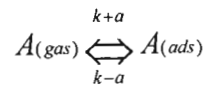
There are two types of reactions, monomolecular or bimolecular. For uni-molecular reactions, where  $A$  is the reactant and  $P$  is the product.



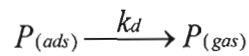
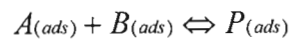
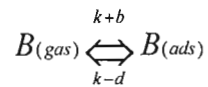
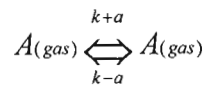
For a kinetic expression, a pseudo steady state for the adsorbed species  $A_{(ads)}$  and  $P_{(ads)}$  can be assumed. The measure of concentrations of these species is the degree of occupation of the surface,  $\theta_A$  and  $\theta_P$ . A pseudo steady state can be assumed for the degrees of occupation of the catalytically active surface area, so that  $\theta_A$  and  $\theta_P$  do not change in time (i.e.  $\frac{d\theta_A}{dt} = \frac{d\theta_P}{dt} = 0$ ).

For a bimolecular reaction, there are two mechanisms:

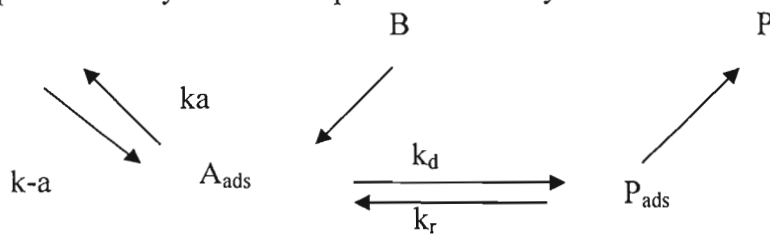
- A. The Eley-Rideal mechanism. One of the reactants is adsorbed on the catalyst surface, the other reacts from the gas phase.



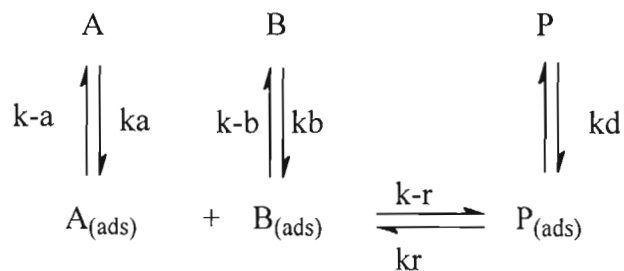
B. Langmuir Hinshelwood mechanism. Both reactants are adsorbed on the catalyst surface.



The pseudo steady state assumption for the Eley Rideal Mechanism:



The pseudo steady state for the Langmuir-Hinshelwood mechanism:



## 1.13 Characterisation Techniques

### 1.13.1 Brunauer Emmett Teller Isotherm

The BET equation is a widely used isotherm for the description of multilayer (physical) adsorption.

Note the assumptions:

1. the first layer of adsorbate is taken up with a fixed heat of adsorption ( $H_i$ ).
2. The second and subsequent layers are all characterised by heats of adsorption equal to latent heats of evaporation ( $H_L$ ).
3. We derive the BET equation by considering a dynamic equilibrium between each layer and the gas phase as:

$$\rho / V (\rho_o - \rho) = 1/Vm^o + c-1/Vm^c \cdot \rho / \rho_o$$

Where  $V$  = volume of gas adsorbed

$\rho$  = pressure of gas

$\rho_o$  = saturated vapour pressure of the liquid at the operating temperature

$Vm$  = volume equivalent to an adsorbed monolayer

BET constant  $c = \exp( H_i - H_L / RT)$

A plot of  $\rho / V (\rho_o - \rho)$  vs  $\rho / \rho_o$  is linear in the range of  $\rho / \rho_o$  from 0.05 to 0.35. The slope yields  $c$  and the intercept yield the monolayer capacity  $Vm$  (31).

#### 1.13.1 (i) Significance of Pore Structure and Surface Area in Heterogeneous Catalysis

Importance of pore structure and surface area:

Gaseous reactions over solid materials occur at the exterior and interior surfaces of the catalyst. Therefore the product formation is proportional to the surface area available. The greater the amount of surface area accessible, the larger the conversions of reactants to products. To increase surface area, metal oxide catalysts are used due to their open pore structure. Narrow pore structures limit the rate of reactions.

An application of surface area measurement was the prediction of catalyst poisoning. If the activity of catalyst declines more rapidly than any decrease in surface area, then poisoning is suspected.

Promoters may increase the surface area available for adsorption or may increase the catalyst activity per unit surface area. Therefore, surface area is important in determining the role of the catalyst. Only a small fraction of the surface area determined by physical techniques is chemically active.

The pore structure is equally important to the surface area although it contributes to the total surface area, but that is a separate factor.

The distribution of pore sizes in a given catalyst preparation maybe such that the internal surface area maybe inaccessible to large reactant molecules. Commercial catalysts usually have high internal surface areas so that the external surface area would not be poisoned and lose activity (31).

Experimental methods used to determine the surface areas are:

1. The volumetric adsorption of an inert gas.
2. The monitoring of adsorption by gravimetric means.
3. A dynamic method employing the continuous flow of an inert gas and adsorbate through an absorbent bed.

The volumetric method will be discussed in detail as this has been used to determine the surface area. There are five types of adsorption isotherms called the Brunauer classification.

An adsorption isotherm shows how the amount adsorbed depends on the equilibrium pressure of the gas at constant temperature: an adsorption isobar, how the amount varies with temperature at constant pressure.

If the gas solid system applies to isotherm types I, II or IV, the volumetric method for the evaluation of surface area of a porous solid can be determined.

If the isotherm is of type I (Fig.1.21), the Langmuir equation can be used to describe the adsorption adequately.

The Langmuir equation:  $V/V_m = bp/(1 + bp)$  (38)

or  $P/V = P/V_m + 1/bV_m$  (39)

$P/V$  vs  $P$  will yield a straight line.

Slope = monolayer volume  $V_m$ .

When the isotherm is of type II or IV, the monolayer capacity may be determined by the BET theory. The BET equation:

$$\frac{P}{V(P_o - P)} = \frac{1}{V_m c} + \frac{(c-1)}{V_m c} \cdot \frac{P}{P_o} \quad (40)$$

may be applied when a plot of  $\left[ \frac{P}{V(P_o - P)} \right]$  vs  $P/P_o$  is a straight line.

Where  $P_o$  = vapour pressure of the adsorbate at the adsorption temperature.

The slope and intercept of which will provide  $V_m$ .

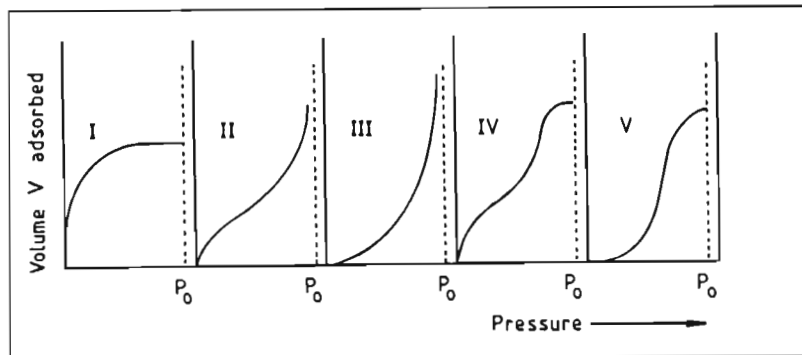


Figure 1.21: The five types of adsorption isotherms in the Brunauer classification

It is therefore simple to calculate the surface area of the adsorbent. If the monolayer volume is recorded in  $\text{m}^3/\text{g}$ , the number of moles adsorbed in the monolayer is  $V_m/0.0224$ .

Multiplying by Avagadro's number ( $6.023 \times 10^{23}$  molecules/mole) gives the number of molecules in the monolayer. If the area occupied by each adsorbate molecule is  $\text{\AA}^2$ , the specific area in  $\text{m}^2/\text{g}$  is clearly:

$$S_g = V_m / 0.0224 \times 6.023 \times 10^{23} \times \text{\AA}^2$$

$$= 2.69 \times 10^{25} \text{ Vm } \text{\AA} \text{ m}^2 \text{ g}^{-1}$$

where  $\text{\AA}$  = Angstroms

If the total specific area of the sample is not less than  $0.2\text{m}^2$ , nitrogen is used for the determination of the monolayer.

The apparatus in Fig. 1.22 shows the determination of samples of more than  $20\text{m}^2$ . Nitrogen from a storage vessel is admitted to the previously evacuated and calibrated. gas burette. The manometer records the pressure when the Hg in the burette is at a particular graduation mark between 2 successive bulbs. The nitrogen is then shared with the evacuated bulb containing the adsorbent sample at 77K and the equilibrated pressure is measured. The apparent volume of the empty adsorbent bulb at 77K will have been determined by volume sharing experiments using nitrogen and by application of the gas laws. After successive doses of nitrogen a BET plot can be drawn and  $V_m$  can be determined. Thereafter the specific surface area ( $S_g$ ) can be calculated.

### 1.13.2 X-Ray Diffraction

Bulk catalysts are analysed by x-ray diffraction. Constituents of catalysts can be determined by available characteristic d spacing and intensities previously studied. X-ray diffractograms can be accumulated from a few milligrams of catalyst, using computer linked digital systems, so as to maximise the detection of minority phases. X-ray diffractograms reveal many important properties, viz:

1. They signify whether the catalyst is crystalline or amorphous.
2. They yield an estimate of the size of micro crystallites that may be present.
3. XRD patterns yield d spacing and unit cell dimensions therefore giving us insight into the atomic constituents of the unit cell.
4. They also indicate the influence reactant gas mixtures exert upon the internal structure as well as the crystalline order of the exterior surface of the catalyst.

Non-crystalline or amorphous catalysts yield no sharp diffraction peaks, but broad features. Micro crystallites yield broadened peaks because the fewer the planes, giving rise to Bragg diffraction, the less sharp the peak. If  $\beta$  is the full width at half the maximum of the broadened peak,  $\lambda$  the x-ray wavelength, and  $t$  is the thickness, then  $t = K\lambda / \beta \cos \theta$



where  $\theta$  is the Bragg angle  
and  $K$  is a constant (25).

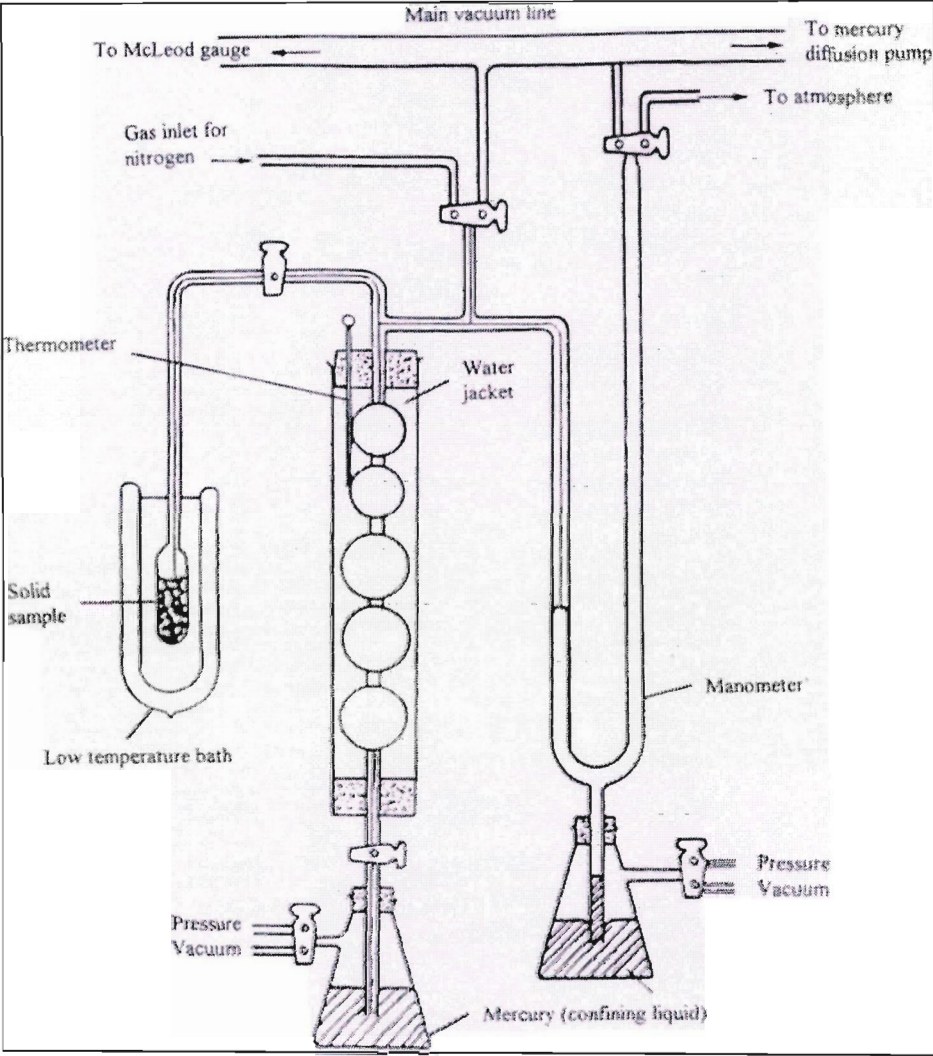


Figure 1.22: Apparatus for the volumetric determination of surface area.

## References:

1. G. J. Hutchings, *Applied Catal.*, **72**, 1991, 119, 1-32
2. G. C. Bond, S. F. Tahir, *Applied Catal.*, **71**, 1991, 1-31
3. Charles N. Satterfield, *Heterogeneous Catalysis In Industrial Practice*, 2<sup>nd</sup> edition, Mcgraw-Hill, New York, 1991
4. G. Centi & F. Trifiro, *Chem. Rev.*, **88**, 1988, 55-80
5. L. M. Cornaglia, C. R. Carrara, J. O. Petunchi, E. A. Lormardo, *Applied Catal. A: General*, **183**, 1999, 177-187
6. S. H. Sookraj and D. Engelbrecht, *Catal. Today*, **49**, 1999, 161
7. G. Ertl, H. Knoginger, J. Weikamp, *Preparation of Solid Catalysts*, Wiley-VCH, Weinheim, Germany, 1999
8. F. Roozeboom and T. Fransen, *Z. Anorg Allg. Chem.*, **449**, 1979, 25
9. A. S. Russell and J. J. Stokes, *Indus. Eng. Chem.*, **38**, 1946, 1074
10. V. Cortes Corberan, S.V. Bellon, *New Developments in Selective Oxidation*, 1994, Elsevier Science, 167
11. M. Abon, J. C. Volta, *Applied Catal.*, **157**, 1997, 173
12. J. Ziolkowski, E. Bordes, P. Courtine, *J. Catal.*, **122**, 1990, 126-150
13. M. T. Sananes, *J. Catal.*, **154**, 1995, 253
14. D.B. Dadyburjor, *Catal.Rev.-Sci. Eng.*, **19**(2), 1979, 293-350
15. B. Chen and E. J. Munson, *J. Am. Chem. Soc.*, **121**, 1999, 11024-11025
16. Y. Zhang-Lin, M. Forissier, J.C. Vedrine, J.C. Volta, *J. Catal.*, **145**, 1994, 267-275
17. G. J. Hutchings, *Applied Catal.*, **72**, 1991, 5
18. C. J. Kiely, A. B. Burrows, S. Sajip, G. J. Hutchings, M. T. Sananea, A. Tuel and J. C. Volta, *J. Catal.*, **162**, 1996, 34
19. G. Busca, F. Cavani, G. Centi and F. Trifiro, *J. Catal*, **99**, 1986, 400
20. B. K. Hodnett & B. Delmon, *Applied Catal.*, **6**, 1983, 254
21. W. H. Cheng, *Applied Catal. A:*, **147**, 1996, 55
22. G. J. Hutchings and R. Higgins, *J. Catal.*, **162**, 1996, 153
23. A. W. Naumann and A. S. Behan Jr, *J. Catal.*, **39**, 1975, 432
24. V.A. Zazhigalov, V. M. Belousov, G. A. Komashko, I Pyatniskaya, T. A. Kriger, O. Y. Polotnyuk and Y. I. Sorokin, *Journal of Applied Chem. Of USSR / Consultants Bureau*, **60**(4), 1987, 820-824
25. M. L. Granados, J. C. Conesa and M. F. Garcia, *J. Catal.*, **141**, 1993, 671

26. M.T. Sananes-Schultz, A. Tuel, G. J. Hutchings and J. C. Volta, *J. Catal.*, **166**, 1997, 391
27. M. Nakamura, K. Kawai and Y. Fujiwara, *J. Catal.*, **34**, 1974, 345
28. H. Scott Fogler, *Elements of Chemical Reaction Engineering*, 1999, Prentice Hall, New Jersey, 6-16
29. G. F. Froment, K.B. Bischoff, *Chemical Reactor Analysis and Design*, 2<sup>nd</sup> edition, John Wiley and Sons, Inc. Canada, 1990
30. R. J. Wijngaarden, A. Kronberg, K. R. Westerterp, *Industrial Catalysis, Optimising Catalysts and Processes*, Wiley-VCH, Weinheim, New York, 1998
31. J. M. Thomas, W. J. Thomas, *Principals and Practice of Heterogeneous Catalysis*, VCH-Publishers, (Federal Republic of Germany), 1997

## 2. Experimental

The following materials were used in the preparation of the catalysts in the table below.

Table 2.1: Table showing supplier and percentage purity of materials used:

Reagents	Molar Mass (g/mol)	Supplier	% Purity
V <sub>2</sub> O <sub>5</sub>	181.88	Aldrich	98+%
Ortho-phosphate	98.00	Fluka	98+%
Benzyl Alcohol	104.14	Aldrich	99%
Iso-Butanol	74.12	Rochelle Chem.	98.5%
RuCl <sub>3</sub> . 3H <sub>2</sub> O	261.47	Acros	99%

### 2.1 Experimental methods of catalyst synthesis

2.1.1 Synthesis 1 (a): Vanadium phosphorus oxide catalyst (VO<sub>2</sub>P<sub>2</sub>O<sub>7</sub>) prepared by the reduction of VOPO<sub>4</sub>.2H<sub>2</sub>O.

Catalyst precursor VOPO<sub>4</sub>.2H<sub>2</sub>O was prepared by adding V<sub>2</sub>O<sub>5</sub> (11.8g, 0.065 mol) to isobutanol (250ml). H<sub>3</sub>PO<sub>4</sub> (16.49g, 0.0168 mol, 85%) was then introduced into the mixture which was then refluxed for 16 hours (1). The lime green suspension was then separated from the organic solution by filtration and washed with isobutanol (200ml), and ethanol (100%, 150ml). The resulting solid was refluxed in water (24ml H<sub>2</sub>O / g solid) and filtered hot.

It was observed that the light green suspension dissolved in the H<sub>2</sub>O as it was being filtered. No product was isolated. It was concluded that 85% H<sub>3</sub>PO<sub>4</sub> was too aqueous for the synthesis of VPO catalyst and therefore 99% H<sub>3</sub>PO<sub>4</sub> should be used.

Synthesis 1 (b): Vanadium Phosphate Catalysts Prepared by the Reduction of VOPO<sub>4</sub>.2H<sub>2</sub>O.

This method is the same as the one before (2.1.1), however, a double filter paper was used.

Mass of V<sub>2</sub>O<sub>5</sub> (98%) = 11.802g, 0.064 moles

Precipitate was dark green in colour.

Mass of precursor = 49.325g

Volume of H<sub>2</sub>O used = 441.305g

After filtrating with water, a dark green precipitate was formed. The yield of product was 24%.

#### 2.1.2 Synthesis 2: Vanadium Phosphate Catalyst (VO<sub>2</sub>P<sub>2</sub>O<sub>7</sub>) prepared by the Reduction of VOPO<sub>4</sub>.2H<sub>2</sub>O

Method is the same as synthesis one, however, 99% H<sub>3</sub>PO<sub>4</sub> was used.

V<sub>2</sub>O<sub>5</sub> = 5.9g, 0.032 moles

Isobutanol = 125ml

H<sub>3</sub>PO<sub>4</sub> (99%) = 8.25g, 0.083moles.

Washed with isobutanol = 100ml, then Ethanol = 75ml

After refluxing for 16hrs, solution turned pale blue.

Mass of precipitate = 15.268g

Volume of H<sub>2</sub>O = 137.412g

Yield of product was 82%

Sample calcined and turned dark brown to greyish in colour.

#### 2.1.3 Synthesis 3: Preparation of undoped VPO Precursors

The synthesis of undoped and doped precursors were followed by Sanane's – Schultz M.T. (1). Undoped precursors were prepared via VOPO<sub>4</sub>.2H<sub>2</sub>O. VOPO<sub>4</sub>.2H<sub>2</sub>O was prepared from V<sub>2</sub>O<sub>5</sub> (12.0g, 0.065mol) and H<sub>3</sub>PO<sub>4</sub> (115.15g, 0.99 moles, 85%) which was refluxed in water (24ml H<sub>2</sub>O / g solid) for 8 hours. The resulting VOPO<sub>4</sub>.2H<sub>2</sub>O was recovered by filtration and washed with water. Then 4g of this solid was refluxed with isobutanol (80ml) for 21 h and the resulting solid was recovered by filtration and dried in air (110°C, 16 hours). Yield recovered was 5%. Colour obtained was pale green.

#### 2.1.4 Synthesis 4: Preparation of doped Fe VPO precursors

Doped precursors were prepared by the method of Hutchings, *et al*, (2). VOPO<sub>4</sub>.2H<sub>2</sub>O was prepared from V<sub>2</sub>O<sub>5</sub> (12.0g, 0.065mol) and H<sub>3</sub>PO<sub>4</sub> (115.5g, 0.99 moles, 85%) which were refluxed in water (24ml H<sub>2</sub>O / g solid) for 8hours.

The resulting  $\text{VOPO}_4 \cdot 2\text{H}_2\text{O}$  was recovered by filtration and washed with water. As per calculation  $\text{V}:\text{M}(\text{Fe}) = 1:0.05$  atomic ratio, 1.5329g, 0.003 moles  $\text{Fe}(\text{acac})_3$  should be dissolved in 80ml isobutanol prior to refluxing  $\text{VOPO}_4 \cdot 2\text{H}_2\text{O}$  with isobutanol. Consequently, 4.000g  $\text{VOPO}_4 \cdot 2\text{H}_2\text{O}$  (solid) was refluxed with the required amount of  $\text{Fe}(\text{acac})_3$  in the isobutanol solution for 21h, and the resulting solid was recovered by filtration and dried in air ( $120^\circ\text{C}$ , 12 h). Yield obtained was 5%.

#### 2.1.5 Synthesis 5: VPO Catalysts for oxidation of Butane to Maleic Anhydride, Influence of $(\text{VO})_2\text{H}_4\text{P}_2\text{O}_9$ Precursor morphology

A typical synthesis was carried out by the method of Horowitz, H.S., (3).  $\text{V}_2\text{O}_5$  (11.81g, 0.064 moles) and  $\text{H}_3\text{PO}_4$  (17.88g, 0.180 moles, 99%) in 236ml isobutanol and 23.6ml benzyl alcohol. After completion of the reaction,  $(\text{VO})_2\text{H}_4\text{P}_2\text{O}_9$  precipitates were recovered by vacuum filtration, washed in excess solvent, air dried for 1h, and then dried at  $110^\circ\text{C}$  in a vacuum oven for 12h. In some instances  $\text{VOPO}_4 \cdot 2\text{H}_2\text{O}$  was reacted in the manner described above to yield 53%  $(\text{VO})_2\text{H}_4\text{P}_2\text{O}_9$ .

#### 2.1.6 Synthesis 6: VPO Catalysts for Oxidation of Butane to Maleic Anhydride

The same as Synthesis 5, however, 85%  $\text{H}_3\text{PO}_4$  was used. The yield obtained was 57%. The colour of the precursor was greenish-blue.

#### 2.1.7 Synthesis 7: Iron Doped VPO Catalysts for Oxidation of Butane to Maleic Anhydride

This is the method to dope the catalyst with  $\text{Fe}(\text{acac})_3$  reported by Horowitz, H.S.*et al*, (3). A typical synthesis involved the reaction of  $\text{V}_2\text{O}_5$  (11.81g, 0.065 moles) and 99%  $\text{H}_3\text{PO}_4$  (17.88g, 0.180 moles) in 236ml isobutanol and benzyl alcohol (23.6ml). Prior to the addition of solvents,  $\text{Fe}(\text{acac})_3$  (1.532g) was dissolved in the isobutanol and then benzyl alcohol was added to the solution. The solution was refluxed for 6 hours.  $(\text{VO})_2\text{H}_4\text{P}_2\text{O}_9$  precipitates with  $\text{Fe}(\text{acac})_3$  were recovered by vacuum filtration, washed in excess solvent, air dried for one hour, then dried at  $110^\circ\text{C}$  in a vacuum oven for 12h. The yield obtained for this reaction was 58%.

#### 2.1.8 Synthesis 8: Ruthenium Doped VPO Catalysts for Oxidation of Butane to Maleic Anhydride (1% Ru promoted catalysts)

Method the same as synthesis 7, except  $\text{RuCl}_3 \cdot 3\text{H}_2\text{O}$  (0.3398g) was added. The mass of product formed was 13.927g. The colour of precipitate was bluish grey. After calcining under nitrogen at  $450^\circ\text{C}$  for 6 hours, the sample turned black in colour. The yield obtained was 61%.

#### 2.1.9 Synthesis 9: The Study of the oxidation of Butane over Vanadyl Pyrophosphate

This method was followed according to Pepera *et al*, (4). For the  $(\text{VO})_2\text{P}_2\text{O}_7$  preparation, vanadium pentoxide (4.556g, 0.025 moles) was stirred into isobutyl alcohol (65ml). Orthophosphoric acid (5.98g, 0.060moles, 99%) was dissolved in 10ml isobutyl alcohol. This was added to the  $\text{V}_2\text{O}_5$  solution. The combined solution was heated to  $110^\circ\text{C}$  and refluxed for 8h. The solution was filtered and washed with 5ml isobutanol and dried overnight in air. The bright blue product formed was  $(\text{VO})_2\text{P}_2\text{O}_7 \cdot 2\text{H}_2\text{O}$ . 8.637g was calcined under nitrogen for 6h at  $400^\circ\text{C}$ . A greyish-brown catalyst was recovered after calcining. The yield for this reaction was 99% successful.

#### 2.1.10 Synthesis 10: 3% Fe Promoted VPO Catalyst for oxidation of Butane to Maleic Anhydride

This method was followed according to Horowitz, H.S. (3).  $\text{Fe}(\text{acac})_3$  (0.917g) was dissolved in isobutanol (236ml) and heated for 30 minutes at  $40^\circ\text{C}$ . Benzyl alcohol (23.6ml) was added to the solution. Thereafter  $\text{V}_2\text{O}_5$  (11.814g, 0.065 moles) and  $\text{H}_3\text{PO}_4$  (18.049g, 0.181moles) were added to the solution. The solution was filtered and a bright powder blue product of mass 32.423g was obtained. This was washed with 50ml isobutanol and left overnight in air to dry. The product  $(\text{VO})_2\text{H}_4\text{P}_2\text{O}_9$  was then calcined at  $400^\circ\text{C}$  for 6h and the colour change was to a dark brown calcined catalyst. The yield obtained was 91%.

#### 2.1.11 Synthesis 11: 1% Fe Promoted Catalyst

This method was followed according to Horowitz, H.S. (3).  $\text{Fe}(\text{acac})_3$  (0.308g) was added to isobutanol (236ml) and was heated for 30 minutes at  $40^\circ\text{C}$ . Benzyl alcohol (23.6ml) was added. Thereafter  $\text{V}_2\text{O}_5$  (11.839g, 0.065 moles) and  $\text{H}_3\text{PO}_4$  (17.749g, 0.181 moles, 99%) were added to the solution and heated to  $110^\circ\text{C}$  and refluxed for 6



hours. The solution was filtered and a bright powder blue product, of mass 22.385g was obtained. The product was washed with isobutanol (50ml) and left to dry in air overnight. The sample was calcined under nitrogen for 6 hours at 450°C and became black in colour. This reaction was 91% successful.

#### 2.1.12 Synthesis 12: 0.6% Ru Promoted Catalyst

This method was followed according to Horowitz, H.S. (3).  $\text{RuCl}_3 \cdot 3\text{H}_2\text{O}$  (0.2039g) was added to isobutanol (236ml) and heated at 40°C for 30 minutes. Benzyl alcohol (23.6ml) was added to the solution. Thereafter  $\text{V}_2\text{O}_5$  (11.81g, 0.065 moles) and  $\text{H}_3\text{PO}_4$  (15.44g, 0.156 moles, 99%) was added to the combined solution and refluxed for 6 hours at 110°C. The precipitate was filtered and left overnight to dry in air. The catalyst appeared grey in colour. Thereafter, it was calcined under nitrogen for 6 hours at 400°C. The yield obtained was 97%.

#### 2.1.13 Synthesis 13: 0.2% Ru Promoted Catalyst

This method was followed according to Horowitz, H.S. (3).  $\text{RuCl}_3 \cdot 3\text{H}_2\text{O}$  (0.0677g) was dissolved in isobutanol (236ml) and heated for 30 minutes at 40°C. Benzyl alcohol was added (23.6ml).  $\text{V}_2\text{O}_5$  (11.81g) was added to the solution, followed by  $\text{H}_3\text{PO}_4$  (15.44g, 0.157 moles, 99%) and the solution was heated to 110°C and refluxed for 6 hours. The precipitate was filtered off after refluxing and the product appeared greenish-blue in colour. The mass obtained was 24.184g. The powder was left overnight in air to dry. The catalyst was calcined under nitrogen for 6 hours at 400°C. The yield obtained was 90% successful.

## 2.2 Characterization Techniques

### 2.2.1 Average Oxidation State

The average oxidation number of vanadium ( $n_v$ ) was determined by a redox titration procedure largely the same as that employed by M. Nakamura, *et al.* (5). About 0.1g catalyst was dissolved in 17ml of 12M  $\text{H}_3\text{PO}_4$  and boiled till a clear solution was obtained. This solution was added to a mixture of 10ml  $\text{H}_2\text{SO}_4$  in 250ml water. Graphite was removed by filtration. All vanadium ions were oxidized to  $\text{V}^{+5}$  by titration with 0.05N  $\text{KMnO}_4$  solution until the end point was reached which turned the



colour of the solution to blue. The pentavalent ions were then reduced by adding  $\text{Fe}(\text{NH}_4)_2(\text{SO}_4)_2$  to give a solution containing  $\text{V}^{+4}$  ions (6). The average oxidation state was calculated as:

$$n_v = 5 - [\text{volume of solution} / \text{volume of } \text{Fe}(\text{NH}_4)_2(\text{SO}_4)_2 \text{ solution}]$$

Indicator = 0.045g / 5ml  $\text{H}_2\text{SO}_4$  i.e. 1% indicator in  $\text{H}_2\text{SO}_4$

To make up 12M  $\text{H}_3\text{PO}_4$ , dissolve 23.549g in 20ml  $\text{H}_2\text{O}$ .

Standards: 0.01M  $\text{KMnO}_4$  i.e. 0.05N/5, therefore 0.05M  $\text{Fe}(\text{NH}_4)_2(\text{SO}_4)_2$  i.e. 0.05N  $\text{Fe}(\text{NH}_4)_2(\text{SO}_4)_2$

Required: 1.580g /  $\text{dm}^3$   $\text{KMnO}_4$  for a 0.01M solution

14.202g /  $\text{dm}^3$   $\text{Fe}(\text{NH}_4)_2(\text{SO}_4)_2$  for 0.05M solution

#### 2.2.2 X-Ray Diffraction (XRD)

The samples (approximately 0.2-0.5g) were packed tightly onto a metal sample plate. This was placed into an aluminium sample holder. The sample holder takes approximately 50 samples which it analyzes systematically. This was carried out on a Phillips PW 1730-10.

#### 2.2.3 Fourier Transform Infrared (FTIR)

A KBr disk was made up. This disk was placed into the Nicolet Impact 400 D instrument. Infrareds of samples were taken.

This was plotted on a XY Plotter DXY-1250 Roland digital.

#### 2.2.4 Scanning Electron Microscopy (SEM) and Electron Dispersive X-Ray Spectroscopy (EDX)

The samples are mounted on a graphite stub using double-sided graphite tape. For EDX analysis the samples are analyzed uncoated (as it is). For SEM images, the samples prepared for EDX analysis are sputter coated with approximately 10nm of gold to minimize charging of the samples under the electron beam.

The samples were analyzed using a Hitachi 5520 scanning electron microscope fitted with a link ISIS energy dispersive x-ray analyzer.

2.2.5 Microwave Digestion

The VPO catalyst samples were digested using a Perkin Elmer Anton Paar Physica Multiwave (Microwave sample preparation system). The microwave digestion method is as follows:

0.1g of the catalyst was weighed out into the reaction vessel. Aqua regia in the ratio 1.5 HNO<sub>3</sub> : 3.5 HCl (conc.) was then pipetted into the reaction vessel. The vessel caps were flared and then closed. The reaction vessels were then placed in the vessel jacket and the caps were tightened. The shell was placed into the microwave and followed the titanium dioxide method which can be seen in the Appendix Figure 5.34.

Table 2.2: Showing power and temperature ramping

Power	0-400W
	400-900W
	900-0W in 15min.
Temperatures	0-250 <sup>0</sup> C
	250-25 <sup>0</sup> C

The samples were then diluted to 100ml in a volumetric flask. It was then further diluted ten fold i.e. 5ml in 50ml volumetric flask. The sample appeared blue in colour. The samples were then ready for ICP-OES.

2.2.6 Inductively Coupled Plasma-Atomic Emission Spectroscopy (ICP-AES )

ICP-AES was carried out using a JOBIN YVON Emission JY 24 ICP Spectrometer. The instrument carried out a zero order search. The instrument was then autosearched to set the correct wavelength. An autosearch was carried out to set the correct voltage. The standards were analyzed to set the calibration graph. To make a 1000ppm standard stock Ru solution:

101.07g RuCl<sub>3</sub>.3H<sub>2</sub>O is 261.42g/mol

Therefore 1g is x

$$x = 2.587\text{g}$$

$$= 1000\text{ppm}$$

$$\text{Therefore, } 1000\text{mg} / 1 \times 250 \text{ ml} / 1000\text{ml} \times 261.429\text{gmol}^{-1} / 101.070 \text{ gmol}^{-1}$$

$$= 0.647\text{g RuCl}_3 \cdot 3\text{H}_2\text{O}$$

1000ppm Vanadium stock solution as supplied by Merck. V= 50.94 Batch number 1013089. 1000ppm Phosphorus stock solution as supplied by Merck. Mixed standard solutions contain 10ml i.e.100ppm V and 5ml i.e. 50ppm P

Table 2.3: Showing phosphorous standards made up

Vol.	Conc.	Conc. In 100ml Vol. Flask	50ppm P	Conc.
1ml	100ppm V	1	1	0.5
2.5	100	2.5	2.5	1.25
5	100	5	5	2.50
10	100	10	10	5.0

### 2.2.7 Brunauer Emmett and Teller (Surface Area Analysis)

This method describes measuring the specific surface area of powders and granulated material using the adsorption of gaseous nitrogen at the temperature of liquid nitrogen. The principle is based on the properties of gases to be adsorbed at the surface of solids, developed by Bruauer, Emmet and Teller. BET is a measure of the developed surface of the particles, expressed in  $\text{m}^2/\text{g}$ .

Mass  $m_1$  was determined by weighing the sample tube and the sample stopper (to the nearest 0.001g). 0.250g-0.300g of sample was placed into the sample tube by the use of an aluminium funnel. The test tube was placed into the Gemini Micromeretic

Flowprep 060 holder which was at 300°C and the sample was treated with nitrogen gas. The sample tube was closed by the use of a rubber stopper. The sample was left for one hour and thereafter was left to cool for 15 minutes. Mass  $m_2$  was obtained by weighing the sample tube, sample and stopper. The mass of sample was  $m_2 - m_1 = m$ . Saturation pressure ( $P_o$ ) was determined, to be 776.17mmHg, by placing two empty tubes into the Gemini with the use of liquid nitrogen. After  $P_o$  measurement, the sample was then ready to be analyzed.

2.2.8 Grain Size Distribution (GSD) using a Laser Beam

This technique was used to measure the size of particle diameter in microns. A spatula of sample was introduced until the obscuration was approximately 15%. At this obscuration, the ultrasonic was increased to 100%. The ultrasonic was kept to 100% for 20 seconds. After 20 seconds ultrasonic was decreased to 0%. The sample measurement was ready to start. The vessel was then cleaned.

2.3 On Line sample Analysis

A Perkin Elmer Gas Chromatograph was used with a CP-Sil 24 CB column. This particular column was used to separate unreacted n-butane, maleic anhydride, acetic acid and phthalic acid. The Flame Ionization Detector (FID) gave retention times as the table indicates:

Table 2.4: Showing retention times for each compound isolated

Retention times	Compound
2.80	n-butane
7.20	Maleic anhydride

The Thermal Conductivity Detector (TCD) Varian 3700 GC has a carboxen™ 1000 column installed. This is used to separate CO, CO<sub>2</sub> and air.

A chromosorb WHPSP pre-column was also installed in the varian 3700 GC and was used to separate the gaseous products from other products at room temperature. Flame Ionisation Detector Settings (FID) and Thermal Conductivity Settings (TCD) can be seen in the table below.

Table 2.5: Flame Ionisation Detector Settings and Thermal Conductivity Detector Settings

Detector Variables	Specifications	Detector Variables	Specifications
PSS1	220°C	Injector	150°C
Cap2	150°C	Column	26°C
Split Total Flow	53ml/min	Detector	130°C
Flow	50ml/min	Column Limit	200°C
FID 1	250°C	Range	0.5mV
Press 1	5.0	Attenuation	1
Press 2	4.9	Output	-ve
Temperature	250°C	Filament	150°C
Lim	5.0psi		
Set off	psi		

### 2.3.1 Reactor Design and Setup

The type of reactor used was a fixed bed micro reactor which was designed and constructed on a small scale. The reactors were set up according to the diagram in Figure 2.1. The fixed bed micro reactor was selected because of the phases present. In this n-butane oxidation to maleic anhydride reaction, a gas-solid phase exists. The tubular reactor is packed with solid catalyst particles. The advantages of a fixed bed reactor are high conversion per unit of mass catalyst, low operating costs and a continuous operation of the process (6).

n-Butane gas in air was fed through stream 1 as shown in Figure 2.1. The feed gas was at a flow rate of 120ml.min<sup>-1</sup>, measured by a flow meter F1. Copper tubing pipes (1/4" diameter) were used for the feed gas entering the reactors at room temperature. The n-butane gas was then subjected to the reactors that were heated at 200° C and thereafter at 50 °C intervals until the catalyst stabilized.

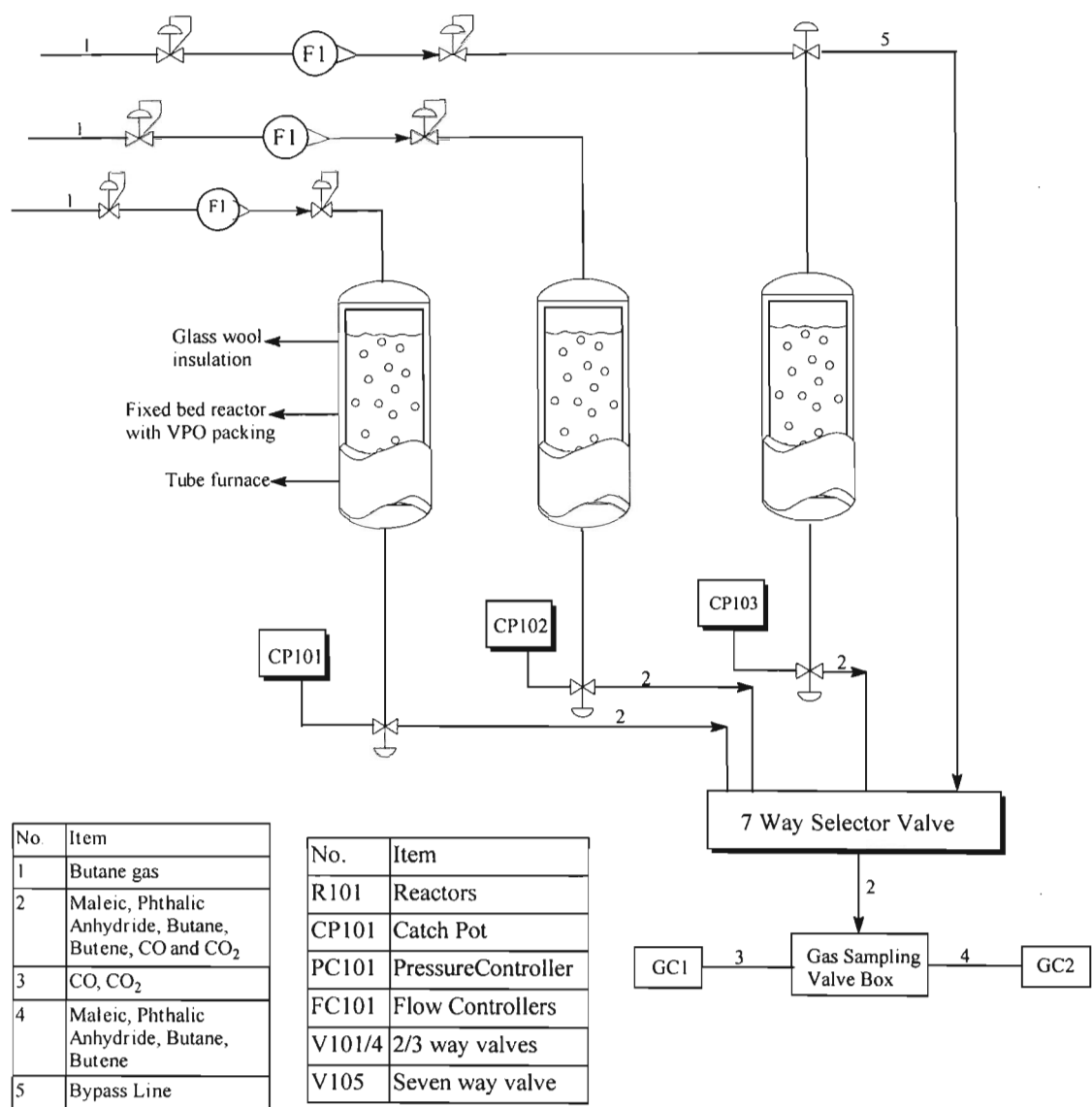


Figure 2.1: The design of the fixed bed reactor showing feed gas and product streams

The fixed bed reactor's dimensions were a 10mm inner diameter stainless steel rod, 40cm in length. This was placed in a furnace with thermocouples attached to a temperature control box. The reactor outlet was a 1/4" stainless steel pipe heated at 120°C to keep the maleic anhydride from condensing in the lines. A two way valve separated the flow to the catch pot or to the detector which is explained in detail below. Maleic anhydride is bubbled to the catch pot which contained a solution of water and acetone (1:1). Maleic anhydride, phthalic anhydride, butane, butene, CO and CO<sub>2</sub> flowed to a stainless steel seven way selector valve.

A gas sampling valve box (GSVB) as can be seen in Figure 2.2 was used with a 6-port Valco rotary valve, a 10-port Valco rotary valve and a heater plate. The GSVB sends the sample to the two GC's. The product stream was kept heated to prevent condensation of maleic anhydride. The product stream enters the GSVB from the reactor and sends the sample to the pre-column of the Varian GC. The Isothermal Varian GC with a TCD separates and detects CO and CO<sub>2</sub> gases. From the pre-column, it goes back to the GSVB and out again to the analytical column of the Varian GC where CO and CO<sub>2</sub> are detected. The sample also exits to the temperature

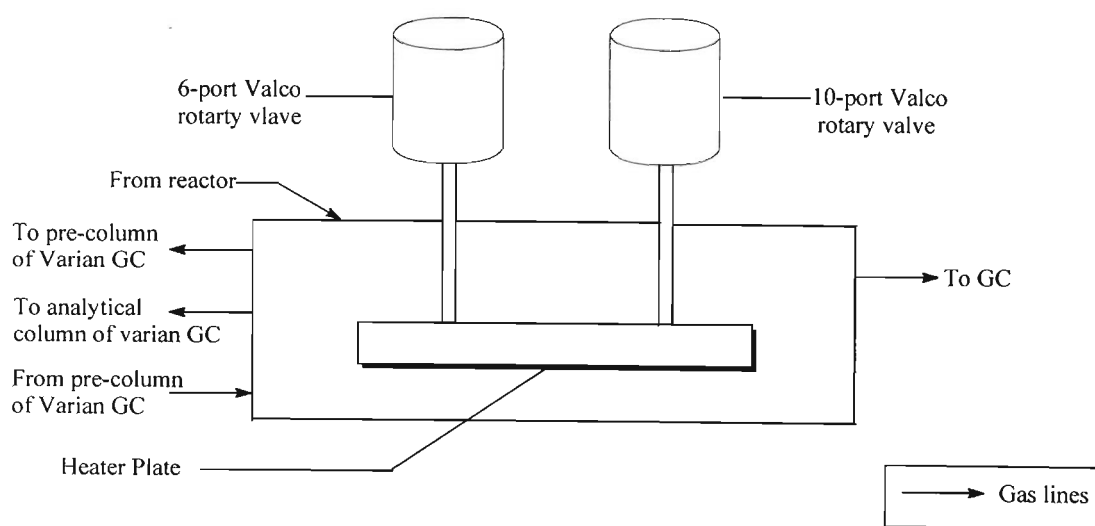
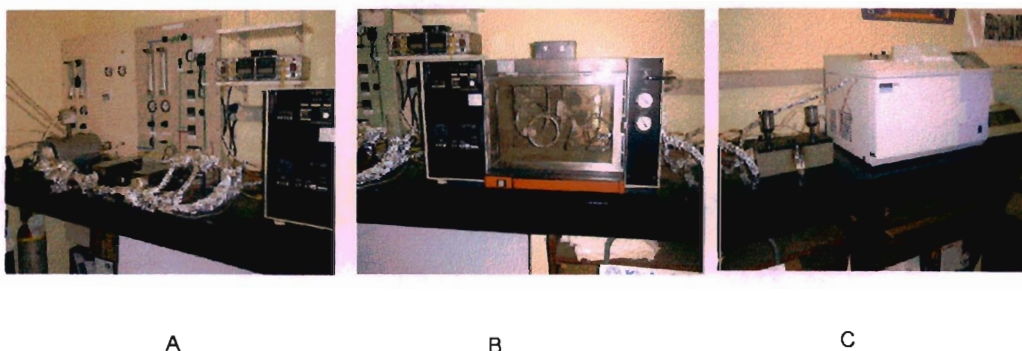


Figure: 2.2: Diagram of the Gas Sampling Valve Box



programmable Perkin Elmer GC with a FID detector which separates and detects maleic anhydride and butane amongst other hydrocarbons.

Figure 2.3 shows pictures of the reactors, control panels with rotameters, the temperature programmable Perkin Elmer GC with FID and an Isothermal Varian GC with TCD.



A: Three reactors and control panels. 1/4" Stainless steel tubing leading to a seven way selector valve. Rotameters for control and monitoring gas flow rates to the reactor.  
B: Isothermal Varian GC with TCD that separates and detects CO and CO<sub>2</sub>.  
C: Gas sampling valve box which separates samples to the two GC's. A Perkin Elmer GC with FID that separates and detects Maleic Anhydride and butane and other hydrocarbons.

Figure: 2.3 Diagram showing reactors and control panels



## References:

1. M. T. Sanane's – Schultz, F. B Abdelouahab, G. J. Hutchings and J. C. Volta, J. Catal., **163**, 1996, 346-347
2. G. J. Hutchings, R. Olier, M. T. Sananes and J.C. Volta, New Developments in Selective Oxidation II, Elsevier Science, 1994, 213
3. H. S. Horowitz, Applied Catal., **38**, 1988, 194
4. M. A. Pepera, J. L. Callahan, M. J. Desmond, E. C. Milberger, P. R. Blum and N. J. Bremer, J. Am. Chem. Soc., **107**, 1985, 4884
5. M. Nakamura, K. Kawai and Y. Fujiwara, J. Catal., **34**, 1974, 345
6. J. S. Buchanan, J. Apostolakis and S. Sundaresan, Applied Catal., **19**, 1985, 66

### 3. Results and Discussion

#### 3.1. Results from the synthesis of catalysts that have been tested

The VPO catalysts were prepared by reaction of  $V_2O_5$  and  $H_3PO_4$  in an organic medium as detailed in Chapter 2. Table 3.1 indicates the colours obtained for each catalyst at each stage i.e. precursor, calcined and used.

Table 3.1: Showing colours obtained for each catalyst

Synthesis	Colour
Undoped Precursor	Bright powder blue
Undoped Calcined	Dark brown
Undoped Used	Light grey
0.2% Ru Precursor	Dull powder-blue
0.2% Ru Calcined	Dark brown
0.2% Ru Used	Dull green
0.6% Ru Precursor	Dull powder-blue
0.6% Ru Calcined	Dark brown
0.6% Ru Used	Dull green
1% Ru Precursor	Bluish-grey
1% Ru Calcined	Black
1% Ru Used	Dull green

The undoped catalyst was prepared in an organic medium using the method shown in Chapter 2, synthesis 5 (1). A bright powder blue product,  $[(VO)_2H_4P_2O_9]$  was obtained. Approximately 1.5g were calcined under nitrogen atmosphere at  $450^\circ\text{C}$  for 6 hours. The calcined catalyst was dark brown in colour.

The catalyst was ready to be introduced into the fixed bed micro reactor, details of which can be viewed in Chapter 2, Section 2.3.

After the catalytic run, the used catalyst had turned light green, and was analysed by different techniques (FTIR, ICP-AES, AV, BET, SEM, EDX, XRD and GSD), as were the precursor and calcined catalysts.

The 0.2%, 0.6% and 1% Ru doped precursors were prepared using the same method as is described in Chapter 2, Section 2.1.13, 2.1.12 and 2.1.8 respectively. A dull blue

product and a bluish grey product were formed respectively and were subjected to the same treatment as the undoped catalyst.

### 3.2 Catalyst Characterization

#### 3.2.1 Average Oxidation State (Av)

The following table shows the average oxidation state obtained by the titration method as described in Chapter 2.2.1

Table 3.2: Showing Oxidation Satate (Nv) and Average Oxidation State (Av)

Sample	Nv	Nv	Nv	Nv	Average Av
Undoped precal. (p)	4.41	4.41	4.41	4.38	4.40
Undoped calcined (c)	4.29	4.29	4.28	4.28	4.29
Undoped used (u)	4.32	4.28	4.31	4.30	4.30
0.2% Ru precal.	4.27	4.28	4.29	4.33	4.29
0.2% Ru calcined	4.08	4.10	4.07	4.11	4.09
0.2% Ru used	4.37	4.39	4.39	4.35	4.38
0.6% Ru precal.	4.43	4.47	4.45	4.43	4.45
0.6% Ru calcined	4.25	4.28	4.30	4.27	4.28
0.6% Ru used	4.35	4.35	4.28	4.30	4.32
1% Ru precal.	4.23	4.24	4.20	4.21	4.22
1% Ru calcined	4.10	4.12	4.16	4.15	4.13
1% Ru used	4.24	4.28	4.32	4.29	4.28

The average vanadium oxidation state estimated by the potentiometric titration (method taken from Buchanan *et al.* (1985)) (2) is shown in Table 3.2.

As can be seen from the results, the average oxidation state is between 4.09 and 4.45. The used catalysts are found to be between 4.28 – 4.38.

Horowitz *et al.* (1988) indicates that the overall oxidation state for highly active and selective VPO catalysts for n-butane oxidation should be close to 4+ (1).

Zang *et al.* (1994) found the presence of small but significant amounts of  $V^{5+}$ . This species is dispersed on the (020) surface of  $(VO)_2P_2O_7$  (3).

The best catalytic performances can be correlated with the presence of  $V^{4+}$  cations and  $V^{4+}$ - $V^{5+}$  dimers (4). These dimers control the catalytic activity for n-butane oxidation

to maleic anhydride. The active catalyst requires the presence of both  $V^{4+}$  and  $V^{5+}$  cations in close proximity (5).

3.2.2 Inductively Coupled Plasma-Atomic Emission Spectroscopy (ICP-AES)

Inductively Coupled Plasma – Atomic Emission Spectroscopy (ICP-AES) was the technique employed to analyze the P: V ratio and the Ru:V molar percent ratio. The powder samples together with aqua regia were digested in a microwave digester. The Ru : V molar percent and P:V molar ratios can be seen in Table 3.3.

Table 3.3: Showing ICP-AES results to determine the Ru:V molar % and P:V molar ratios

Conc. Ru(%)	Ru : V (% molar ratio)	P: V (molar ratio)
Undoped p	0	0.82
Undoped c	0	0.83
Undoped u	0	0.78
0.2% p	0.15	0.83
0.2% c	0.17	0.80
0.2% u	0.13	0.82
0.6% p	0.22	0.83
0.6% c	0.26	0.83
0.6% u	0.19	0.83
1% p	0.45	0.84
1% c	0.52	0.83
1% u	0.47	0.84

From the results depicted in Table 3.3, the P:V ratio is between 0.78 and 0.84 molar ratio. It can be observed that with an increase in Ru:V promoter loading there is an increase in P: V molar ratio.

According to Hodnett (1985), the P:V ratio is a crucial factor in determining the redox properties of VPO catalysts. Hodnett and Delmon (1984) showed that the reactivity of these catalysts was found to be strongly dependent upon the P: V ratio.

An increase in P: V ratio also results in larger, more defined plate-like morphology which can be seen in Appendix 1, Figures 5.21-5.32.

### 3.2.3 Electron Dispersive X-Ray Spectroscopy (EDX)

Electron Dispersive X-Ray Spectroscopy (EDX) is the study of a specific area on the catalyst surface. The samples were analyzed uncoated i.e. the powder catalyst was mounted on a graphite stub as it appeared. An example of an EDX spectrum can be seen in Appendix 1, Figure 5.33.

P: V molar ratios and Ru: V molar percent were calculated from the output data from the EDX instrument. These ratios can be seen in Table 3.4.

Table 3.4: The EDX results below ((molar % Ru: V and P: V molar ratio) were obtained for the compounds studied

Sample ID	Average molar (%) Ru: V	Average P: V molar ratio
Undoped precursor (p)	0	0.53
Undoped calcined (c)	0	0.50
Undoped used (u)	0	0.57
0.2% Ru p	0.19	0.55
0.2% Ru c	0.16	0.57
0.2% Ru u	0.15	0.61
0.6% Ru p	0.20	0.66
0.6% Ru c	0.16	0.80
0.6% Ru u	0.10	0.70
1% Ru p	0.41	0.72
1% Ru c	-	0.64
1% Ru u	0.45	0.69

The P: V molar ratios are in the range of 0.50-0.80. P: V molar ratios from ICP-AES were in the range of 0.78-0.84. Lower P: V molar ratios obtained in EDX study was due to EDX being a surface study technique. Higher P: V ratios obtained in ICP-AES indicate that a greater content of phosphorous may be below the catalyst surface in the bulk.

### 3.2.4 Brunauer Emmett and Teller (BET)

The BET surface area obtained for all catalysts were between 6-14m<sup>2</sup>/g. This can be seen in Table 3.5 below.

Table 3.5: Results Showing BET (surface area) of Catalysts

Sample Name	Sample mass (g)	Surface area (m <sup>2</sup> /g)
Undoped precal.	0.2398	14.1470
Undoped calcined	0.2741	8.9618
Undoped spent	0.2503	21.8048
0.2% Ru precal.	0.2733	8.0860
0.2% Ru calcined	0.2168	9.8677
0.2% Ru used	0.2461	20.8337
0.6% Ru precal.	0.2544	6.9127
0.6% Ru calcined	0.2485	10.1550
0.6% Ru used	0.2456	21.6072
1% Ru precal.	0.2544	11.7265
1% Ru calcined	0.2746	9.0338
1% Ru used	0.2413	20.0528

The BET results obtained for the catalysts showed that with an increase in Ru loading, the surface area decreased for the catalyst precursor. The activated catalysts show surface areas between 8-10m<sup>2</sup>/g. As the catalyst doping increased in percentage, the surface area increased for the activated catalyst, however, the calcined 1% Ru catalyst showed a decrease in surface area. This indicated an optimum percentage loading for the 0.6% Ru catalyst for the highest surface area. Hodnett (1985) stated that an optimum promoter: V ratio exists for a maximum surface area. Further promoter doping may lead to segregation as can be seen for the calcined 1% Ru promoted catalysts.

The production of VOHPO<sub>4</sub>.0.5H<sub>2</sub>O, after activation gives rise to VPO catalysts with higher BET area (8). The used catalysts have surface areas between 20-21m<sup>2</sup>/g. This large surface area indicates a smaller degree of crystallinity as can be seen in Appendix 1, Figures 5.23, 5.26, 5.29 and 5.32. It does appear that an increase in surface area results in an initial increase in conversion, however, once a certain maximum surface area has been attained, there does not seem to be any improvement in conversion. Also, it does not seem that an increase in surface area results in any significant difference in maleic anhydride yield (9).



3.2.5 Scanning Electron Microscopy (SEM)

The SEM images (Appendix 1, Figures 5.21 - 5.32) may help to identify the nature of the active site. Kiely *et al.* (1996) also stated that reduction of the  $(VO)_2P_2O_7$  phase was observed and surface modification showed extended shear defects. These defects could be sites where  $V^{4+}$  and  $V^{5+}$  cations co-exist.

Scanning electron micrographs for each stage of the catalyst, precursor, calcined and used can be seen in Appendix 1, Figures 21-32. The SEM images show that the material has a plate like texture. These plate-like structures show a tendency to agglomerate / cluster to form structures resembling “flattened flowers” in which each “petal” corresponds to individual platelets. The plate diameters are 10-15  $\mu m$  and have a thickness of less than 1  $\mu m$  (Table 3.6).

Table 3.6: Showing Particle Diameter in Microns ( $\mu m$ )

Sample Name	Diameter ( $\mu m$ )
Undoped precal.	10
Unoped calcined	10
0.2% Ru precal.	10-15
0.2% Ru calcined	10-15
0.6% Ru precal.	10-15
0.6% Ru calcined	10-15
1% Ru precal.	10-15
1% Ru calcined	10-15

The SEM images of calcined compounds still show “flattened-rose” type morphology as was seen in their corresponding precursors. This indicates that a topotactic transformation may have occurred, from  $VOHPO_4 \cdot 0.5H_2O$  to  $(VO)_2P_2O_7 + H_2O$  (10).

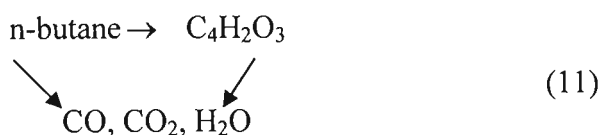
SEM images for the Ru promoted catalysts appear to have more exposed “flattened flowers” and more exposed “petals” corresponding to platelets as compared to the undoped catalysts. Horowitz *et al.* (1988) state that an increasing P: V ratio produce larger, more well formed vanadyl hydrogen phosphate crystals, which after topotactic transformation, lead to equally large and well formed vanadyl pyrophosphate crystals.

This rosette morphology is characteristic of the precursor synthesized by solvents such as isobutanol – benzyl alcohol. It is also stated by Horowitz *et al.* (1988) that the

most likely cause for the larger and better defined crystals with increasing P: V ratio is simply a higher solubility for the crystalline product in the synthesis medium due to increased acidity.

### 3.2.6 Fourier Transform Infra-Red Spectroscopy (FT-IR)

FTIR has been a useful technique in identifying the different vibrational bands identified on the surface of the catalysts analysed. Consider the following reaction:



Water, CO and CO<sub>2</sub> are products of the reaction of n-butane to maleic anhydride. Infrared Spectroscopy was able to detect CO, CO<sub>2</sub>, H<sub>2</sub>O, PO<sub>3</sub>, V=O and P-O-P as will be discussed in detail below.

FTIR was carried out for all of the catalysts at different stages of treatment such as precalcined, calcined and used. The spectra are in Appendix 1, Figures 5.9-5.20. Table 3.7 shows a summary of the peaks obtained to give the respective bands.

A sharp band at 1620-1640cm<sup>-1</sup> identifies adsorbed water (11). The bands for coordinated water can clearly be seen by a very broad band due to hydrogen – bonded OH in the 3600-2600cm<sup>-1</sup> region (11, 12, 13). A weak, sharp band can also be observed at 3600cm<sup>-1</sup> and can be assigned to the free hydroxyl groups (12). The calcined and used catalysts show the anhydrous state of the catalysts.

Adsorbed CO<sub>2</sub> is indicated by two bands in the 2350-2340cm<sup>-1</sup> regions. Gaseous CO and CO<sub>2</sub> are identified by intense vibrational-rotational bands at 2143 and 2350cm<sup>-1</sup> respectively (11).

The IR absorption in the region of 900-1300cm<sup>-1</sup> may be attributed to phosphate stretches. This substance has been identified as vanadyl hydrogen phosphate hemihydrate VO(HPO<sub>4</sub>).0.5H<sub>2</sub>O (2). It is worth noting that the vanadyl band in VO(HPO<sub>4</sub>).0.5H<sub>2</sub>O and in (VO)<sub>2</sub>P<sub>2</sub>O<sub>7</sub> occurs at 976 and 970cm<sup>-1</sup> respectively (14).



Table 3.7: Showing FTIR peaks in wavelength ( $\text{cm}^{-1}$ ) from catalysts tested in a KBr matrix.

Sample name	Ads water	Ads $\text{CO}_2$	$\text{CO} \& \text{CO}_2$	$\text{H}_2\text{O}$	$(\text{PO}_3)$	Polyortho phosphate	$\text{V}=\text{O}$	$(\text{P}-\text{O}-\text{P})$	$(\text{PO}_3)$
Undoped precal.	3382.5	2371.9	2336	1637.1	1098.7	1045	976		640
Undoped calcined	3432.6	2342.0		1620.5	1237	1141.3	965.3	736	
Undoped used	3431.6	2369.7	2336.8	1626.7	1242.7	1136	971.5	741.3	
0.2% Ru precal.	3375.4	2378.9	2336.8	1642.5	1194.7		970.7		634.7
0.2% Ru calcined	3438.6	2350.9	2325.3	1663.2	1237.3	1141.3	965.3	736	
0.2% Ru used	3452.6	2371.9	2336	1653.3	1232	1136	970.7	741.3	
0.6% Ru precal.	3382.5	2368.0	2362	1637.3	1194.7	1098	970.7		640
0.6% Ru calcined	3424.6	2363.6	2345.1	1630.0	1241	1142.6	963.8	741.2	
0.6% Ru used	3431.6	2368	2350.9	1621.3	1237.3	1136	970.7	741.3	
1% Ru precal.	3375.4	2368	2343.9	1632.1	1194.7	1087	970.7		640
1% Ru calcined	3438.6	2368	2350.9	1637.3	1141.3		960	736	
1% Ru used	3438.6	2368	2350.9	1653.3	1242.7	1136	970.7	741.3	

The precalcined catalysts all have a single broad band centred around  $1030\text{cm}^{-1}$  in the IR spectra which can be interpreted as  $\text{PO}_3$  due to polyorthophosphate as can be seen in Table 3.8 below. Crystalline  $\text{VO}(\text{HPO}_4) \cdot 0.5\text{H}_2\text{O}$  was obtained by drying of the solution (14).

Table 3.8: Showing polyorthophosphate peaks.

Sample	Polyorthophosphate Peaks ( $\text{cm}^{-1}$ )
Undoped precalcined	1045
0.2% Ru doped precalcined	-
0.6% Ru doped precalcined	1098
1% Ru doped precalcined	1087

The strong bonding of the pyrophosphate ion is reflected in the high frequency of the peaks which are observed as weak bands at  $1142\text{cm}^{-1}$  in the calcined catalyst and  $1136\text{cm}^{-1}$  in the used catalyst.

For  $\text{PO}_3$  in  $\text{VOPO}_4$ , very weak bands can be seen in the region of  $640\text{cm}^{-1}$  for all the precalcined catalysts. Peaks due to P-O-P in  $(\text{VO})_2\text{P}_2\text{O}_7$  can be observed in the calcined and used catalysts at  $736\text{cm}^{-1}$  and  $741\text{cm}^{-1}$ .

### 3.2.7 X-Ray Diffraction (XRD)

X-Ray diffraction data for the undoped, 0.2%, 0.6% and 1% Ru doped can be viewed in Appendix 1, Table 5.1-5.12. XRD data was obtained for the precursor (Table 3.9) and used catalysts (Table 3.10) due to their crystalline nature after they reacted with n-butane in the fixed bed reactor. The XRD spectra for the calcined catalysts were not recorded as they were found to be amorphous in nature.

The spectra of the catalyst precursors (Appendix 1, Fig. 5.1-5.8) indicate the presence of the vanadyl hydrogenphosphate hemihydrate,  $\text{VO}(\text{HPO}_4) \cdot 0.5\text{H}_2\text{O}$  and  $(\text{VO})_2\text{H}_4\text{P}_2\text{O}_9$ .  $\text{VO}(\text{HPO}_4) \cdot 0.5\text{H}_2\text{O}$  and  $(\text{VO})_2\text{H}_4\text{P}_2\text{O}_9$  gave IR signals in the region of  $900\text{-}1300\text{ cm}^{-1}$  for all catalyst precursors and can be viewed in Appendix 1, 5.9-5.20. Due to the crystallinity observed in the XRD spectrum, the used catalysts show an orthorhombic structure (15). This structure consists of two dimensional layers of  $\text{HPO}_4^{2-}$  anions and pairs of antiferromagnetically coupled  $\text{V}^{4+}$  cations. When calcination at  $450^\circ\text{C}$  under nitrogen,  $\text{VO}(\text{HPO}_4) \cdot 0.5\text{H}_2\text{O}$  undergoes topotactic dehydration to  $(\text{VO})_2\text{P}_2\text{O}_7$ . This phase makes it an active and selective catalyst for the oxidation of butane to maleic anhydride (2).

Calcined catalysts showed an amorphous state and the used catalyst showed crystallinity as stated above and from the XRD spectra. See Appendix Figures 5.1-5.8). A thermal transformation therefore occurred from the calcined stage to the used stage of the undoped, 0.2% Ru promoted, 0.6 Ru promoted and 1% Ru promoted catalyst.

Table 3.9: Table showing phase assignments for 2 degree theta for the precursor catalysts

Undoped precursor				0.2% Ru promoted				0.6% Ru promoted				1% Ru promoted			
d	RI	2°	hkl	d	RI	2°	hkl	d	RI	2°	hkl	d	RI	2°	hkl
spacing		theta		spacing		theta		spacing		theta		spacing		theta	
2.93	100	35.49	112 <sup>15</sup>	2.93	100	35.49	112	2.93	100	35.48	112	2.93	100	35.49	112
3.28	26.2	31.61	031 <sup>15</sup>	3.28	19.84	31.60	031	3.27	19.67	31.72	031	3.28	22.55	31.62	031
5.70	18.47	18.05	020 <sup>15</sup>	5.64	11.66	18.24	020	5.65	13.24	18.21	020	5.68	16.51	18.10	020
4.50	15.37	22.92	111 <sup>15</sup>	4.51	10.50	22.86	111	4.51	12.07	22.92	111	4.51	13.68	22.83	111
5.60	14.87	18.36	020 <sup>15</sup>	3.65	10.26	28.31	201	3.66	12.07	28.22	201	3.65	12.99	28.36	201
2.39	13.42	43.79	132 <sup>15</sup>	2.39	12.87	43.80	321	2.40	12.87	43.74	321	2.39	11.89	43.85	321
2.79	11.34	37.41	040 <sup>15</sup>	2.79	7.37	37.34	040	2.78	9.16	37.48	040	2.78	8.31	37.41	040

Table 3.10: Table showing phase assignments for 2 degree theta for used catalysts

Undoped precursor				0.2% Ru promoted				0.6% Ru promoted				1% Ru promoted			
d spacing	RI	2° theta	hkl	d spacing	RI	2° theta	hkl	d spacing	RI	2° theta	hkl	d spacing	RI	2° theta	hkl
3.13	100	33.26	102 <sup>15</sup>	3.13	100	33.10	102	3.14	100	33.10	102	3.13	100	33.22	102
2.51	59.42	41.61	400 <sup>15</sup>	2.56	16.04	40.89	400					2.42	12.13	43.24	400
2.98	57.38	34.95	112 <sup>15</sup>	2.98	51.85	34.89	112					2.98	49.01	34.99	112
3.88	47.95	26.62	121 <sup>15</sup>					3.86	48.94	26.75	121				
4.78	13.95	21.58	111	4.78	13.67	21.54	111	4.78	13.32	21.54	111	4.78	10.92	21.55	111
				2.65	13.90	39.44	202								

### 3.3 Reactor studies

#### 3.3.1 The Gas Hourly Space Velocities (GHSV)

The GHSV can be viewed in the table below. Most of the catalytic runs were kept at a constant GHSV of  $2170\text{hr}^{-1}$ , however the 0.2% Ru doped catalyst was at  $2063\text{hr}^{-1}$ .

Table 3.11: GHSV( $\text{hr}^{-1}$ ) readings for catalysts at varying temperatures:

Temperature ( $^{\circ}\text{C}$ )	Undoped	0.2% Ru cat.	0.6% Ru. cat	1% Ru cat.
200	2170	2063	1960	2170
250	2170	2063	1960	2170
300	2170	2508	1960	2170
350	2170	2063	1263	2170
400	2170	2063	2170	1960
450	2170	2063	2170	1960

#### 3.3.2 Catalyst Degradation

Products rich in carbon such as CO and  $\text{CO}_2$  are sometimes formed after a series of consecutive reaction steps. These levels could block active catalytic sites on the catalyst surface and thus lead to deactivation of the catalyst. Deactivation rates could also depend on the conversion level.

### 3.4 Catalyst Testing

#### 3.4.1 Undoped Catalyst

As can be seen from the figure (Fig. 3.1) below, with an increase in temperature of fifty degree intervals, the conversions of n-butane showed an increase to a maximum of 99.2% conversion at four hundred and fifty degrees.

The average selectivities to maleic anhydride for the undoped catalyst can be seen in Figure 3.2. The trend shows an increase in selectivity to a maximum of 55.6% at  $400^{\circ}\text{C}$ . Thereafter the selectivity decreases.

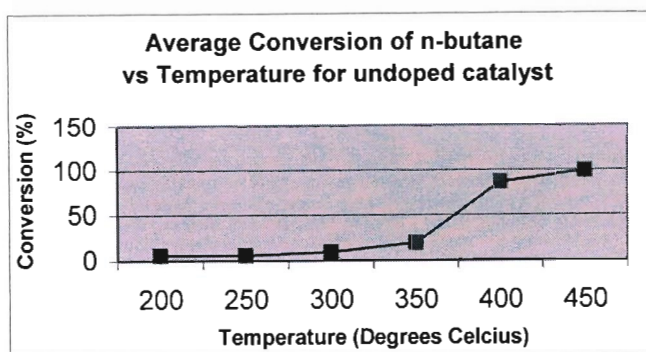


Figure 3.1: Graph showing the average conversions of butane at increasing temperatures for the undoped catalyst

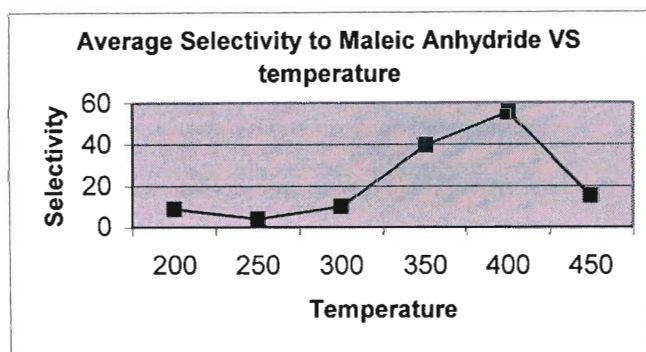


Figure 3.2: Graph showing selectivity for maleic anhydride for varying temperatures for the undoped catalyst

The yield of maleic anhydride shows an increase with an increasing temperature up to 400°C. Thereafter the yield decreases. This can be seen in Figure 3.3 below.

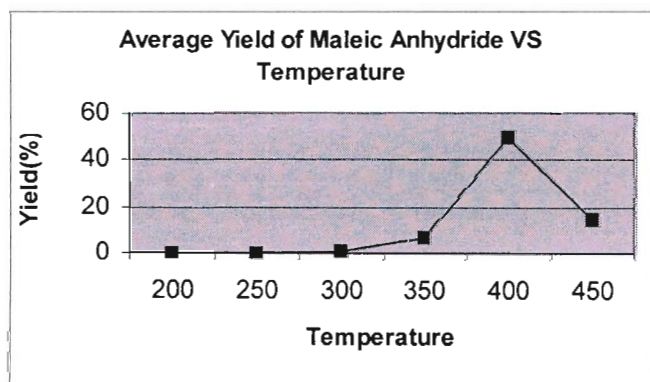


Figure 3.3: Graph showing yield of maleic anhydride at varying temperatures for the undoped catalyst

3.4.2 Catalyst testing of 0.2% Ru Promoted Catalyst

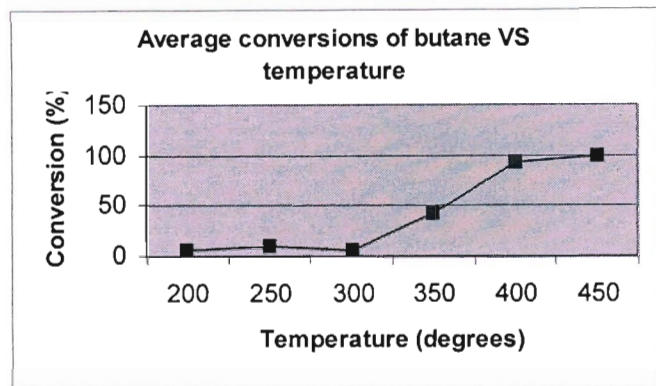


Figure 3.4: Graph showing trends of n-butane conversions with varying times

Figure 3.4 shows the increase in conversion with increasing temperature. The maximum conversion of 99.6% of n-butane for the 0.2% Ru promoted catalyst is at 450°C.

The trend of the selectivity of this catalyst can be seen in Figure 3.5 below. For this catalyst, an increase in selectivity occurs up until 350°C showing a value of 72.3% and thereafter decreases.

0.2% Ru promoted catalyst showed a maximum yield of 35% at 400°C. The yield decreased to 29.2% at 450°C. This can be seen in Figure 3.6.

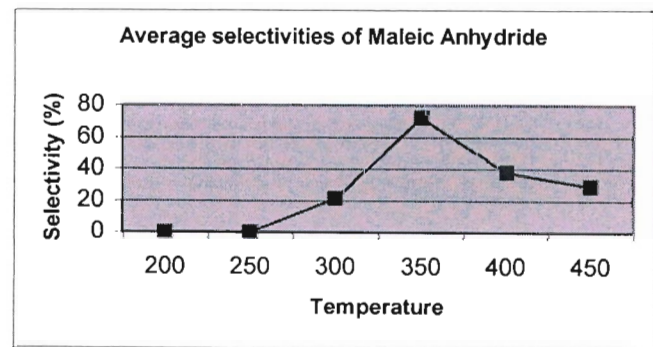


Figure 3.5: Showing selectivity of maleic anhydride at varying temperatures



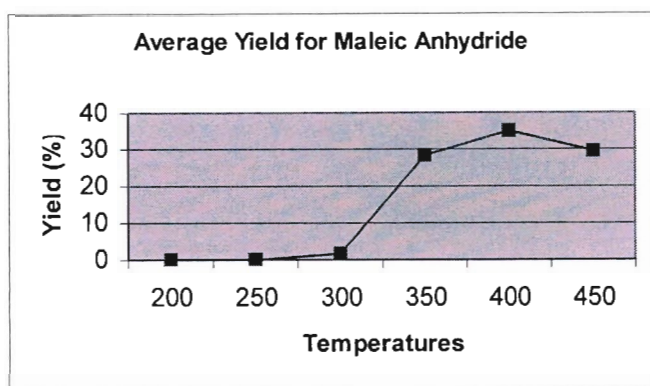


Figure 3.6: Showing the yield of maleic anhydride at varying temperatures

### 3.4.3 Catalyst Testing of 0.6% Ru Promoted Catalyst

The conversions of n-butane can be seen in Figure 3.7 below. The conversions increased at a steady rate to a conversion of 50% at a GHSV of 2170. A maximum of 95% can be seen at 450°C.

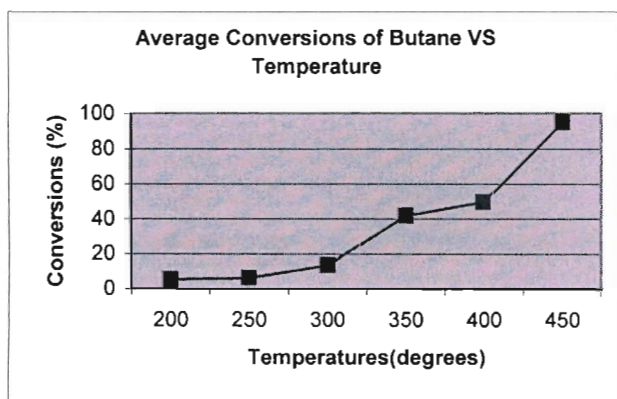


Figure 3.7: Showing conversions of n-butane at varying temperatures

The selectivity to maleic anhydride is shown in Figure 3.8. The selectivity increases from 200°C to 400°C. Thereafter it decreases. A maximum of 70.2% selectivity was obtained at 400°C.

The yield of maleic anhydride is shown in Figure 3.9. The yield shows a typical trend of an increase with an increase in temperature. The maximum yield of 37% is observed at 450°C.



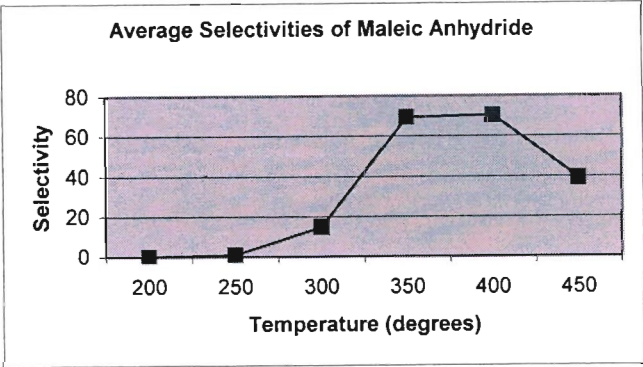


Figure 3.8: Showing selectivity to maleic anhydride at varying temperatures

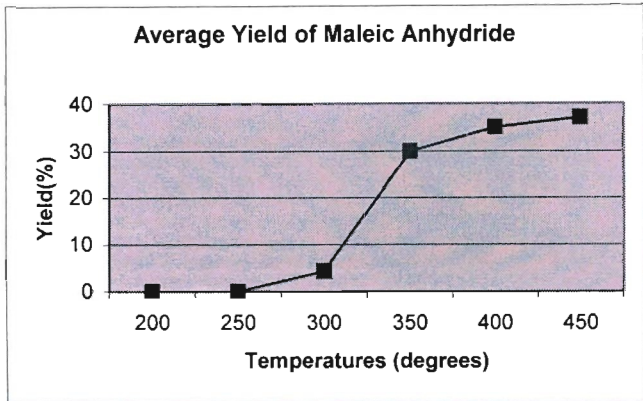


Figure 3.9: Yield of maleic anhydride at varying temperatures for the 0.6% Ru catalyst

3.4.4 Catalyst Testing of 1% Ru Promoted Catalyst

Figure 3.10 below shows an increase in conversion with an increase in temperature. The maximum conversion was 99.7% at 450°C. This was at a GHSV of  $1960\text{hr}^{-1}$ .

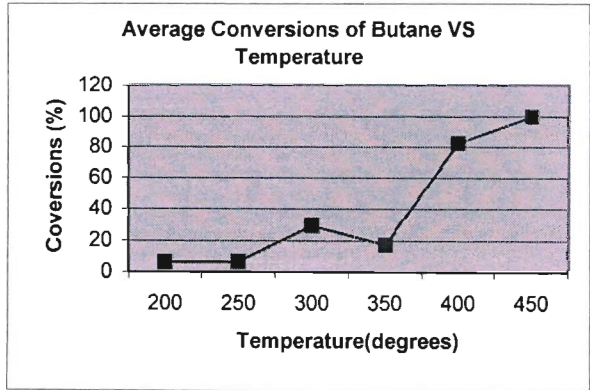


Figure 3.10: Showing conversions of n-butane at varying temperatures for the 1% Ru promoted catalyst

The selectivity of the 1% Ru can be seen in Figure 3.11 below.

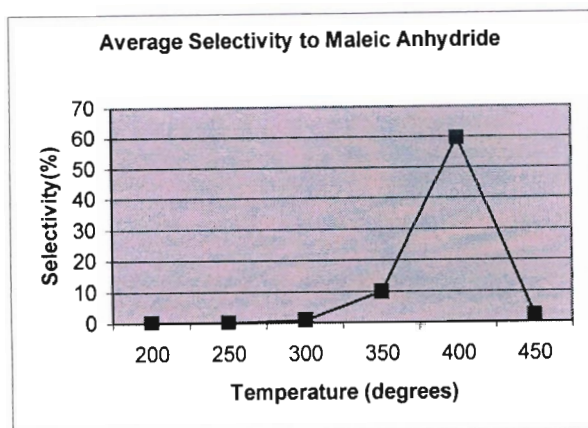


Figure 3.11: Shows the selectivity to maleic anhydride with varying temperature

The selectivity shows a gradual increase up to 350°C. Thereafter it increases rapidly to 60% at 400°C. After it has reached its peak, it dropped drastically to 2% at 450°C. The GHSV was also 1960hr<sup>-1</sup>.

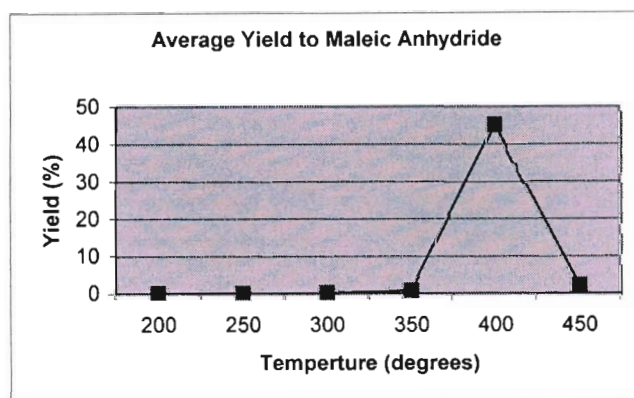


Figure 3.12: Shows the Yield of maleic anhydride at varying temperatures

The yield in this catalyst to maleic anhydride increased gradually (Figure 3.12) but remained below 10% at 350°C. A sharp increase of 45% was observed at 400°C but a drop was also noted at 450°C to 2%. This occurred at a GHSV of 1960hr<sup>-1</sup>.

### 3.4.5 Comparison of Conversions, Selectivity and Yield for all Catalysts at Varying Temperatures

The optimum temperature at which maximum conversions are obtained is found to be at 450°C (Fig. 3.13). There is not much of a difference in the conversion between the undoped and the 1% Ru promoted catalyst. A slight decrease can be observed with the 0.6% Ru promoted catalyst but this difference is minimal.

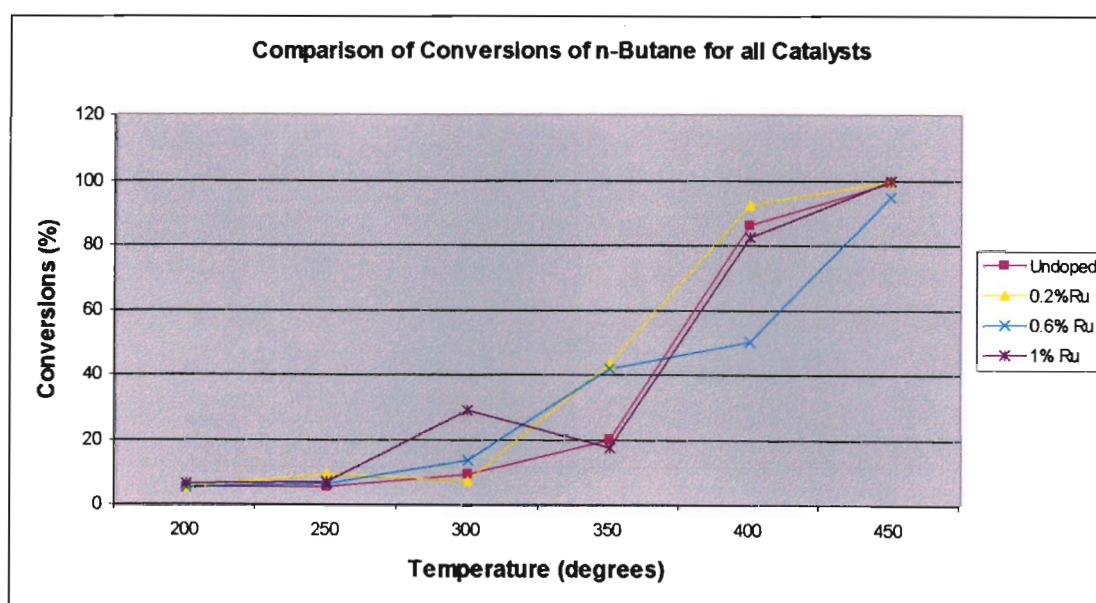


Figure 3.13: Graph of conversion vs. temperature for all catalysts prepared

Figure 3.14 shows a comparison of the selectivity with temperature. The highest selectivity obtained was found with the 0.2% Ru promoted catalyst at a temperature of 350°C. The selectivity to maleic anhydride reached a maximum for all catalysts and thereafter decreased. Maximum selectivity for the other catalysts was obtained at 400°C.

The highest yield to Maleic Anhydride was obtained at 49.5% for the undoped catalyst at a temperature of 400°C (Fig. 3.15). Optimum yields for all catalysts were obtained at 400°C and thereafter decreased.

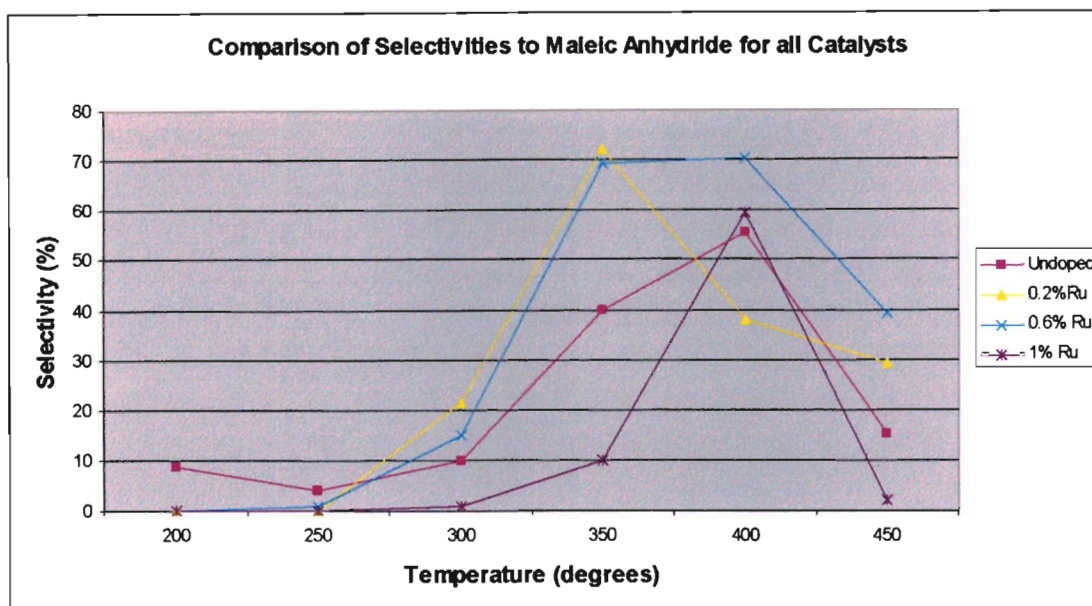


Figure 3.14: Graph showing selectivity to maleic anhydride vs. temperature

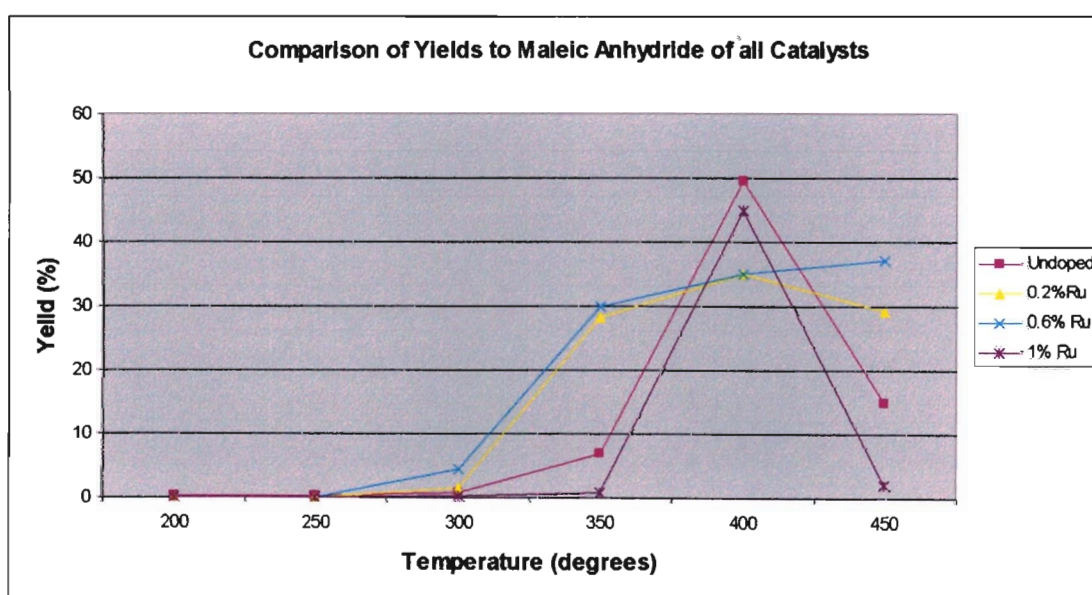


Figure 3.15: Shows a comparison of yield (%) to maleic anhydride for all catalysts tested at constant conversion of 99%

Figure 3.16 and Fig. 3.17 clearly show an increase in selectivity with an increase in promoter loading from the undoped catalyst to 0.6% Ru promoted catalyst. There was a decrease in selectivity for the 1% Ru promoter catalyst at 80% and 99% conversion.



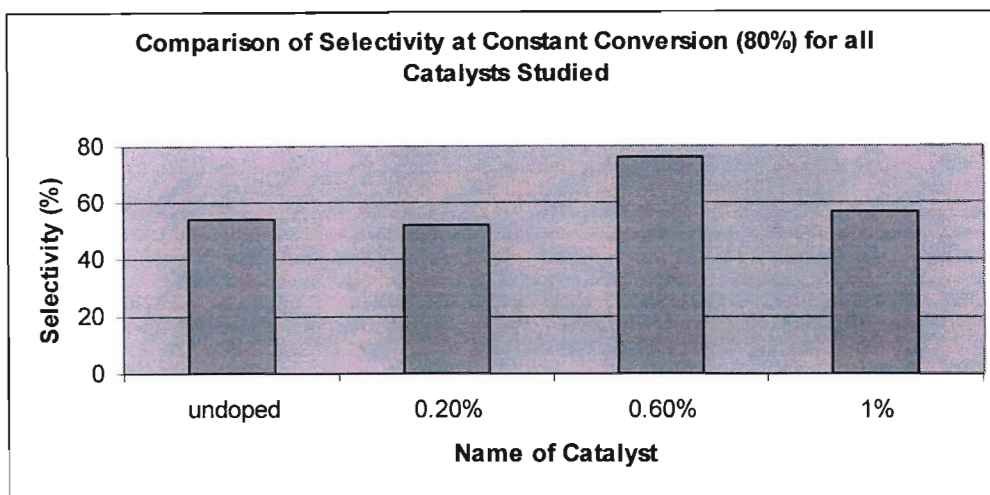


Figure 3.16: Graph showing comparison of selectivity at constant conversion (80%) for all catalysts studied

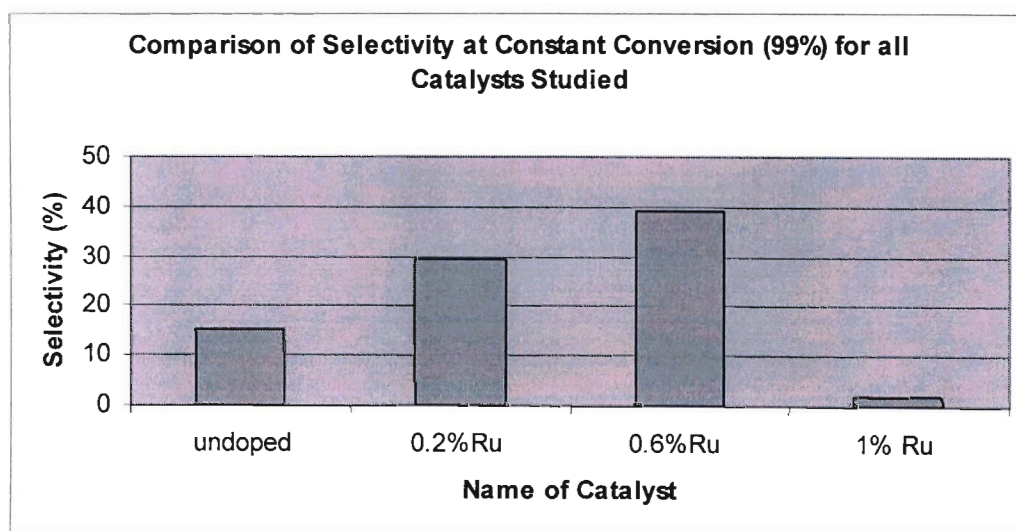


Figure 3.17: Comparison of selectivity at constant conversion of 99% for all catalysts studied

The 0.6% Ru promoted catalyst showed the highest selectivity and could be due to a number of contributing factors:

1. The P: V ratio studied by ICP-AES results for the catalyst increased as the Ru loading increased (Table 3.3).
2. EDX results (Table 3.4) showed that the 0.6% Ru catalyst had the greatest P: V ratio.
3. BET surface area for the calcined 0.6% Ru catalyst was the greatest surface area obtained compared to all other catalysts.

4. The overall oxidation state was close to  $4^+$  which is reported to give highly active and selective catalysts.
5. SEM images of the catalyst showed much more exposed plate-like structures and “petals” due to their preparation and increased Ru loading as compared to other catalysts.
6. XRD data and phase assignments indicates two phases present  $(VO)_2H_4P_2O_9$  and  $VO(HPO_4) \cdot 0.5H_2O$  which undergo topotactic dehydrogenation to form  $(VO)_2P_2O_7$ , which is the active phase. The (020) plane observed (Table 3.9) considerably influences catalytic activity and redox preparation.

The graphs below (Fig. 3.18) show a trend with an increase in Ru loading, there is an increase of maleic anhydride yield from the 0.2%Ru loaded catalyst onwards, for constant conversion of 80%, however, the undoped catalyst, gave the highest maleic anhydride yield .

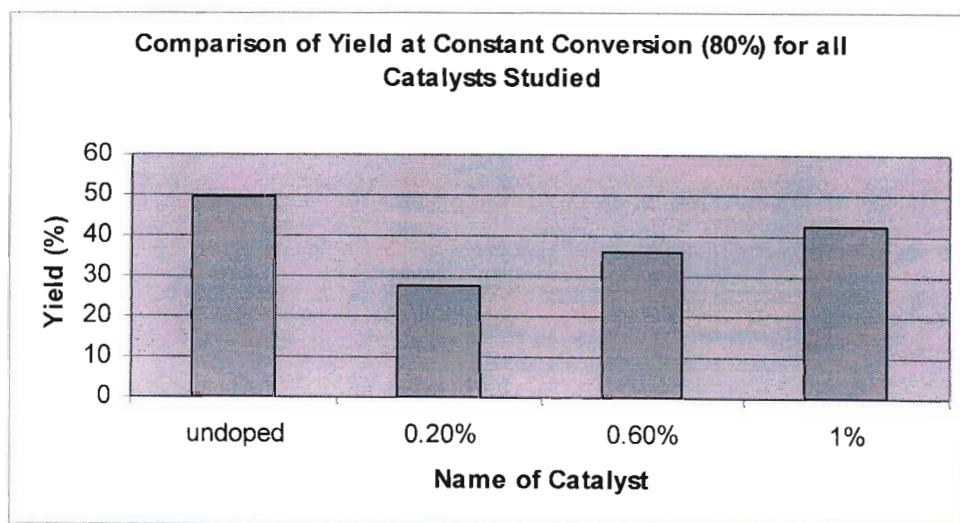


Figure 3.18: Graph showing comparison of maleic anhydride yield at constant conversion (80%) for all catalysts studied

At a conversion of 99%, an increase of maleic anhydride yield was observed with the optimum yield occurring with the 0.6% Ru doped catalyst. There was a drop in the yield for the 1% Ru doped catalyst. Hutchings (1991) indicated that additional levels of promoters usually lead to a distinct decrease in maleic anhydride yield.

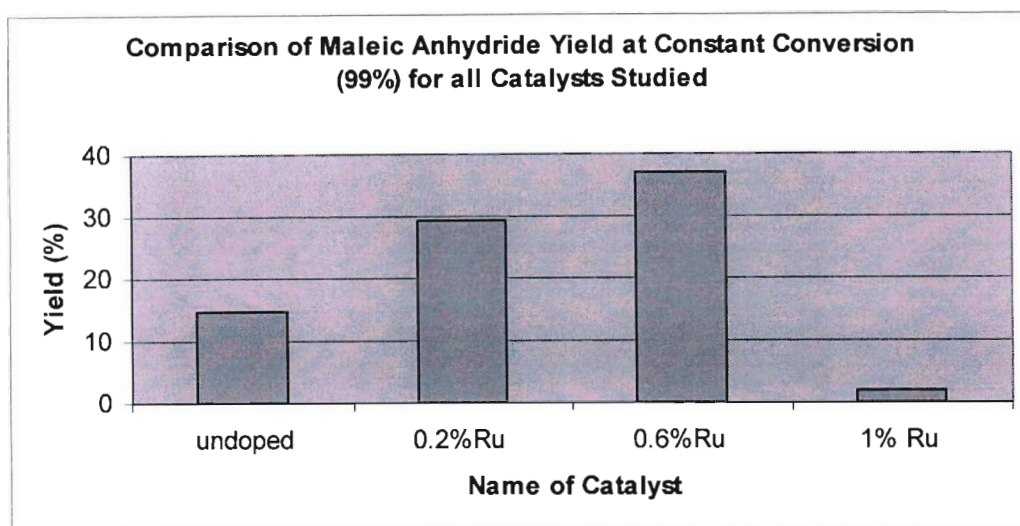


Figure 3.19: Graph showing a comparison of yield to maleic anhydride at constant conversion of 99% for all catalysts studied

The 0.2% Ru and 0.6% Ru promoted catalysts show a stable selectivity over a wider temperature range than the 1% Ru promoted catalyst. Naumann and Behan (1975) (16) stated that Ru showed adverse effects on selectivity which can be true for the additional levels such as 1% Ru loading as the results indicate low selectivity and yield to maleic anhydride.

## References:

1. H. S. Horowitz, C. M. Blackstone, A. W. Sleight, G. Teufer, *Applied Catal.*, **38**, 1988, 194
2. J. S. Buchanan, J. Apostolakis, S. Sundaresan, *Applied Catal.*, **19**, 1985, 66
3. Y. Zang-Lin, M. Forissier, J. C. Vedrine and J. C. Volta, *J. Catal.*, **145**, 1994, 267
4. M. T. Sananes-Schultz, A. Tuel, G. J. Hutchings and J. C. Volta, *J. Catal.*, **166**, 1997, 388
5. C. J. Kiely, A. Burrows, S. Sajip, G. J. Hutchings, M. T. Sananes, A. Tuel and J. C. Volta, *J. Catal.*, **162**, 1996, 31
6. B. K. Hodnett, *Catal. Rev.-Sci. Eng.*, **27** (3), 1985, 37
7. B. K. Hodnett and B. Delmon, *J. Catal.*, **88**, 1984, 43
8. G. J. Hutchings, R. Olier, M. T. Sananes and J. C. Volta, *New Developments in Selective Oxidation*, 1994, 213
9. G. J. Hutchings, M. T. Sananes, S. Sajip, C. J. Kiely, A. Burrows, I. J. Ellison and J. C. Volta, *Catal. Today*, **33**, 1997, 161
10. G. Busca, F. Cavani, G. Centi and F. Trifiro, *J. Catal.*, **99**, 1986, 400
11. R. W. Wenig and G. L. Schrader, *J. Phy. Chem.*, **90**, 1986, 6480
12. Cavani, F., Centi, G. and Trifiro, F., *Applied Catal.*, **9**, 1984, 191
13. G. Busca, C. Centi, F. Trifiro, and V. Lorenzelli, *J. Phy. Chem.*, **90**, 1986, 1337
14. G. Centi, F. Trifiro and G. Poli, *Applied Catal.*, **19**, 1985, 225
15. J. W. Johnson, D. C. Johnston, A. J. Jacobson, and J. F. Brody, *J. Am. Chem. Soc.*, **106**, 1984, 8123
16. A. W. Naumann and A. S. Behan Jr, *J. Catal.*, **39**, 1975, 432



#### 4. Conclusion

The vanadyl pyrophosphate catalyst was prepared from its precursor  $\text{VOHPO}_4 \cdot 0.5\text{H}_2\text{O}$  and promoted with Ruthenium metal in an organic medium. The organic medium was preferred since it gives superior performance. Metal promoters are known to give superior performance when added in relatively small amounts. The catalyst precursor was tested with increasing levels of metal promoters. The fixed bed micro-reactor was selected since fixed bed reactors are used in industry for major catalytic processing. These catalysts were tested at various temperatures while the GHSV was maintained constant. It was found that with increasing temperatures, the conversions of the catalysts increased until  $450^\circ\text{C}$  and thereafter the catalyst degenerated at temperatures higher than  $450^\circ\text{C}$ . The outstanding catalyst that showed greatest selectivity was the 0.6% Ru promoted catalyst.

The undoped catalyst, and the 0.2%, 0.6% and 1% Ru promoted catalyst were characterized at different stages: precursor, calcined and used. The XRD confirmed that the initial phase was the  $\text{VOHPO}_4 \cdot 0.5\text{H}_2\text{O}$  which undergoes transformation to the active catalyst  $(\text{VO})_2\text{P}_2\text{O}_7$  when subjected to temperatures higher than  $350^\circ\text{C}$ . The FTIR data showed the polyorthophosphate peaks and vanadyl peaks indicative of the catalysts. The average oxidation state for the 0.6% Ru promoted catalyst was found to be +4.28 which is evident for best catalytic performance. Catalysts with the V:P ratio of 1 is theoretically known to give higher activity and selectivity, however, the V:P ratio obtained from the elemental techniques such as ICP-AES and EDX, showed the V:P ratio to be 0.8. The catalysts studied, however, still showed high conversions and selectivity. The BET surface area of the 0.6% Ru catalyst showed a value of  $10.16\text{m}^2/\text{g}$  which was the highest surface area obtained in the calcined stage amongst all catalysts. An increase in surface area shows an increase in conversion except for the 1% Ru catalyst.

The trends observed for the catalysts were consistent with literature, namely Hutchings (1991). Hutchings (1991) stated that with an increase in promoter loading, there is an increase in maleic anhydride yield, however, with additional promoter loading, a decrease in maleic anhydride yield is observed and this can be seen in the results presented in Chapter 3.

**Appendix 1**

Table 5.1: XRD data for the undoped precalcined catalyst

Used Wavelength:		K-Alpha				
K-Alpha1 wavelength (Å):		1.78897				
K-Alpha2 wavelength (Å):		1.79285				
K-Alpha2/K-Alpha1 intensity ratio:		0.5				
K-Alpha wavelength (Å):		1.78897				
Peak search parameter search:		As measured intensities:				
Set created:		04/28/1999 12:06				
Peak positions defined by:		Minimum of second derivative				
Minimum peak tip width (°2 Theta):		0				
Minimum peak tip width (°2 Theta):		1				
Peak base width (°2 Theta)		2				
d-spacing (Å)	Relative intensity (%)	Angle (°2 Theta)	Peak Height (counts/sec)	Background (counts/sec)	Tip width (°2 Theta)	(phases)
9.37127	12.5	10.95438	115.03	30.1	0.08	
5.84875	10.63	17.59419	97.83	29.56	0.12	
5.70287	18.47	18.04797	169.99	28.81	0.16	
5.60458	14.87	18.36717	136.9	28.27	0.16	
5.22941	0.47	19.69757	4.37	26.05	0.24	
4.79443	7.03	21.505	64.68	24.39	0.06	
4.5017	15.37	22.92178	141.41	23.62	0.24	(VO <sub>2</sub> )P <sub>2</sub> O <sub>7</sub> ·2H <sub>2</sub> O <sup>1</sup>
4.09458	2.07	25.23662	19.07	22.37	0.32	
3.67419	15.21	28.18055	140.02	22.64	0.16	(VO <sub>2</sub> )P <sub>2</sub> O <sub>7</sub> ·2H <sub>2</sub> O <sup>1</sup>
3.64651	12.88	28.39889	118.56	22.77	0.2	
3.28329	26.22	31.61836	241.3	23.18	0.2	VO(HPO <sub>4</sub> )·0.5H <sub>2</sub> O <sup>2</sup>
3.10281	13.01	33.51019	119.76	22.37	0.32	α-VOPO <sub>4</sub> <sup>3</sup>
2.93433	100	35.4963	920.34	21.53	0.18	(VO <sub>2</sub> )P <sub>2</sub> O <sub>7</sub> ·2H <sub>2</sub> O <sup>1</sup>
2.78892	11.34	37.41375	104.38	20.72	0.24	
2.66196	6.15	39.2697	56.59	19.93	0.4	
2.60701	8.28	40.13247	76.21	19.56	0.2	
2.5422	1.48	41.20153	13.62	19.11	0.12	
2.45419	1.3	42.75016	11.97	18.51	0.32	
2.39875	13.42	43.78848	123.51	18.16	0.1	
2.34078	3.14	44.9314	28.88	17.77	0.12	
2.26321	2.08	46.56032	19.11	17.21	0.32	
2.2319	5.7	47.25298	52.46	16.97	0.24	
2.11574	1.63	50.01991	15	16.03	0.32	
2.05015	3.88	51.73609	35.71	15.44	0.32	
2.02853	10.28	52.3291	94.63	15.24	0.06	VO(PO <sub>3</sub> ) <sub>2</sub> <sup>3</sup>
1.958	3.63	54.36598	33.38	16.34	0.12	
1.89605	7.73	56.29734	71.16	23.59	0.28	
1.85522	14.94	57.65094	137.53	30.02	0.36	
1.76342	4.22	60.96079	38.81	23.57	0.28	
1.71002	1.15	63.0786	10.62	20.9	0.2	

<sup>1</sup> B. K. Hodnett, Catal. Rev. – Sci. Eng., 27(3), 1985, 373-424<sup>2</sup> J. W. Johnson, D. C. Johnston, A. J. Jacobson and J. F. Brody, J. AM. Chem. Soc., 106, 1984, 8125<sup>3</sup> E. Bordes and P. Courtine, J. Catal., 57, 1979, 240

1.69225	1.22	63.81877	11.27	19.96	0.48
1.64893	5.09	65.70272	46.83	17.58	0.24
1.63525	6.69	66.3229	61.55	16.8	0.32
1.59955	3.08	68.00211	28.32	14.68	0.4
1.53999	3.13	71.019	28.79	15.46	0.2
1.51639	3.8	72.29642	34.97	15.88	0.2
1.46598	8.03	75.20216	73.92	16.84	0.24
1.43386	2.05	77.319248	18.84	17.85	0.48
1.42151	2.55	77.98959	23.45	18.53	0.48
1.37397	2.36	81.23681	21.72	18.02	0.24
1.34867	2.21	83.09352	20.35	19.01	0.56
1.30979	3.09	86.14498	28.45	20.7	0.24
1.27865	1.71	88.78243	15.71	18.56	0.24

Table 5.2: XRD data for the undoped calcined catalyst

Used Wavelength: K-Alpha

K-Alpha1 wavelength (Å): 1.78897  
K-Alpha2 wavelength (Å): 1.79285  
K-Alpha2/K-Alpha1 intensity ratio: 0.5  
K-Alpha wavelength (Å): 1.78897

Peak search parameter search: As measured intensities:  
Set created: 04/28/1999 12:06  
Peak positions defined by: Minimum of second derivative  
Minimum peak tip width (°2 Theta): 0  
Minimum peak tip width (°2 Theta): 1  
Peak base width (°2 Theta): 2  
Minimum significance 0.6

d-spacing (Å)	Relative intensity (%)	Angle (°2 Theta)	Peak Height (counts/sec)	Background (counts/sec)	Tip width (°2 Theta)
14.76807	1.84	6.94491	2.25	36.69	0.4
6.19138	10.13	16.61345	12.42	29.54	0.24
5.84082	15.42	17.61827	18.9	30.51	0.06
5.26897	5.21	19.54823	6.39	32.37	0.96
4.77772	28.71	21.58114	35.19	34.39	0.16
3.77613	25.36	27.40468	31.08	65.1	0.48
3.13197	100	33.18916	122.59	53.69	0.48
2.97512	68.42	34.99387	83.87	51.27	0.32
2.64757	8.62	39.49192	10.57	37.94	0.64
2.39937	12.73	43.77676	15.6	34.56	0.64
2.34047	29.76	44.93759	36.48	29.14	0.16
2.08059	28.29	50.92475	34.68	28.74	0.48
2.02855	64.57	52.32848	79.16	30.61	0.12
1.57679	10.58	69.12159	12.97	34.48	0.8
1.43239	12.6	77.2862	15.44	29.86	0.4
1.37715	5.21	81.01018	6.38	25.07	0.4

Table 5.3: XRD data for the undoped used catalyst

Used Wavelength:		K-Alpha				
K-Alpha1 wavelength (Å):		1.78897				
K-Alpha2 wavelength (Å):		1.79285				
K-Alpha2/K-Alpha1 intensity ratio:		0.5				
K-Alpha wavelength (Å):		1.78897				
Peak search parameter search:		As measured intensities:				
Set created:		04/28/1999 12:06				
Peak positions defined by:		Minimum of second derivative				
Minimum peak tip width (°2 Theta):		0				
Minimum peak tip width (°2 Theta):		1				
Peak base width (°2 Theta)		2				
Minimum significance		0.6				
d-spacing (Å)	Relative intensity (%)	Angle (°2 Theta)	Peak Height (counts/sec)	Background (counts/sec)	Tip width (°2 Theta)	phases
8.69806	0.49	12.27242	2.44	24.27	0.8	
6.23753	9.62	16.48965	48.22	24.82	0.12	(VO) <sub>2</sub> P <sub>2</sub> O <sub>7</sub> <sup>1</sup>
5.6705	3.07	18.15186	15.37	24.32	0.8	(VO) <sub>2</sub> P <sub>2</sub> O <sub>7</sub> <sup>1</sup>
4.77685	13.95	21.58511	69.91	21.03	0.08	(VO) <sub>2</sub> P <sub>2</sub> O <sub>7</sub> <sup>1</sup>
3.88482	47.95	26.62367	240.3	32.41	0.28	VO(PO <sub>3</sub> ) <sub>2</sub> <sup>3</sup>
3.84235	39.53	26.92347	198.11	31.93	0.2	
3.12541	100	33.26082	501.14	35.13	0.12	
2.98546	55.17	34.86868	276.46	33.55	0.08	
2.97859	57.38	34.95174	287.56	33.47	0.08	
2.66168	12.35	39.27392	61.87	22.56	0.24	
2.51807	59.42	41.61453	297.77	20.38	0.06	(VO) <sub>2</sub> P <sub>2</sub> O <sub>7</sub> <sup>1</sup>
2.43824	13.16	43.04376	65.96	20.15	0.16	
2.39744	6.59	43.81383	33.04	20.02	0.16	
2.34167	8.58	44.91327	43.01	19.85	0.16	
2.08789	30.14	50.7341	151.06	20.59	0.12	
2.0293	16.23	52.30778	81.34	20.97	0.1	
1.93518	6.01	55.061	30.09	21.64	0.64	
1.90458	4.67	56.02295	23.38	21.87	0.24	
1.83979	12.39	58.1806	62.07	22.4	0.56	
1.63371	8.17	66.39337	40.93	22.71	0.16	
1.59806	6.42	68.07441	32.17	21.38	0.32	
1.57331	15.69	69.29616	78.62	20.41	0.36	
1.47545	6.12	74.63683	30.66	26.68	0.48	
1.45982	6.73	75.57528	33.72	25.87	0.64	
1.43322	3.71	77.23306	18.62	26.61	0.16	
1.3816	4.72	80.69541	23.64	21.33	0.24	
1.37521	2.68	81.14838	13.44	20.48	0.2	
1.35053	2.13	82.95413	10.7	17.07	0.64	
1.30587	34.67	86.46667	173.75	19.11	0.08	

Table 5.4: XRD data for the 0.2% Ru precalcined catalyst

Used Wavelength:		K-Alpha				
K-Alpha1 wavelength (Å):		1.78897				
K-Alpha2 wavelength (Å):		1.79285				
K-Alpha2/K-Alpha1 intensity ratio:		0.5				
K-Alpha wavelength (Å):		1.78897				
Peak search parameter search:		As measured intensities:				
Set created:		04/28/1999 12:06				
Peak positions defined by:		Minimum of second derivative				
Minimum peak tip width (°2 Theta):		0				
Minimum peak tip width (°2 Theta):		1				
Peak base width (°2 Theta)		2				
Minimum significance		0.6				
d-spacing (Å)	Relative intensity (%)	Angle (°2Theta)	Peak Height (counts/sec)	Background (counts/sec)	Tip width (°2Theta)	Tip width (phases)
5.85229	10.02	17.58345	84.96	32.97	0.12	
5.64225	11.66	18.24352	98.83	31.11	0.4	(VO) <sub>2</sub> P <sub>2</sub> O <sub>7</sub> ·2H <sub>2</sub> O <sup>1</sup>
5.06875	17.83	20.32845	151.2	26.09	0.04	
4.78891	6.07	21.53011	51.49	25.94	0.08	
4.51354	10.5	22.86081	89.06	25.77	0.4	(VO) <sub>2</sub> P <sub>2</sub> O <sub>7</sub> ·2H <sub>2</sub> O <sup>1</sup>
4.08524	1.67	25.29527	14.18	25.46	0.48	
3.657	10.26	28.31578	86.96	29.78	0.8	(VO) <sub>2</sub> P <sub>2</sub> O <sub>7</sub> ·2H <sub>2</sub> O <sup>1</sup>
3.28471	19.84	31.60434	168.2	31.37	0.2	(VO) <sub>2</sub> P <sub>2</sub> O <sub>7</sub> ·2H <sub>2</sub> O <sup>1</sup>
3.09323	8.97	33.61704	76.07	30.13	0.2	
2.9342	100	35.49789	847.8	28.97	0.22	(VO) <sub>2</sub> P <sub>2</sub> O <sub>7</sub> ·2H <sub>2</sub> O <sup>1</sup>
2.79416	7.37	37.34104	62.5	27.83	0.48	
2.65765	4.96	39.33599	42.04	26.6	0.4	
2.6006	5.99	40.23568	50.82	26.04	0.56	
2.39803	12.87	43.80231	109.15	23.06	0.08	
2.33927	1.95	44.96192	16.57	20.78	0.2	
2.22982	4.77	47.29953	40.4	19.09	0.48	
2.13038	1.74	49.65276	14.79	18.29	0.24	
2.071	2.34	51.17753	19.85	17.78	0.06	
2.04809	3.12	51.79205	26.47	17.57	0.32	
2.0276	7.84	52.35512	66.44	17.38	0.24	
1.95594	2.58	54.42823	21.91	19.04	0.32	
1.9013	7.43	56.12804	63.03	26.16	0.16	
1.85627	14.66	57.61525	124.32	33.91	0.16	
1.77211	3.15	60.63029	26.68	30.05	0.32	
1.69391	1	63.74882	8.49	25.32	0.32	
1.64962	4.1	65.67195	34.73	22.3	0.64	
1.63391	5.82	66.38429	49.36	21.19	0.2	
1.59787	1.94	68.08369	16.47	18.53	0.96	
1.5384	2.39	71.10356	20.22	19.26	0.56	
1.51576	2.72	72.33109	23.03	18.87	0.4	

1.47007	7.16	74.95694	60.71	18.03	0.2
1.43163	2.35	77.33505	19.95	17.8	0.24
1.42051	2.7	78.05499	22.87	18.03	0.48
1.3964	1.03	79.66752	8.71	18.54	0.12
1.37599	1.85	81.09298	15.68	19	0.48
1.34458	2.13	83.40301	18.03	20.78	0.48
1.30933	3.29	86.18233	27.92	23.77	0.24

Table 5.5: XRD data for the 0.2% Ru calcined

Used Wavelength: K-Alpha

K-Alpha1 wavelength (Å): 1.78897  
K-Alpha2 wavelength (Å): 1.79285  
K-Alpha2/K-Alpha1 intensity ratio: 0.5  
K-Alpha wavelength (Å): 1.78897

Peak search parameter search: As measured intensities:  
Set created: 04/28/1999 12:06  
Peak positions defined by: Minimum of second derivative  
Minimum peak tip width (°2 Theta): 0  
Minimum peak tip width (°2 Theta): 1  
Peak base width (°2 Theta): 2  
Minimum significance: 0.6

d-spacing (Å)	Relative intensity (%)	Angle (°2Theta)	Peak Height (counts/sec)	Background (counts/sec)	Tip width (°2Theta)
6.1911	6.59	16.61419	13.14	34.34	0.64
4.79179	13.78	21.51702	27.49	37.39	0.16
4.07614	9.8	25.35269	19.55	57.63	0.56
3.93858	16.18	26.25372	32.29	64.68	0.8
3.11906	78.78	33.33051	157.15	53.55	0.36
2.97266	52.34	35.02372	104.41	48.55	0.4
2.81319	9.42	37.07926	18.8	42.53	0.06
2.67457	100	39.0969	199.49	40.28	0.06
2.63277	6.47	39.72318	12.9	39.76	0.64
2.44823	7.78	42.85937	15.51	36.67	0.64
2.34191	11.09	44.9086	22.13	30.42	0.2
2.08264	18.96	50.87098	37.82	31.79	0.8
2.02684	48.39	52.37618	96.53	32.13	0.16
1.96897	4.86	54.03833	9.7	32.57	0.08
1.93187	2.36	55.16351	4.72	32.96	0.96
1.91776	5.94	55.60429	11.86	33.12	0.06
1.85704	3.5	57.58936	6.97	35.08	0.96
1.69831	3.47	63.56433	6.93	27.62	0.08
1.61982	4.69	67.03759	9.35	32.73	0.2
1.59818	7.51	68.06867	14.98	32.49	0.1
1.56862	10.25	69.53304	20.44	32.14	0.64
1.43121	4.67	77.36162	9.32	31.57	0.48

Table 5.6: XRD data for the used 0.2% Ru promoted catalyst

Used wavelength:	K- alpha					
K-Alpha1 wavelength (Å):	1.78897					
K-Alpha2 wavelength (Å):	1.79285					
K-Alpha2/K-Alpha1 intensity ratio:	0.5					
K-Alpha wavelength (Å)	1.78897					
Peak search parameter search:	As measured intensities:					
Set created:	04/28/1999 12:06					
Peak positions defined by:	Minimum of second derivative					
Minimum peak tip width (°2 Theta):	0					
Minimum peak tip width (°2 Theta):	1					
Peak base width (°2 Theta)	2					
Minimum significance	0.6					
d-spacing (Å)	Relative intensity (%)	Angle (°2Theta)	Peak Height (counts/sec)	Background (counts/sec)	Tip width (°2Theta)	(phases)
27.99308	0.92	3.66225	4.85	41.04	0.80	
13.21567	12.21	7.76189	64.28	32.09	0.08	
7.02095	1.37	14.63897	7.24	25.33	0.64	
6.26634	8.65	16.41333	45.53	24.59	0.20	
5.64864	2.89	18.22271	15.2	23.83	0.96	
4.78738	13.67	21.53708	71.94	23.45	0.20	
3.87003	40.68	26.72727	214.16	40.30	0.24	(VO) <sub>2</sub> P <sub>2</sub> O <sub>7</sub> <sup>1</sup>
3.13938	100.00	33.10852	526.41	36.06	0.10	(VO) <sub>2</sub> P <sub>2</sub> O <sub>7</sub> <sup>1</sup>
2.98301	51.85	34.89826	272.96	34.30	0.10	(VO) <sub>2</sub> P <sub>2</sub> O <sub>7</sub> <sup>1</sup>
2.66074	12.19	39.28842	64.16	24.65	0.16	
2.65081	13.90	39.44172	73.16	24.55	0.12	(VO) <sub>2</sub> P <sub>2</sub> O <sub>7</sub> <sup>1</sup>
2.56059	16.04	40.89228	84.45	23.62	0.06	
2.44202	10.78	42.97369	56.73	22.28	0.40	
2.34205	6.64	44.90563	34.98	21.03	0.08	
2.18966	1.61	48.22162	8.48	21.65	0.08	
2.17984	1.64	48.46138	8.62	21.59	0.16	
2.09220	26.39	50.62213	138.90	21.34	0.16	
2.03020	24.91	52.28291	131.13	21.23	0.08	
1.97714	2.31	53.79700	12.18	21.13	0.16	
1.93266	5.53	55.13903	29.09	21.04	0.48	
1.84247	9.74	58.08786	51.29	20.84	0.40	
1.78596	1.75	60.11142	9.24	20.70	0.24	
1.63482	6.29	66.34282	33.12	25.35	0.40	
1.59914	6.24	68.02198	32.85	24.46	0.16	
1.57768	14.75	69.07723	77.64	23.91	0.16	
1.47405	5.75	74.71957	30.28	27.37	0.48	
1.45866	6.31	75.64594	33.24	26.66	0.40	
1.43294	4.76	77.25152	25.07	26.86	0.20	
1.38217	4.29	80.65543	22.56	21.17	0.96	
1.35171	1.91	82.86570	10.08	16.86	0.64	
1.30127	2.01	86.84762	10.57	18.95	0.80	



Table 5.7: XRD data for the 0.6% Ru precalcined catalyst

Used Wavelength:	K-Alpha
K-Alpha1 wavelength (Å):	1.78897
K-Alpha2 wavelength (Å):	1.79285
K-Alpha2/K-Alpha1 intensity ratio:	0.5
K-Alpha wavelength (Å):	1.78897
Peak search parameter search:	As measured intensities:
Set created:	04/28/1999 12:06
Peak positions defined by:	Minimum of second derivative
Minimum peak tip width (°2 Theta):	0
Minimum peak tip width (°2 Theta):	1
Peak base width (°2 Theta)	2
Minimum significance	0.6

d-spacing (Å)	Relative intensity (%)	Angle (°2Theta)	Peak Height (counts/sec)	Background (counts/sec)	Tip width (°2Theta)	(phases)
7.9891	1.39	12.85696	12.02	32.12	0.06	
5.86532	8.22	17.54409	70.95	35.18	0.16	
5.65181	13.24	18.2124	114.24	34.49	0.56	(VO) <sub>2</sub> P <sub>2</sub> O <sub>7</sub> .2H <sub>2</sub> O <sup>1</sup>
4.79661	6.53	21.49514	56.32	27.06	0.08	
4.5013	12.07	22.92381	104.16	26.86	0.72	(VO) <sub>2</sub> P <sub>2</sub> O <sub>7</sub> .2H <sub>2</sub> O <sup>1</sup>
4.09729	1.8	25.21969	15.52	26.55	0.24	
3.66906	12.07	28.22073	104.13	28.59	0.16	(VO) <sub>2</sub> P <sub>2</sub> O <sub>7</sub> .2H <sub>2</sub> O <sup>1</sup>
3.27337	19.67	31.71677	169.71	29.95	0.4	
3.09764	11.26	33.5678	97.15	28.81	0.24	
2.9355	100	35.48174	862.89	27.63	0.12	(VO) <sub>2</sub> P <sub>2</sub> O <sub>7</sub> .2H <sub>2</sub> O <sup>1</sup>
2.78375	9.16	37.48592	79.07	26.39	0.16	VO(HPO <sub>4</sub> ).0.5H <sub>2</sub> O <sup>2</sup>
2.66622	6.05	39.20428	52.24	25.33	0.32	
2.60418	6.45	40.17799	55.62	24.73	0.4	
2.40086	12.87	43.74803	111.02	21.28	0.28	
2.34502	0.78	44.84561	6.77	20.37	0.14	
2.23033	5.32	47.28821	45.94	19.22	0.32	
2.11552	1.14	50.02537	9.85	17.93	0.8	
2.04775	4.24	51.80144	36.55	17.09	0.4	
2.02564	18.62	52.40944	160.63	16.8	0.1	
1.95748	3.02	54.38172	26.08	17.3	0.28	
1.8988	8.2	56.2084	70.8	19.42	0.2	
1.8547	17.12	57.66852	147.7	21.12	0.24	
1.77123	4.26	60.66346	36.75	24.6	0.48	
1.69078	0.66	63.88043	5.66	25.37	0.64	
1.65174	4.35	65.57709	37.57	22.02	0.32	
1.63402	5.74	66.37941	49.55	20.54	0.24	
1.60153	3.36	67.90662	29.01	17.73	0.2	
1.58535	0.96	68.69619	8.29	16.31	0.12	
1.54172	4.4	70.92726	37.98	16.06	0.16	
1.51604	3.68	72.31568	31.72	16.33	0.24	
1.46909	8.63	75.01521	74.47	16.84	0.24	
1.43228	2.69	77.29332	23.21	17.28	0.32	
1.4195	2.53	78.12088	21.82	17.44	0.4	

1.38143	2.14	80.70719	18.42	17.93	0.4
1.34739	2.8	83.19009	24.16	19.55	0.4
1.30979	2.82	86.14448	24.31	23.37	0.4

Table 5.8: XRD data for the 0.6% Ru calcined catalyst

Used Wavelength:	K-Alpha
K-Alpha1 wavelength (Å):	1.78897
K-Alpha2 wavelength (Å):	1.79285
K-Alpha2/K-Alpha1 intensity ratio:	0.5
K-Alpha wavelength (Å):	1.78897
Peak search parameter search:	As measured intensities:
Set created:	04/28/1999 12:06
Peak positions defined by:	Minimum of second derivative
Minimum peak tip width (°2 Theta):	0
Minimum peak tip width (°2 Theta):	1
Peak base width (°2 Theta)	2
Minimum significance	0.6

d-spacing (Å)	Relative intensity (%)	Angle (°2 Theta)	Peak Height (counts/sec)	Background (counts/sec)	Tip width (°2 Theta)
9.2587	4	11.08797	7.71	30.28	0.28
6.24082	7.46	16.48091	14.36	33.98	0.64
4.77933	20.41	21.57376	39.28	35.39	0.24
3.92321	22.03	26.35843	42.41	63.31	0.8
3.12534	100	33.26161	192.52	54.61	0.32
2.9784	62.88	34.95406	121.05	49.88	0.2
2.64241	10.17	39.5722	19.58	37.21	0.56
2.44412	9.36	42.93498	18.02	33.35	0.48
2.39702	12.97	43.82186	24.97	31.3	0.24
2.3405	10.29	44.93704	19.8	28.73	0.16
2.08278	26.13	50.86727	50.3	28.88	0.48
2.02833	25.21	52.33464	48.54	30.44	0.28
1.84557	8.25	57.98111	15.88	33.96	0.64
1.75938	2.35	61.11575	4.53	26.76	0.16
1.63047	4.63	66.54237	8.91	30.19	0.96
1.57485	14.46	69.21877	27.85	33	0.64
1.46981	6.55	74.97237	12.61	32.4	0.8
1.43154	6.77	77.34057	13.03	28.74	0.24

Table 5.9: XRD data for the used 0.6% Ru promoted catalyst

Used Wavelength:	K-Alpha
K-Alpha1 wavelength (Å):	1.78897
K-Alpha2 wavelength (Å):	1.79285
K-Alpha2/K-Alpha1 intensity ratio:	0.5
K-Alpha wavelength (Å):	1.78897
Peak search parameter search:	As measured intensities:

Set created:	04/28/1999 12:06
Peak positions defined by:	Minimum of second derivative
Minimum peak tip width (°2 Theta):	0
Minimum peak tip width (°2 Theta):	1
Peak base width (°2 Theta)	2
Minimum significance	0.6

d-spacing (Å)	Relative intensity (%)	Angle (°2 Theta)	Peak Height (counts/sec)	Background (counts/sec)	Tip width (°2 Theta)	
10.62858	2.42	9.65524	10.05	28.77	0.16	
7.06463	2.76	14.54797	11.46	26.78	0.48	
6.26179	8.47	16.42533	35.15	26.85	0.32	
5.67499	3.88	18.13737	16.11	26.91	0.64	
4.78607	13.32	21.54301	55.23	25.49	0.24	(VO) <sub>2</sub> P <sub>2</sub> O <sub>7</sub> <sup>3</sup>
3.86681	48.94	26.74998	202.95	44.11	0.8	(VO) <sub>2</sub> P <sub>2</sub> O <sub>7</sub> <sup>1</sup>
3.14085	100	33.09253	414.73	37.3	0.06	(VO) <sub>2</sub> P <sub>2</sub> O <sub>7</sub> <sup>1</sup>
2.97705	58.42	34.97043	242.3	37.46	0.32	
2.65092	13.03	39.43992	54.02	25.58	0.16	
2.4351	14.23	43.10188	59.02	24.68	0.56	
2.33773	5.43	44.9932	22.5	23	0.16	
2.09084	29.7	50.65741	123.16	25.56	0.32	
2.02627	22.87	52.39208	94.85	27.72	0.14	
1.93064	4.34	55.20151	17.98	33.52	0.96	
1.83851	9.35	58.22485	38.76	30.83	0.64	
1.71429	1.07	62.9033	4.43	22.61	0.8	
1.63517	4.31	66.32672	17.86	28.17	0.8	
1.59848	5.98	68.05395	24.8	27.18	0.16	
1.57822	15.82	69.05014	65.6	26.61	0.1	
1.47415	6.29	74.71414	26.1	27.96	0.64	
1.45869	6.42	75.64377	26.64	26.82	0.64	
1.43236	4.08	77.28842	16.93	24.8	0.32	
1.38818	5.78	80.23509	23.97	21.19	0.06	
1.37876	4.24	80.89603	17.57	20.38	0.8	
1.35164	2.88	82.87092	11.95	17.96	0.8	
1.29865	1.87	87.06736	7.76	20.64	0.8	
1.29066	0	87.74258	0	22.71	0.06	

Table 5.10: XRD data for the 1% Ru precalcined catalyst

Used Wavelength:	K-Alpha
K-Alpha1 wavelength (Å):	1.78897
K-Alpha2 wavelength (Å):	1.79285
K-Alpha2/K-Alpha1 intensity ratio:	0.5
K-Alpha wavelength (Å):	1.78897
Peak search parameter search:	As measured intensities:
Set created:	04/28/1999 12:06
Peak positions defined by:	Minimum of second derivative
Minimum peak tip width (°2	0

Theta):  
Minimum peak tip width (°2  
Theta): 1  
Peak base width (°2 Theta) 2  
Minimum significance 0.6

d-spacing (Å)	Relative intensity (%)	Angle (°2 Theta)	Peak Height (counts/sec)	Background (counts/sec)	Tip width (°2 Theta)	(phases)
8.72318	1.22	11.77101	10.16	30.93	0.12	
5.8383	8.85	17.62593	73.72	35.53	0.2	
5.68428	16.51	18.10747	137.45	35.38	0.24	(VO <sub>2</sub> )P <sub>2</sub> O <sub>7</sub> .2H <sub>2</sub> O <sup>1</sup>
4.78643	5.41	21.54137	45.07	27.57	0.16	
4.51824	13.68	22.83671	113.89	27.52	0.16	(VO <sub>2</sub> )P <sub>2</sub> O <sub>7</sub> .2H <sub>2</sub> O <sup>1</sup>
4.07501	2.04	25.35986	17.02	27.42	0.48	
3.65061	12.99	28.36633	108.16	31.02	0.36	(VO <sub>2</sub> )P <sub>2</sub> O <sub>7</sub> .2H <sub>2</sub> O <sup>1</sup>
3.28267	22.55	31.62453	187.73	31.07	0.28	VO(HPO <sub>4</sub> ).0.5H <sub>2</sub> O <sup>2</sup>
3.10116	10.81	33.52858	90.02	30.65	0.2	
2.93422	100	35.49767	832.64	30.21	0.14	(VO <sub>2</sub> )P <sub>2</sub> O <sub>7</sub> .2H <sub>2</sub> O <sup>1</sup>
2.78521	8.31	37.46554	69.2	29.77	0.4	
2.65941	5.18	39.30891	43.16	29.36	0.32	
2.60333	6.42	40.19168	53.47	29.16	0.32	
2.39551	11.89	43.85091	99.01	23.98	0.14	
2.33889	1.82	44.96977	15.15	22.19	0.2	
2.22914	5.12	47.31487	42.61	21.63	0.32	
2.12261	1.67	49.84693	13.88	21.03	0.48	
2.0482	4.28	51.78917	35.62	20.57	0.24	
2.02789	16.22	52.3468	135.06	20.44	0.1	
1.95526	2.6	54.44861	21.65	22.19	0.32	
1.89852	7.01	56.21754	58.37	28.75	0.2	
1.85402	16.34	57.69173	136.04	35.27	0.28	
1.76154	2.87	61.03266	23.89	30.05	0.56	
1.69248	0.84	63.80868	7.01	26.16	0.64	
1.6485	4.81	65.72215	40.08	23.48	0.24	
1.63372	5.85	66.39298	48.7	22.55	0.32	
1.60327	3.08	67.82281	25.67	20.54	0.2	
1.54239	3.33	70.89137	27.75	19.01	0.24	
1.51739	3.05	72.24114	25.43	19.01	0.2	
1.46798	8.83	75.08173	73.53	19.02	0.32	
1.43262	2.89	77.2717	24.1	19.94	0.24	
1.41994	3.03	78.09205	25.2	20.92	0.24	
1.37526	1.97	81.14498	16.37	20.01	0.24	
1.34733	3.57	83.195	29.68	19.73	0.24	
1.30949	2.46	86.16911	20.46	22.51	0.96	

Table 5.11: XRD data for the 1% Ru calcined catalyst

Used Wavelength:	K-Alpha
K-Alpha1 wavelength (Å):	1.78897
K-Alpha2 wavelength (Å):	1.79285
K-Alpha2/K-Alpha1 intensity ratio:	0.5
K-Alpha wavelength (Å):	1.78897
Peak search parameter search:	As measured intensities:
Set created:	04/28/1999 12:06
Peak positions defined by:	Minimum of second derivative
Minimum peak tip width (°2 Theta):	0
Minimum peak tip width (°2 Theta):	1
Peak base width (°2 Theta)	2
Minimum significance	0.6

d-spacing (Å)	Relative intensity (%)	Angle (°2 Theta)	Peak Height (counts/sec)	Background (counts/sec)	Tip width (°2 Theta)
8.11693	6.98	12.65365	7.25	32.81	0.1
6.19707	7.89	16.59807	8.19	35.14	0.32
4.76272	9.34	21.64991	9.7	44.51	0.48
3.95683	11.71	26.13047	12.15	64.36	0.96
3.52572	8.28	29.3934	8.59	60.64	0.24
3.12526	81.4	33.26247	84.48	62.94	0.48
2.9704	52.92	35.05122	54.92	58.94	0.32
2.6396	8.22	39.61607	8.53	45.85	0.64
2.3377	18.22	44.99375	18.91	35.66	0.2
2.07593	22.6	51.04724	23.45	34.08	0.96
2.02873	100	52.32347	103.77	34.86	0.24
1.83538	3.68	58.334	3.82	36.53	0.8
1.46916	4.11	75.01147	4.27	33.36	0.96
1.43113	20.62	77.36706	21.4	28.96	0.24

Table 5.12: XRD data for the used 1% Ru promoted catalyst

Used Wavelength:	K-Alpha
K-Alpha1 wavelength (Å):	1.78897
K-Alpha2 wavelength (Å):	1.79285
K-Alpha2/K-Alpha1 intensity ratio:	0.5
K-Alpha wavelength (Å):	1.78897
Peak search parameter search:	As measured intensities:
Set created:	04/28/1999 12:06
Peak positions defined by:	Minimum of second derivative
Minimum peak tip width (°2 Theta):	0
Minimum peak tip width (°2 Theta):	1
Peak base width (°2 Theta)	2
Minimum significance	0.6

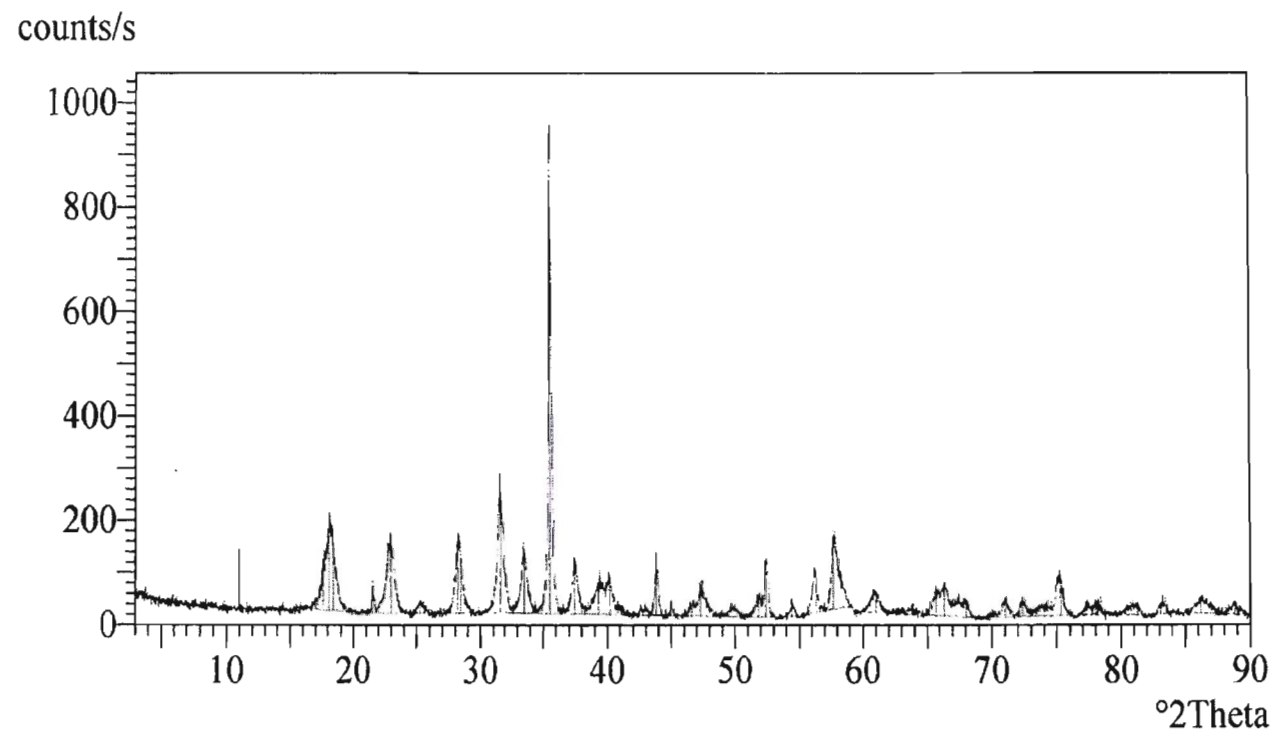
d-spacing (Å)	Relative intensity (%)	Angle (°2Theta)	Peak Height (counts/sec)	Background (counts/sec)	Tip width (°2Theta)	Phases
6.65671	1.98	15.44474	13.44	24.71	0.24	
6.25228	7.13	16.45048	48.32	24.23	0.24	
5.71025	3.27	18.02443	22.19	23.47	0.32	
4.78351	10.92	21.55468	74.01	23.51	0.2	(VO) <sub>2</sub> P <sub>2</sub> O <sub>7</sub> <sup>3</sup>
3.84728	52.02	26.88829	352.49	43.26	0.4	(VO) <sub>2</sub> P <sub>2</sub> O <sub>7</sub> <sup>1</sup>
3.1294	100	33.2172	677.66	34.65	0.18	
2.97566	49.01	34.98729	332.11	31.96	0.16	β-VOPO <sub>4</sub> <sup>3</sup>
2.82336	1.4	36.94085	9.5	28.98	0.48	
2.7739	0.96	37.624	6.49	27.94	0.1	
2.65595	12.41	39.3621	84.12	25.94	0.2	
2.57906	1.35	40.58646	9.13	24.66	0.04	
2.42741	12.13	43.24527	82.17	22.38	0.28	(VO) <sub>2</sub> P <sub>2</sub> O <sub>7</sub> <sup>3</sup>
2.33917	4.44	44.96406	30.07	20.97	0.2	
2.24343	1.33	46.99542	9.04	20.33	0.8	
2.18708	1	48.28214	6.77	20.31	0.8	
2.09103	23.3	50.6525	157.89	21.14	0.16	
2.02446	16.66	52.44233	112.93	22.05	0.12	
1.92742	7.58	55.30162	51.38	23.51	0.24	
1.83867	9.44	58.21953	63.95	24.99	0.48	
1.70723	1.04	63.19371	7.04	22.3	0.64	
1.67001	0.18	64.77106	1.19	22.49	0.12	
1.63333	5.5	66.41107	37.28	22.95	0.4	
1.59544	4.58	68.20135	31.04	23.46	0.16	
1.57589	14.05	69.16662	95.18	23.73	0.2	
1.51119	1.36	72.58453	9.22	20.26	0.8	
1.47338	8.15	74.75975	55.23	19.6	0.32	
1.45639	7.21	75.78463	48.84	19.3	0.32	
1.43085	3.24	77.38478	21.95	18.82	0.28	
1.41587	2.52	78.3596	17.06	18.53	0.64	
1.3819	4.85	80.67439	32.86	17.83	0.48	
1.34959	1.88	83.02482	12.73	17.13	0.64	
1.30231	1.39	86.76162	9.41	19.6	0.64	



Table 5.13 Showing Phases of VPO Catalysts

Phase	Description
$\beta - \text{VOPO}_4$ <sup>1</sup>	Isostructural with $\beta - \text{VOSO}_4$ ; V in the 5+ oxidation state. Features corner-sharing distorted $\text{VO}_6$ octahedra
$\alpha - \text{VOPO}_4$	Isostructural with $\alpha - \text{VOSO}_4$ ; V in 5+ oxidation state. Features corner-sharing distorted $\text{VO}_6$ octahedra
$(\text{VO})_2\text{P}_2\text{O}_7 \cdot 2\text{H}_2\text{O}$ or the $\alpha$ - phase	Often cited as a precursor; decomposed at $\approx 380^\circ\text{C}$
$(\text{VO})_2\text{P}_2\text{O}_7$	V in the 4+ oxidation state. Features edge-sharing $\text{VO}_6$ octahedra
$\beta$ - phase	Said to be the $\text{V}^{4+}$ containing part of the B-phase. Tri-polyphosphate structure assigned on the basis of IR spectra.
$\text{VO}(\text{PO}_3)_2$	Present in VPO catalysts with P:V ratio close to 2:1

<sup>1</sup> B. K. Hodnett, Catal. Rev. – Sci. Eng., 27(3), 1985, 373-424



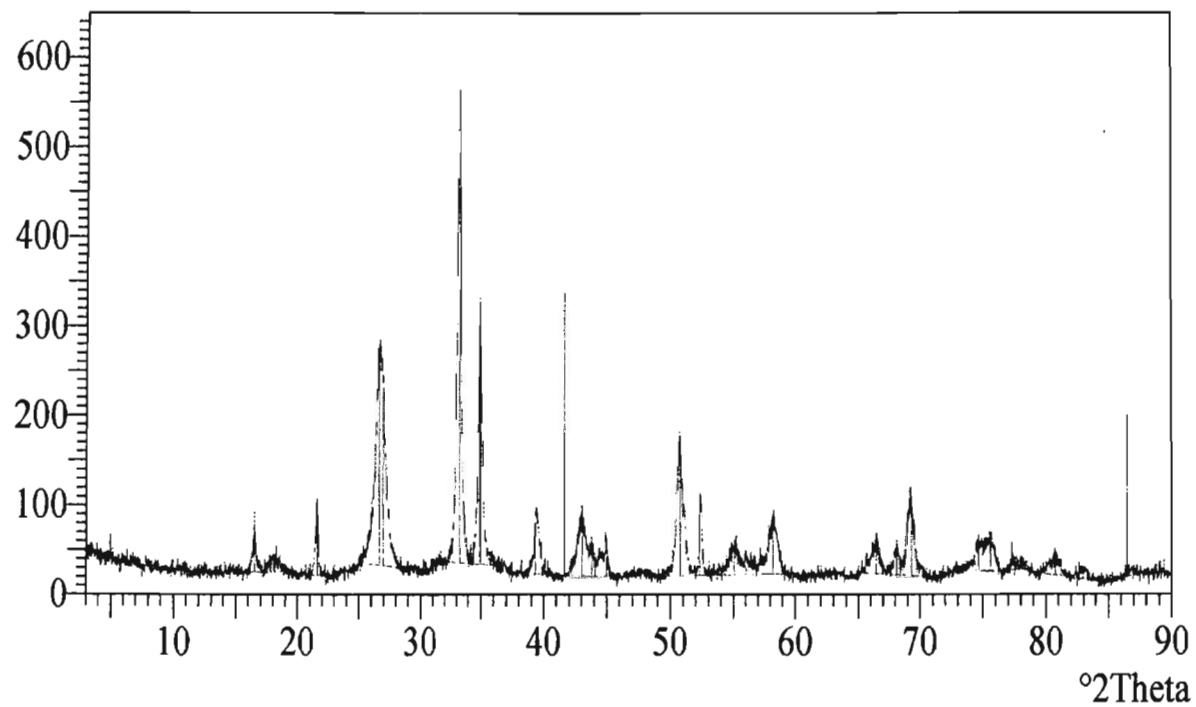
2°Theta	Phase
22.92, 28.12, 35.49	$(\text{VO})_2\text{P}_2\text{O}_7$ <sup>1</sup>
33.50	$\alpha\text{-VOPO}_4$ <sup>3</sup>
31.61	$\text{VO}(\text{HPO}_4) \cdot 0.5\text{H}_2\text{O}$ <sup>2</sup>

Philips Analytical

Figure 5.1: XRD spectrum of undoped catalyst precursor



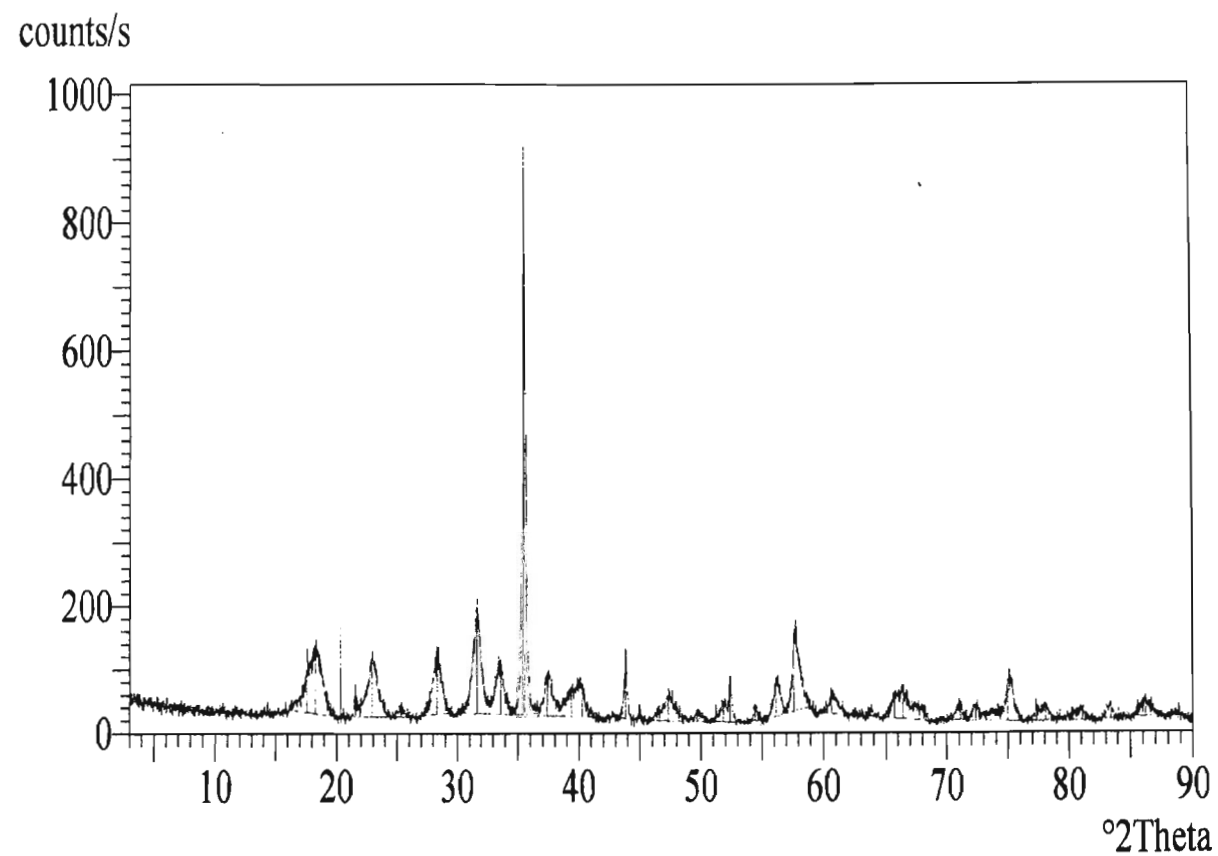
counts/s



2°Theta	Phase
16.48, 18.15, 21.58, 33.26, 34.86	$(VO)_2P_2O_7$ <sup>1</sup>
26.62	$VO(PO_3)_2$ <sup>3</sup>

Philips Analytical

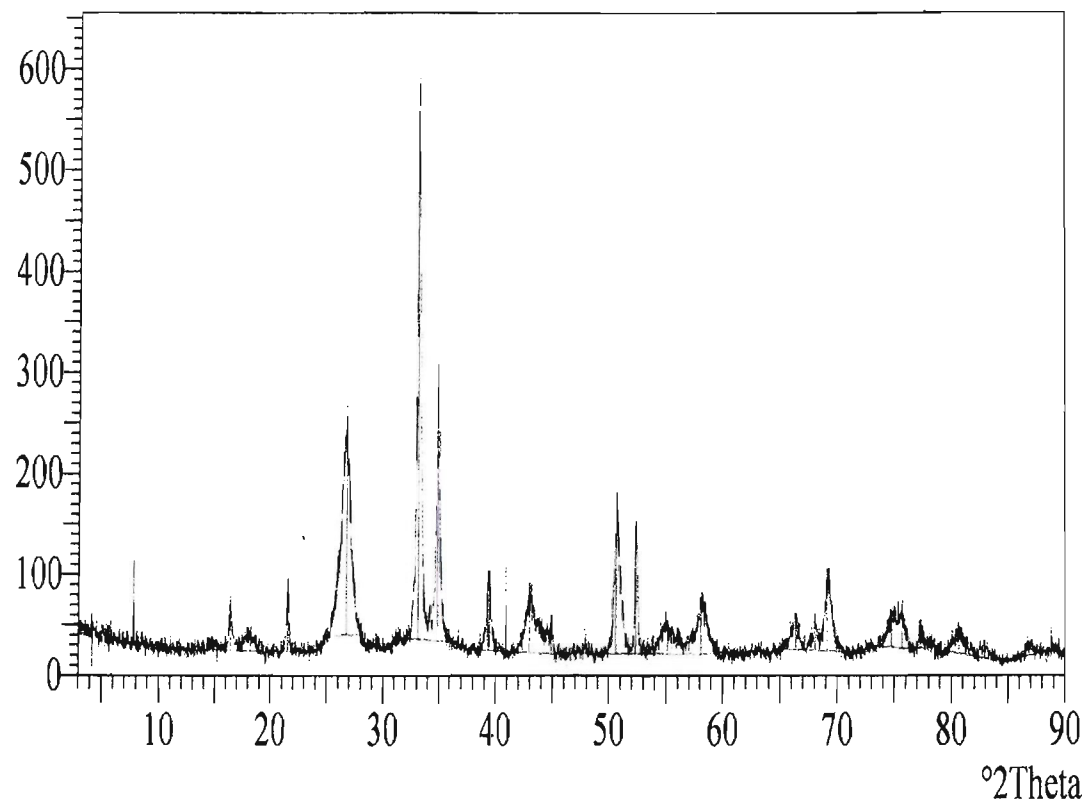
Figure 5.2: XRD spectrum of used undoped catalyst



2° theta	phases
18.24, 22.86, 35.49	$(\text{VO})_2\text{P}_2\text{O}_7^1$
31.60	$\text{VO}(\text{HPO}_4)0.5\text{H}_2\text{O}^2$

Figure 5.3: XRD spectrum of 0.2% Ru promoted catalyst precursor

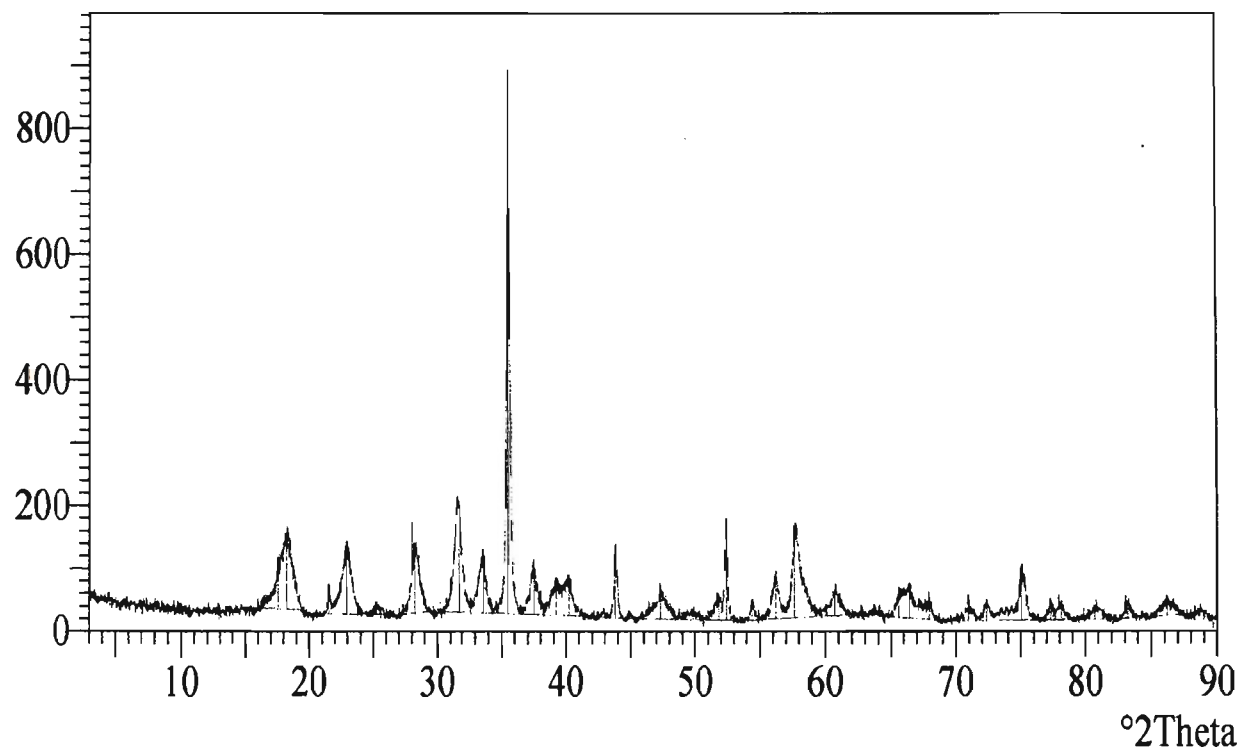
counts/s



2° theta	Phases
26.72, 33.10, 34.89, 39.44	(VO) <sub>2</sub> P <sub>2</sub> O <sub>7</sub>

Figure 5.4: XRD spectrum of 0.2% Ru promoted used catalyst

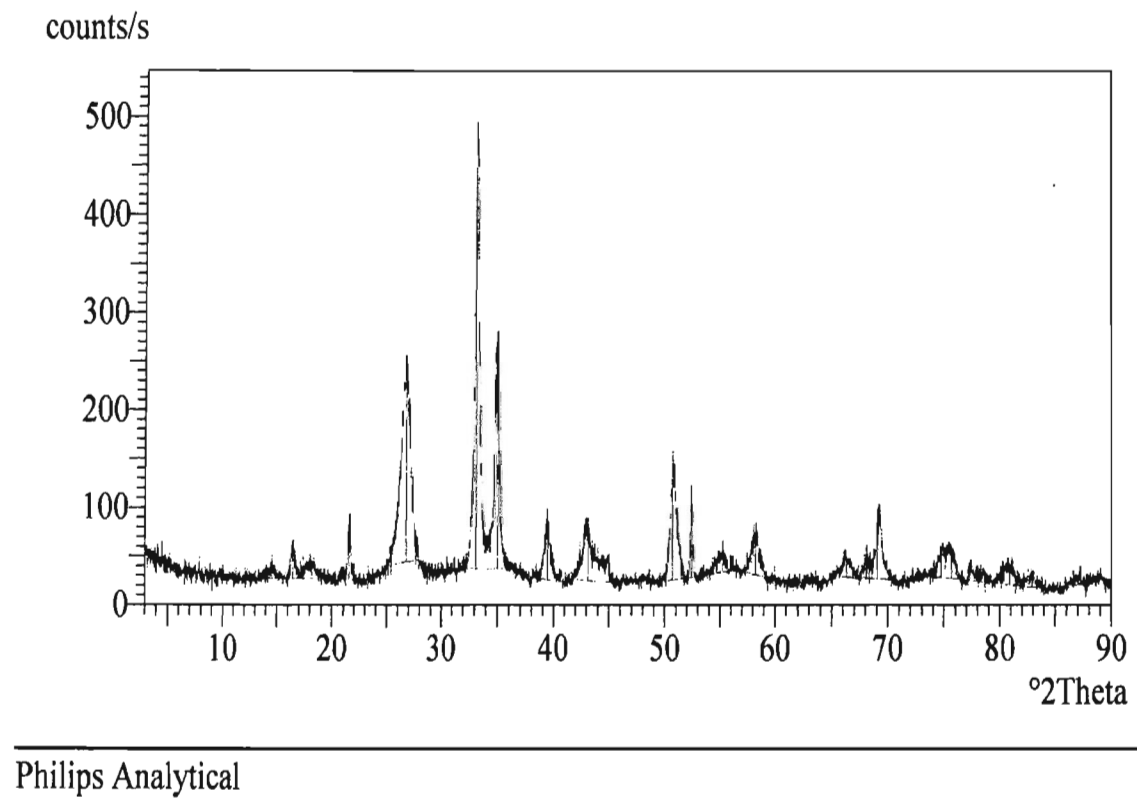
counts/s



2° theta	Phases
18.21, 22.92, 28.22, 35.48	(VO) <sub>2</sub> P <sub>2</sub> O <sub>7</sub> ·2H <sub>2</sub> O <sup>1</sup>
37.48	VO(HPO) <sub>4</sub> ·0.5H <sub>2</sub> O <sup>2</sup>

Philips Analytical

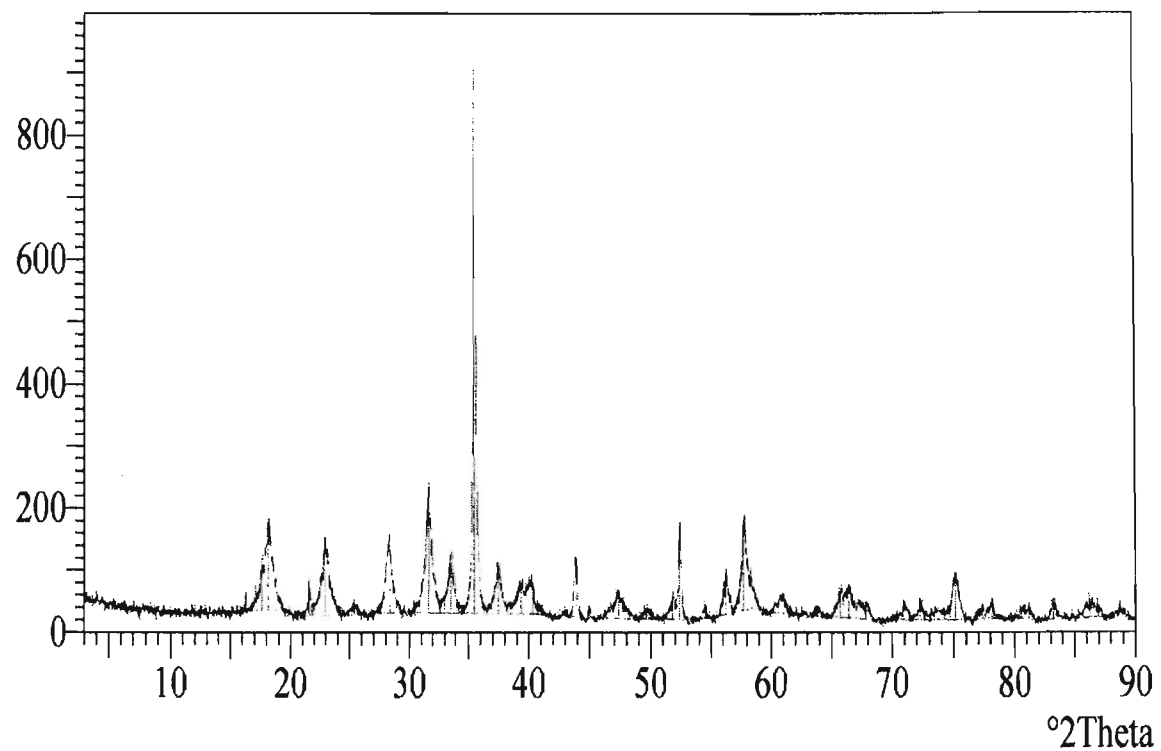
Figure 5.5: XRD spectrum of 0.6% Ru promoted catalyst precursor



2° theta	Phases
21.54, 26.74, 33.09	(VO) <sub>2</sub> P <sub>2</sub> O <sub>7</sub> <sup>3</sup>

Figure 5.6: XRD spectrum of 0.6% Ru promoted used catalyst

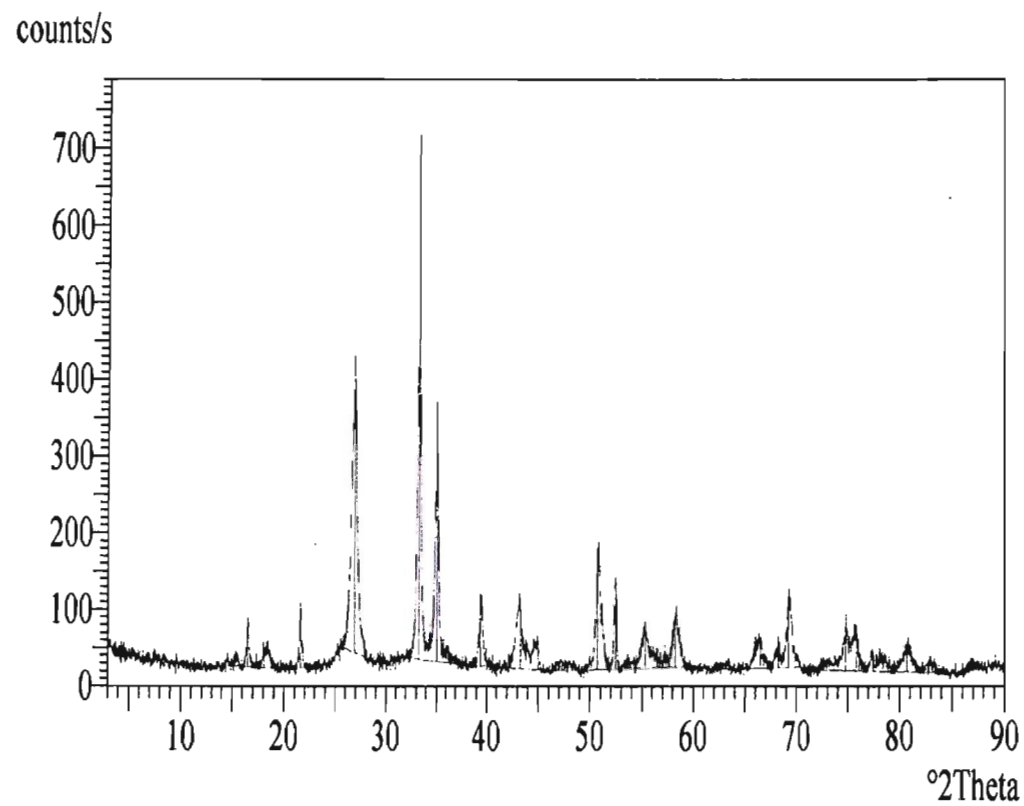
counts/s



Philips Analytical

2° theta	Phase
18.10, 22.83, 28.36, 35.49	$(\text{VO})_2\text{P}_2\text{O}_7 \cdot 5\text{H}_2\text{O}^1$
31.62	$\text{VO}(\text{HPO}_4 \cdot 0.5\text{H}_2\text{O})^2$

Figure 5.7: XRD spectrum of 1% Ru promoted precursor



2° theta	phase
21.55, 43.24	$(\text{VO})_2\text{P}_2\text{O}_7^3$
34.98	$\beta\text{-VOPO}_4^3$
33.21	$(\text{VO})_2\text{P}_2\text{O}_7^1$

Philips Analytical

Figure 5.8: XRD spectrum of 1% Ru promoted used catalyst

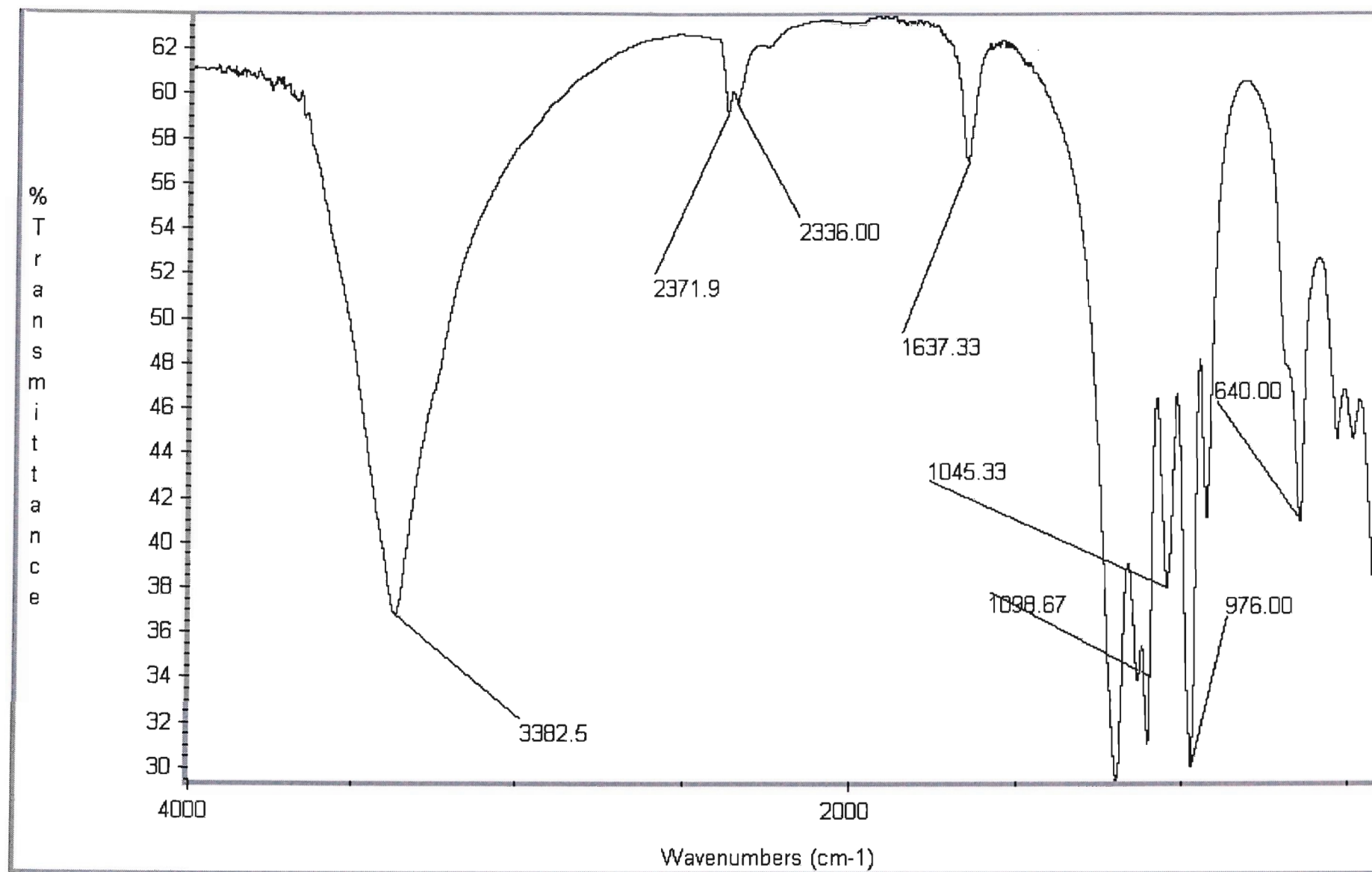


Figure 5.9: FTIR spectrum of undoped catalyst of the precalcined stage.



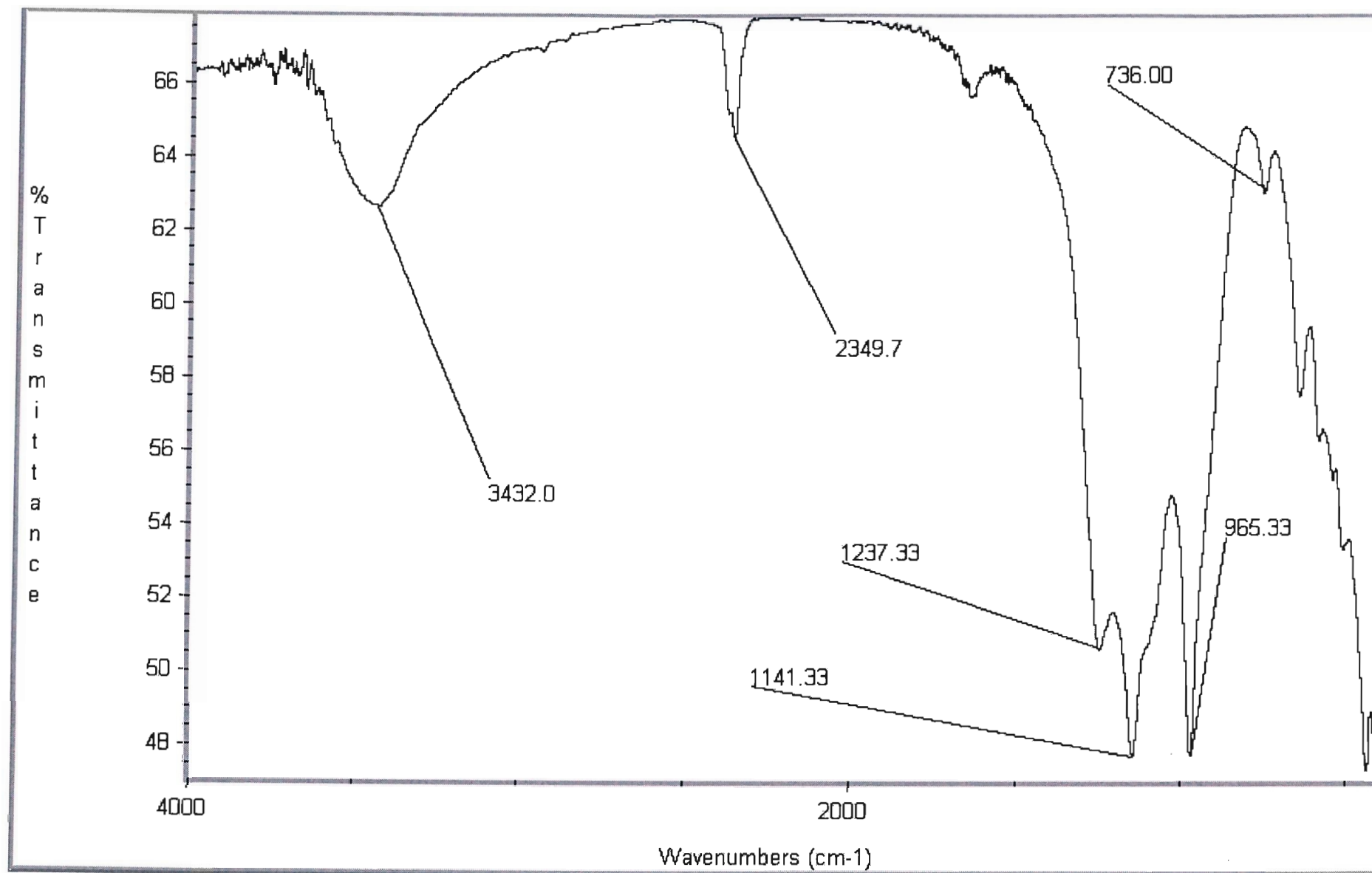


Figure 5.10: FTIR spectrum of undoped catalyst of the calcined stage.

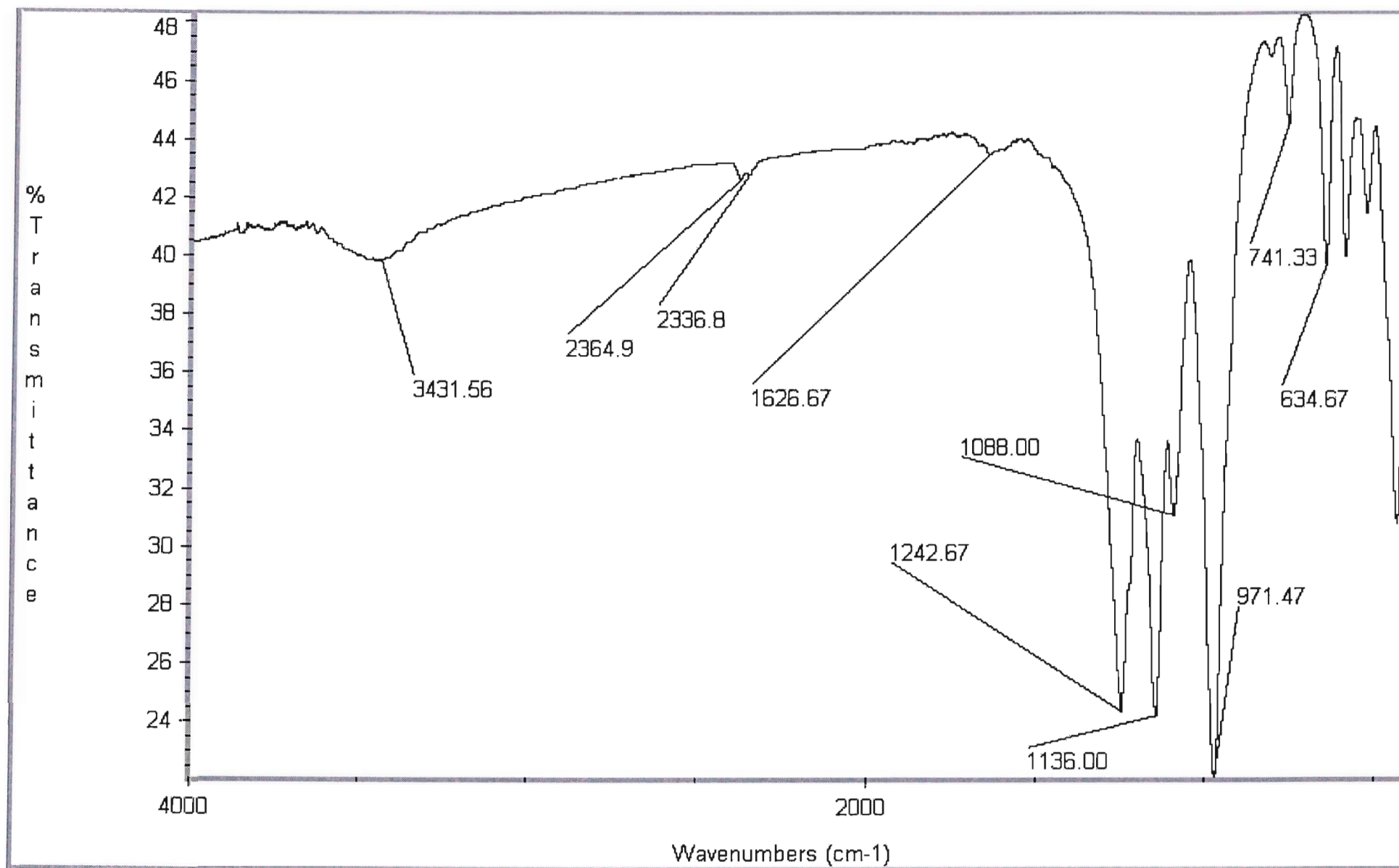


Figure 5.11: FTIR spectrum of the undoped catalyst of the used stage

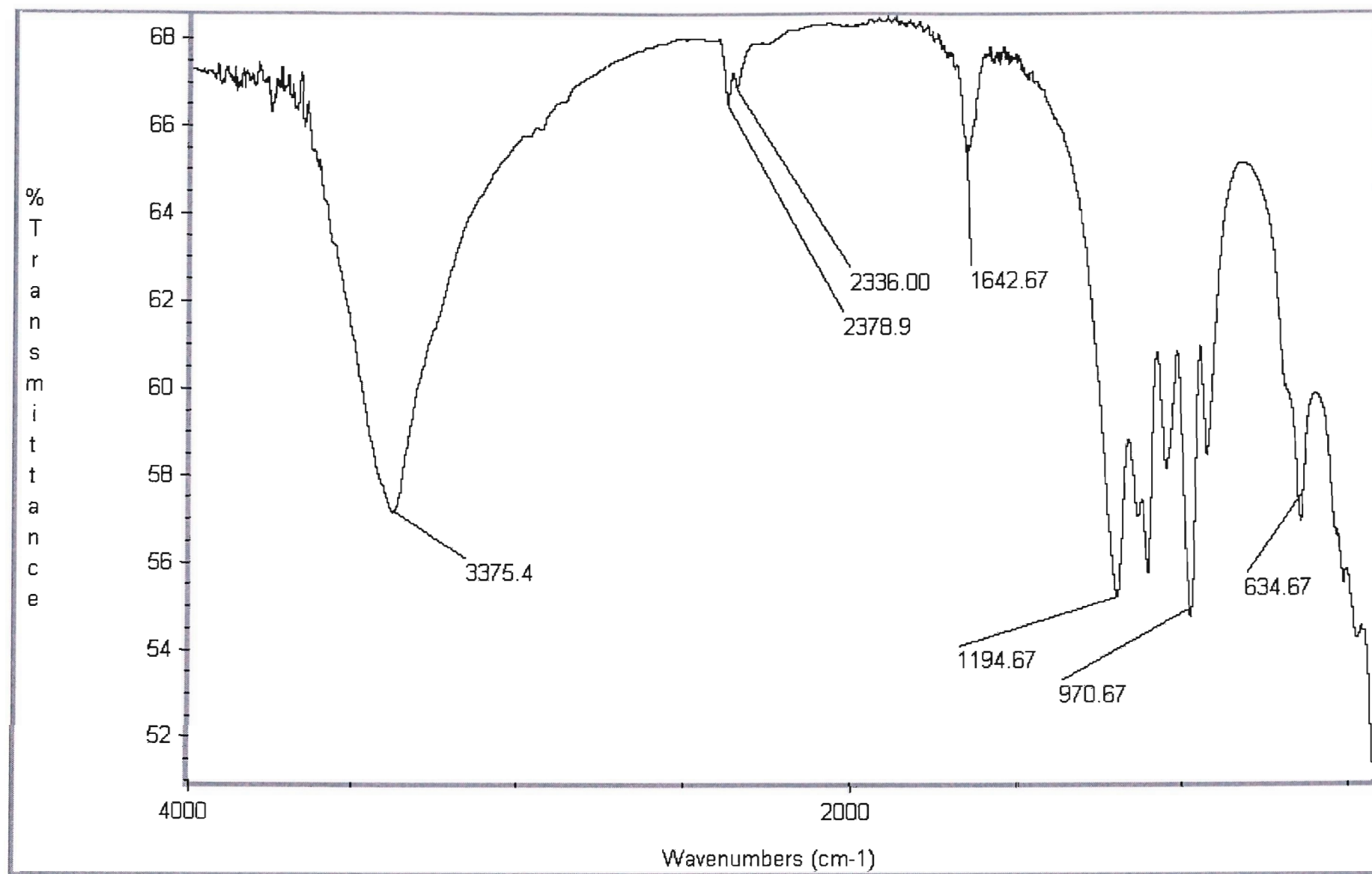


Figure 5.12: FTIR spectrum of 0.2% Ru promoted catalyst in the precursor stage.

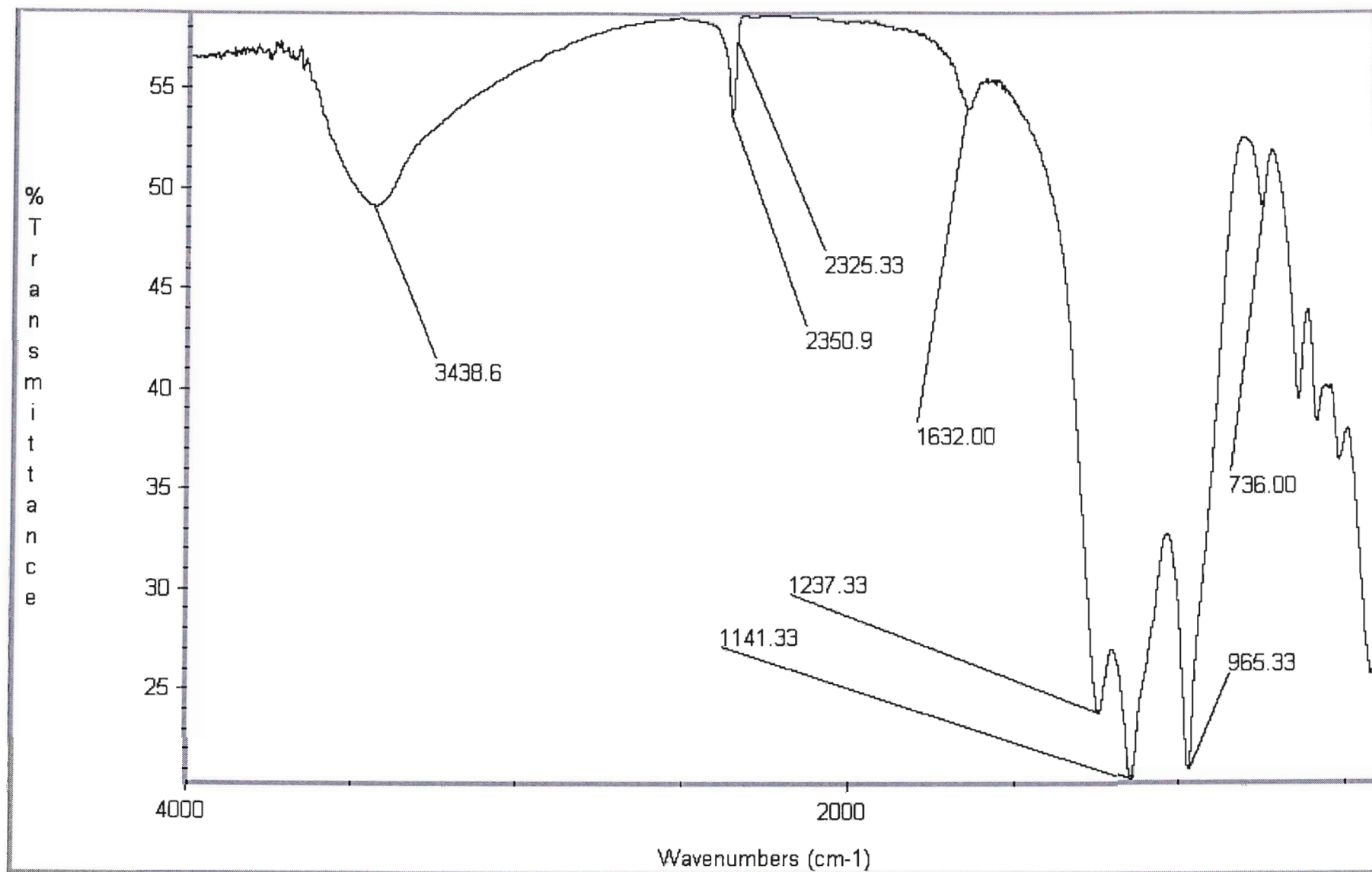


Figure 5.13: FTIR spectrum of the 0.2% Ru promoted catalyst of the calcined stage.

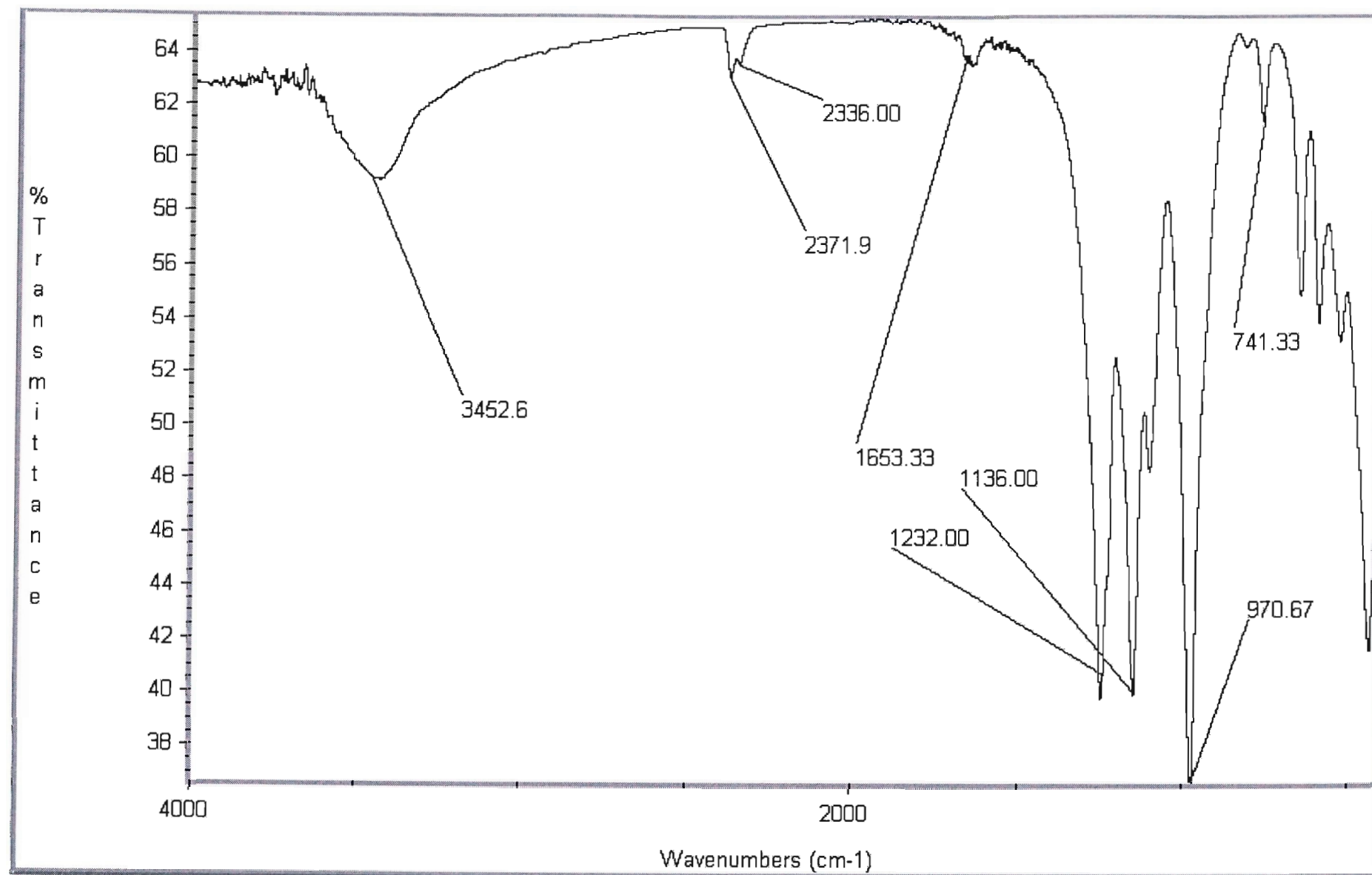


Figure 5.14: FTIR spectrum of the 0.2% Ru promoted catalyst of the used stage

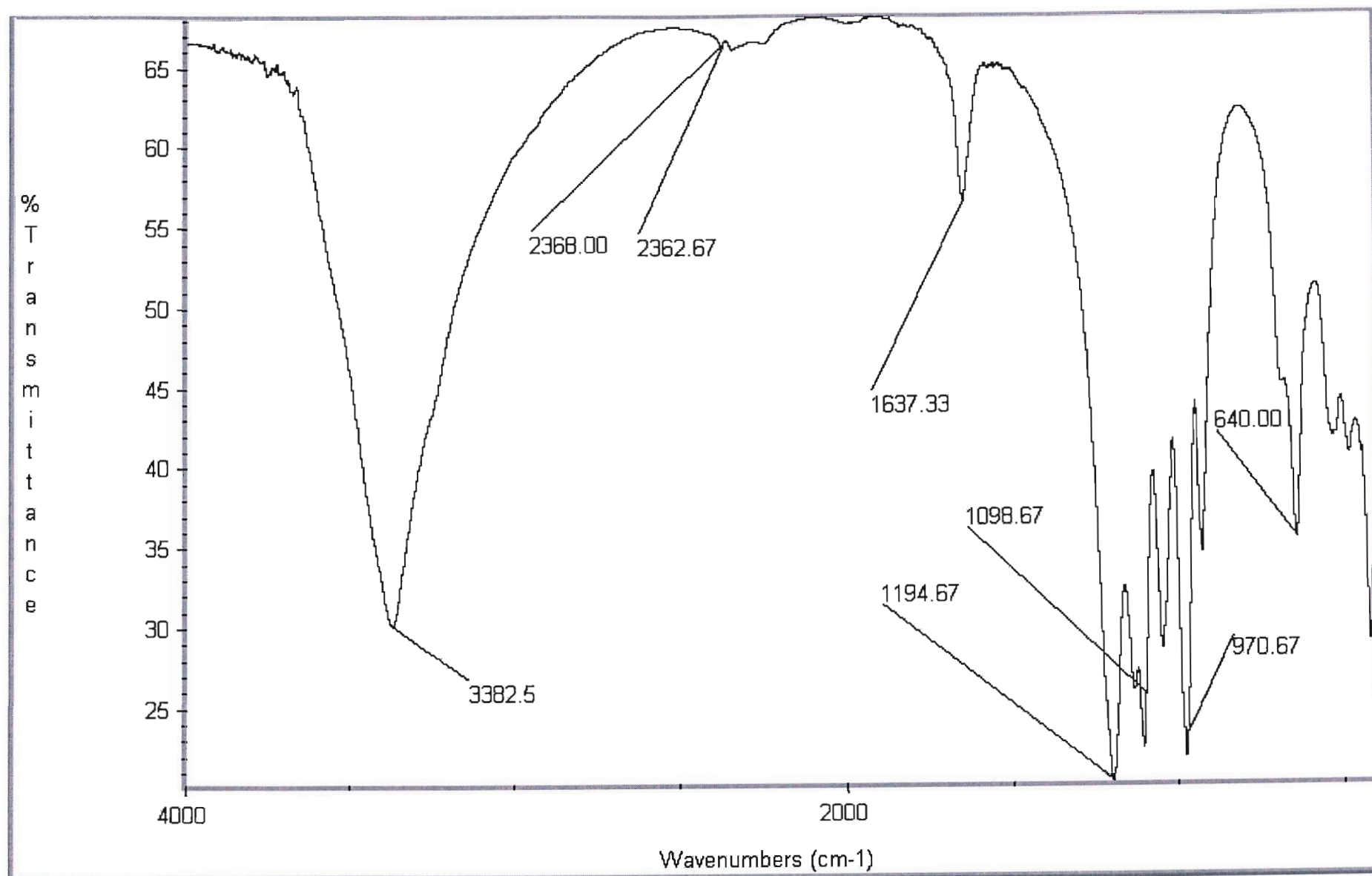


Figure 5.15: FTIR spectrum of the 0.6% Ru promoted catalyst of the precursor stage.

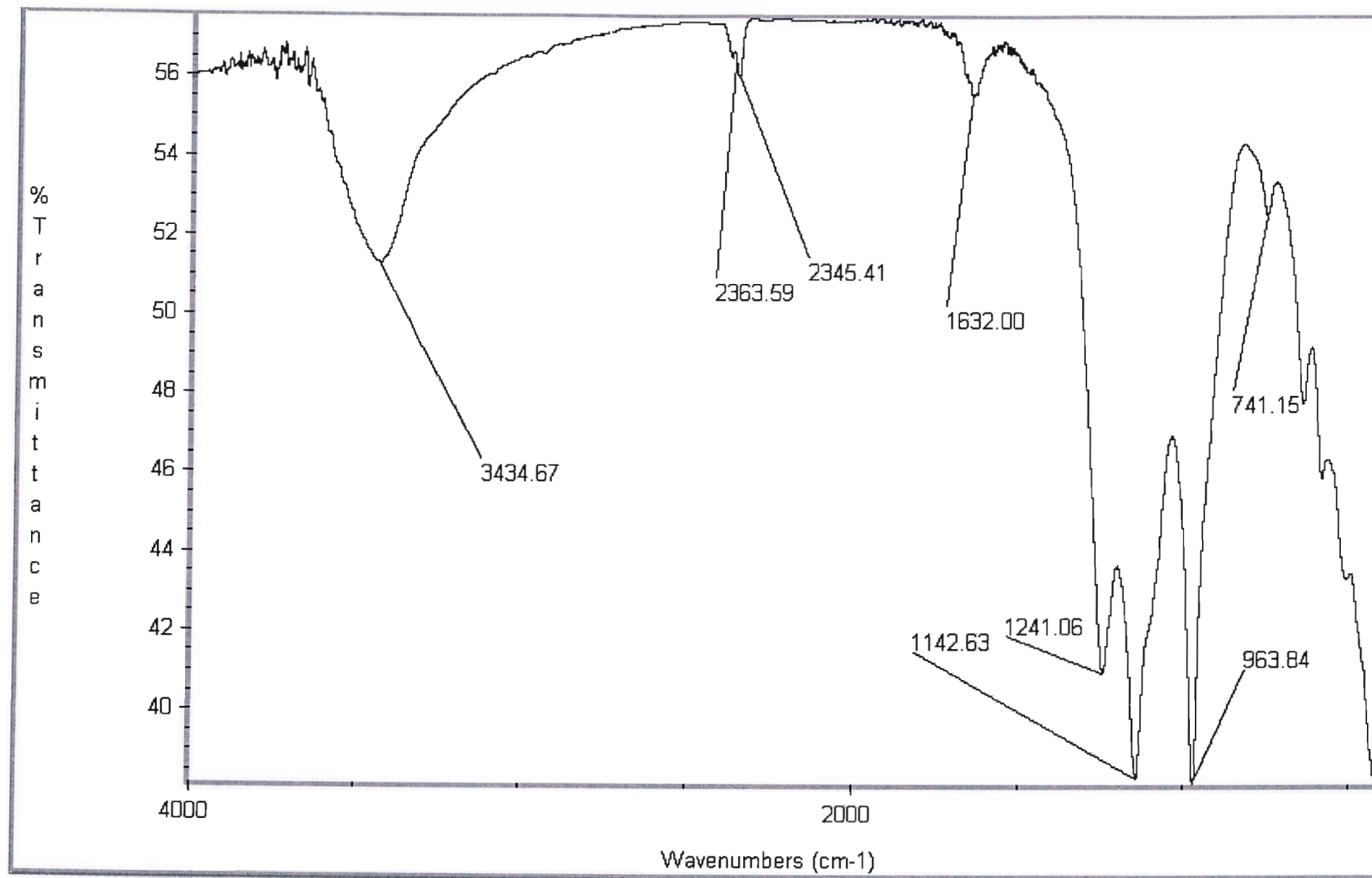


Figure 5.16: FTIR spectrum of the 0.6% Ru promoted catalyst of the calcined stage.

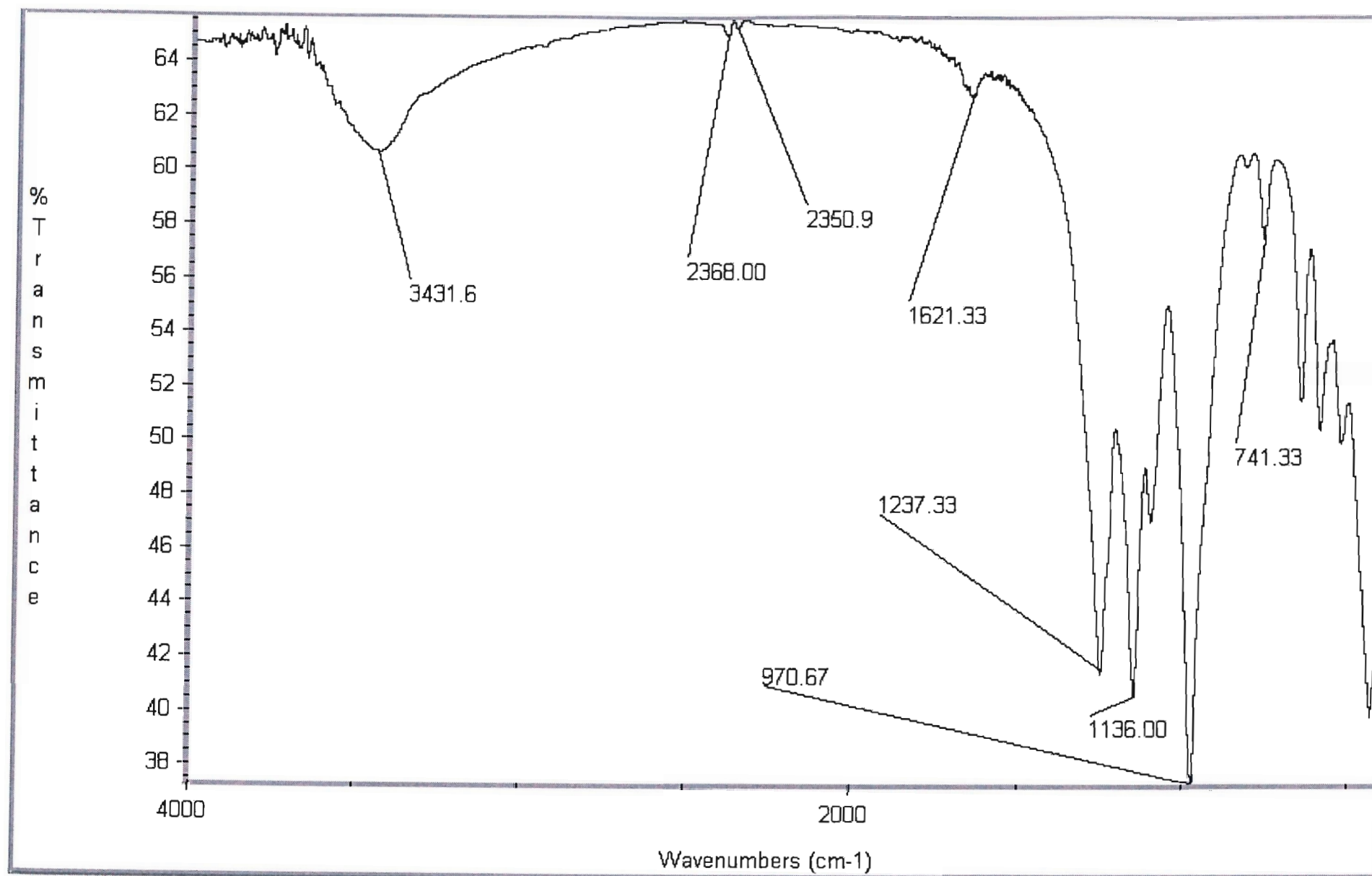


Figure 5.17: FTIR spectrum of the 0.6% Ru promoted catalyst of the used stage



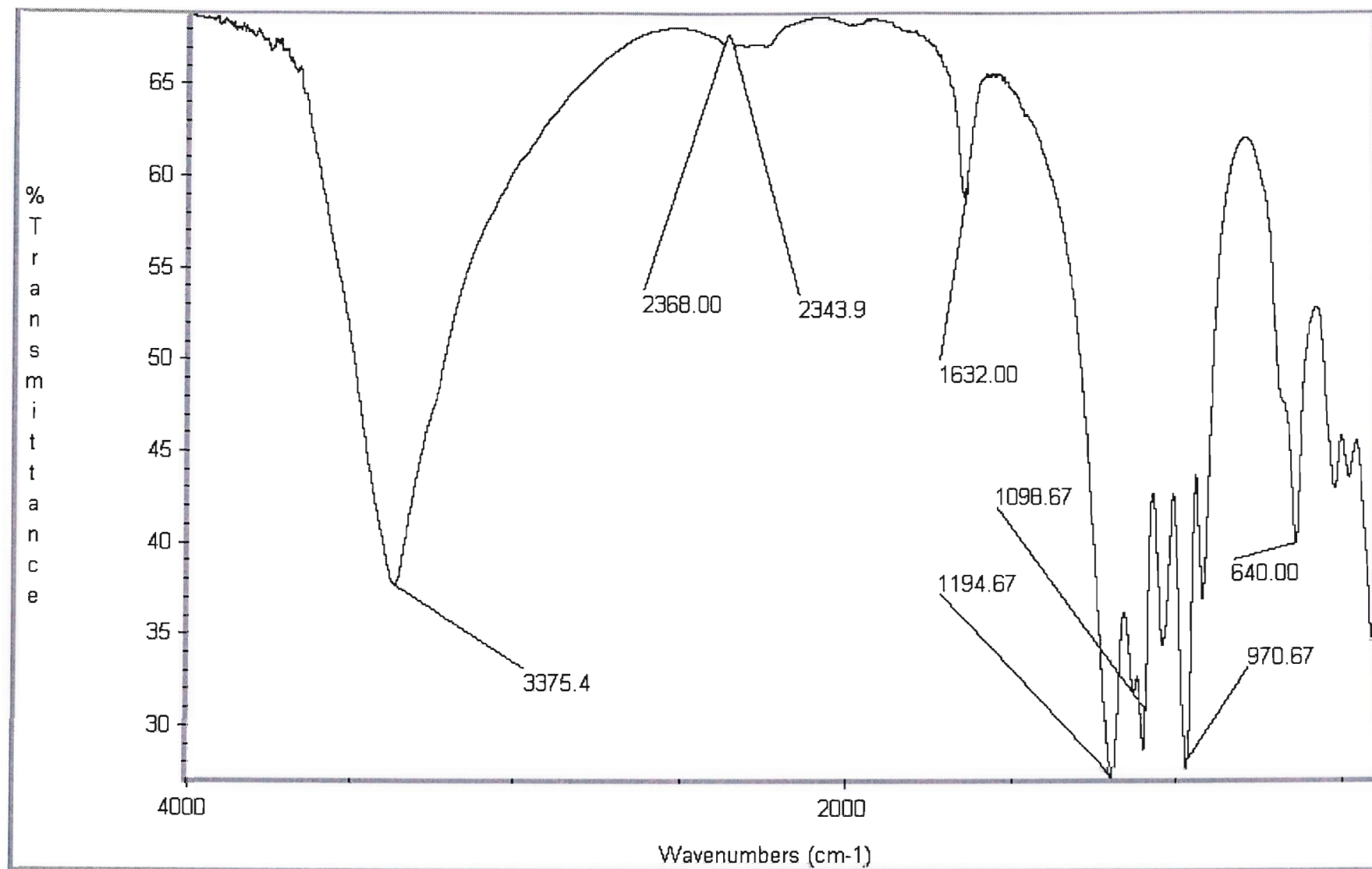


Figure 5.18: FTIR spectrum of the 1% Ru promoted catalyst of the precursor stage.

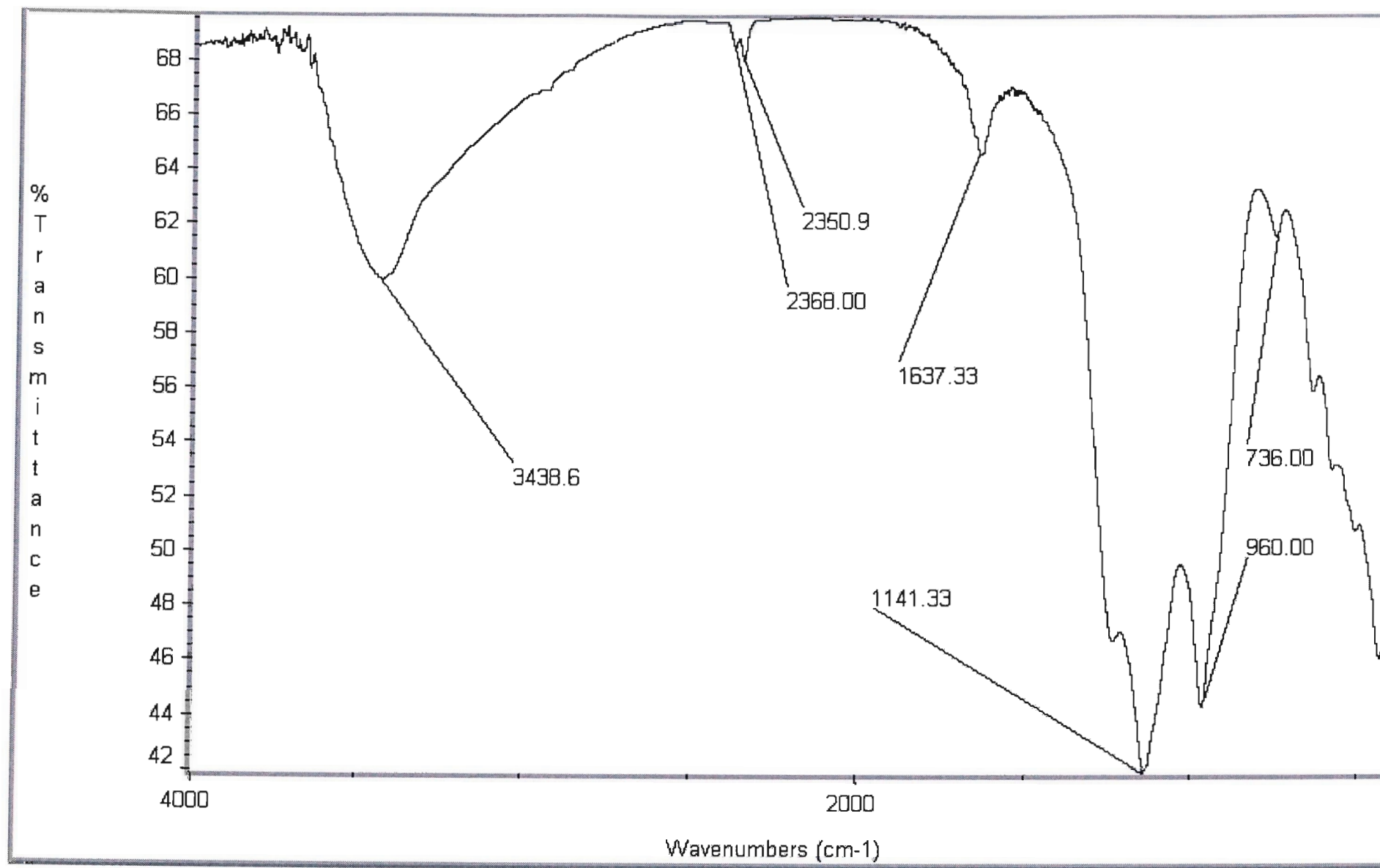


Figure 5.19: FTIR spectrum of the 1% Ru promoted catalyst of the calcined stage.

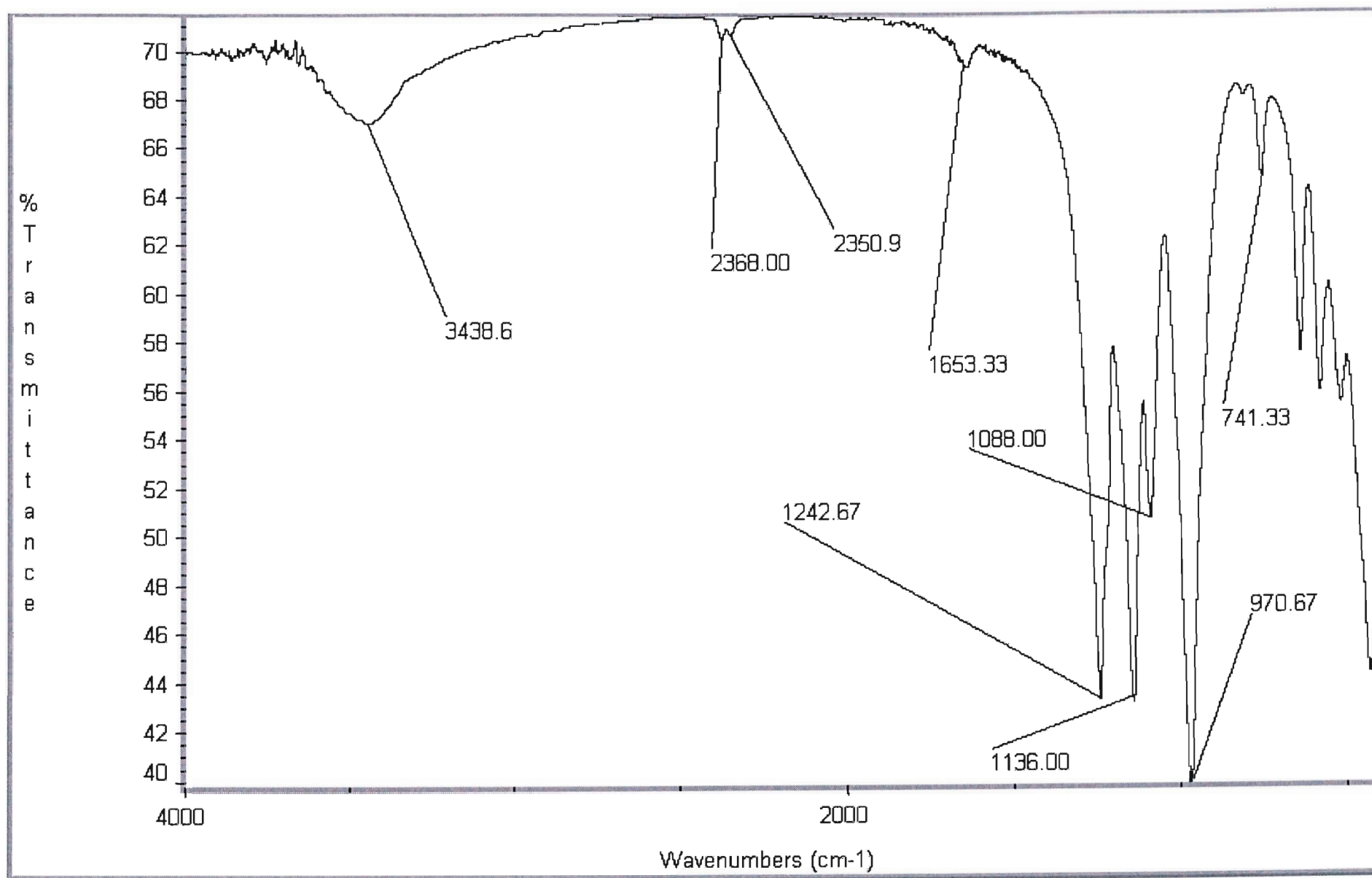


Figure 5.20: FTIR spectrum of the 1% Ru promoted catalyst of the used stage

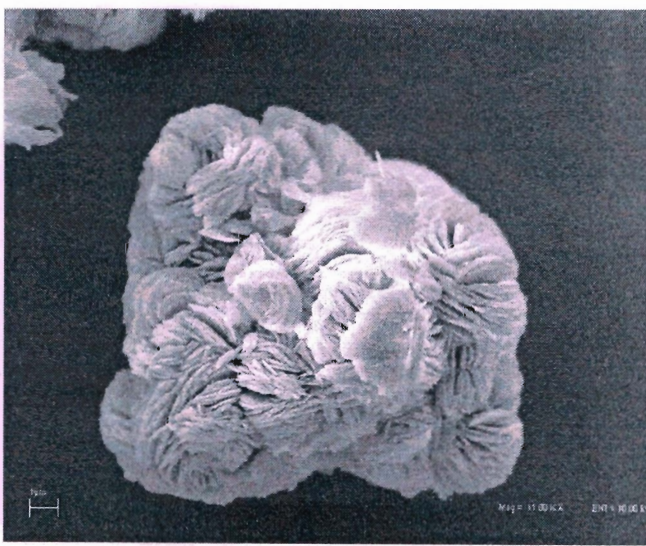
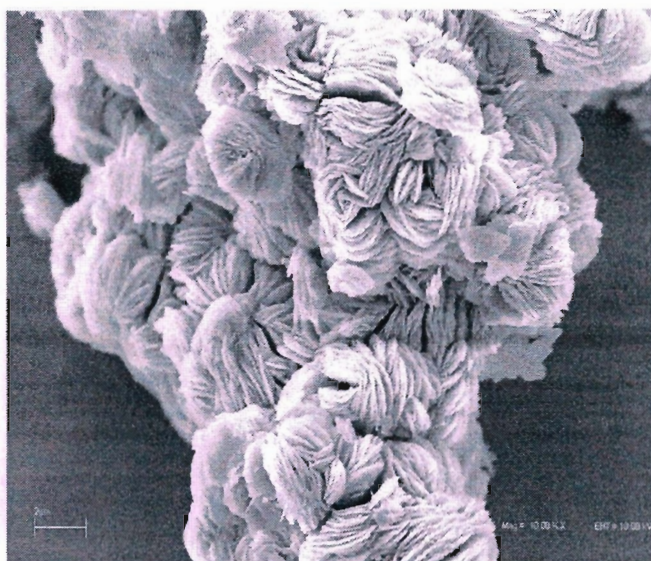
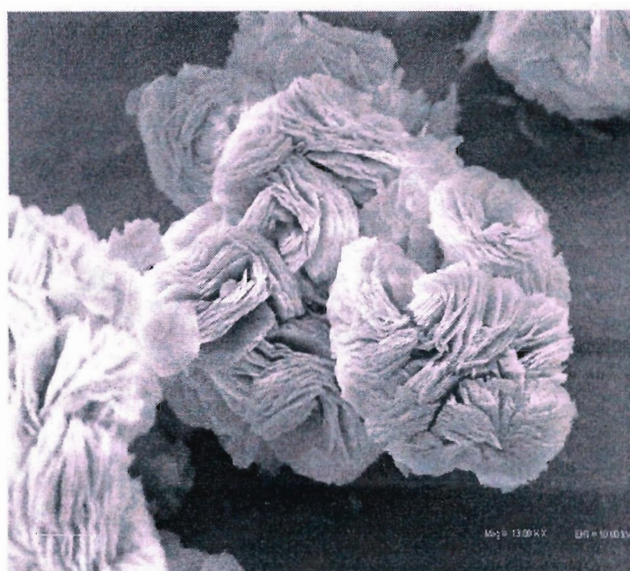


Figure 5.21: SEM images of undoped catalyst precursor



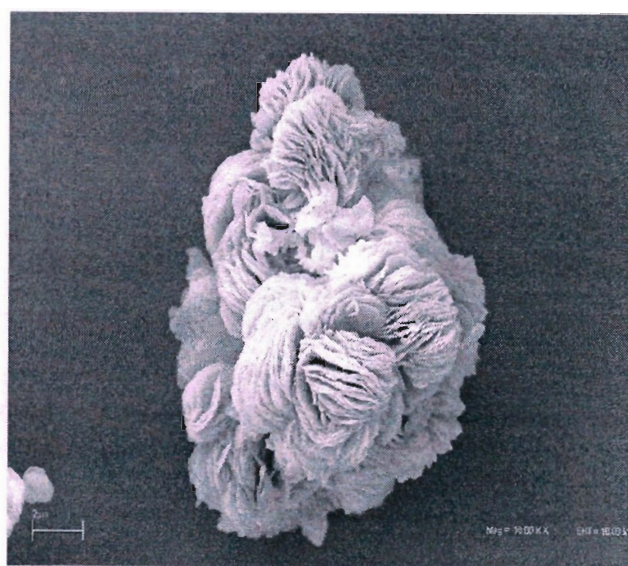
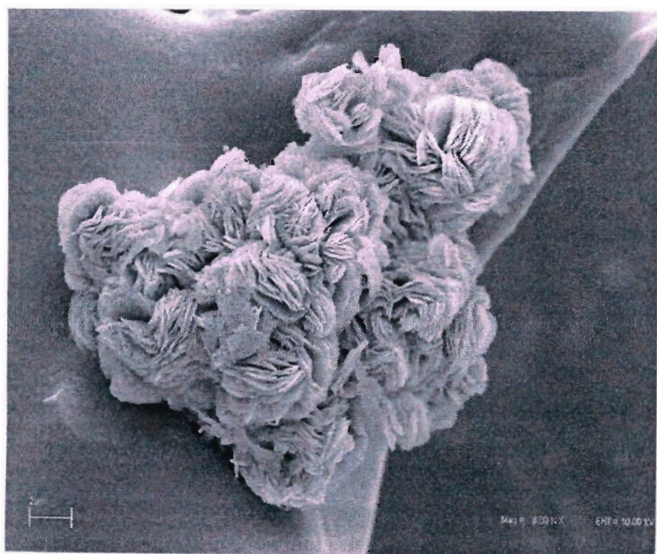
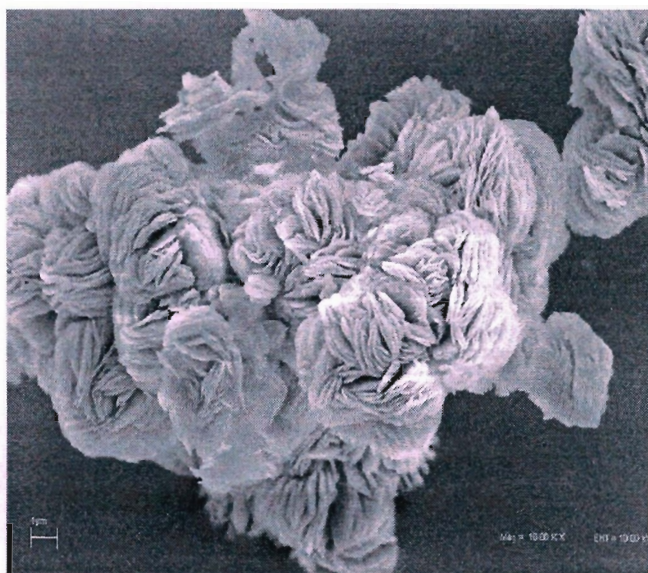
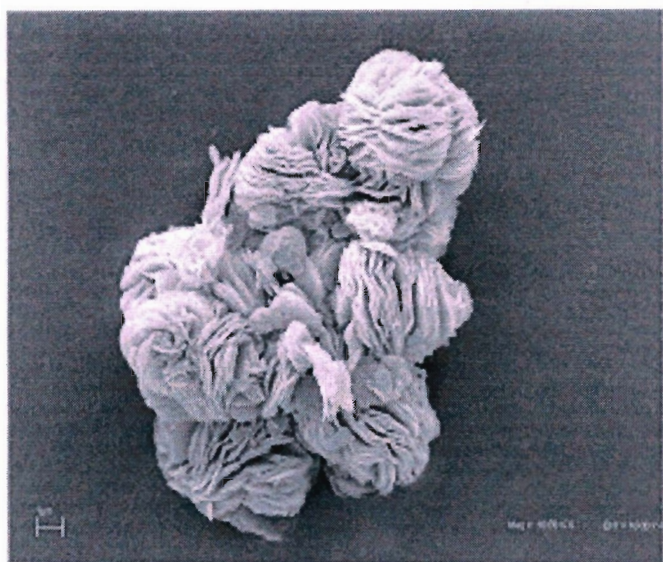


Figure 5.22: SEM images of undoped catalyst calcined



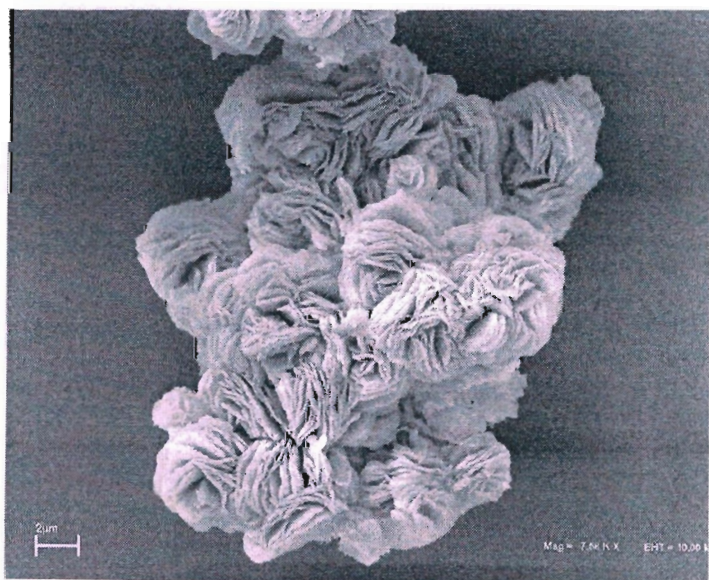
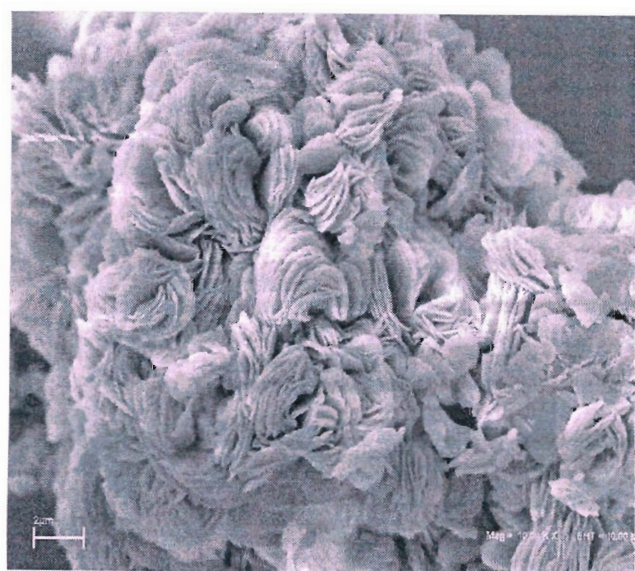
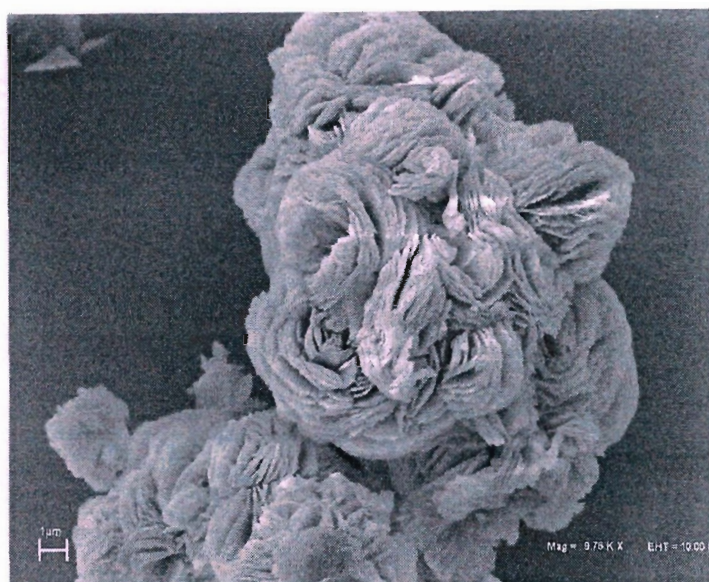


Figure 5.23: SEM images of used undoped catalyst



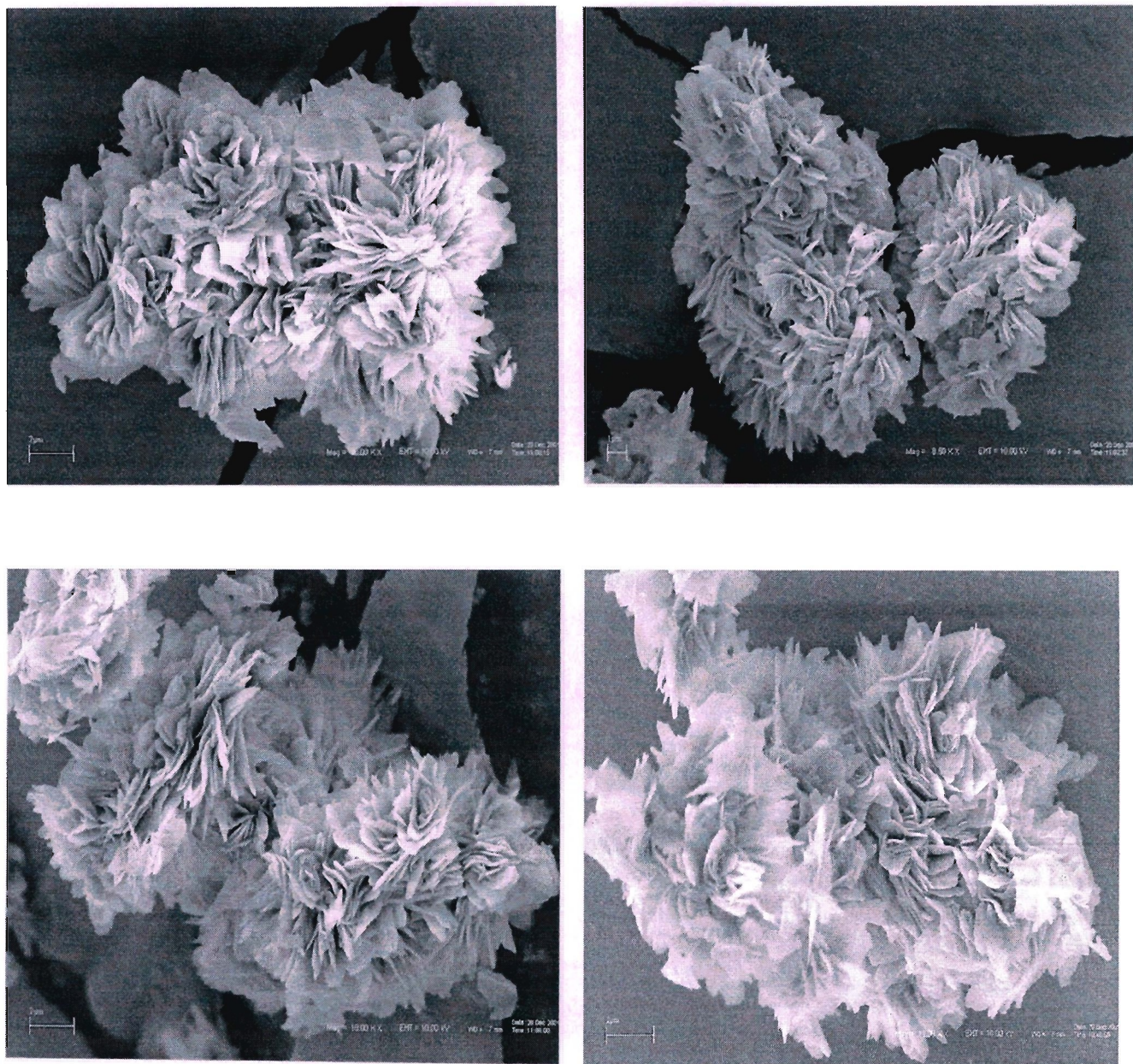


Figure 5.24: SEM images of 0.2% Ru promoted catalysts precursor



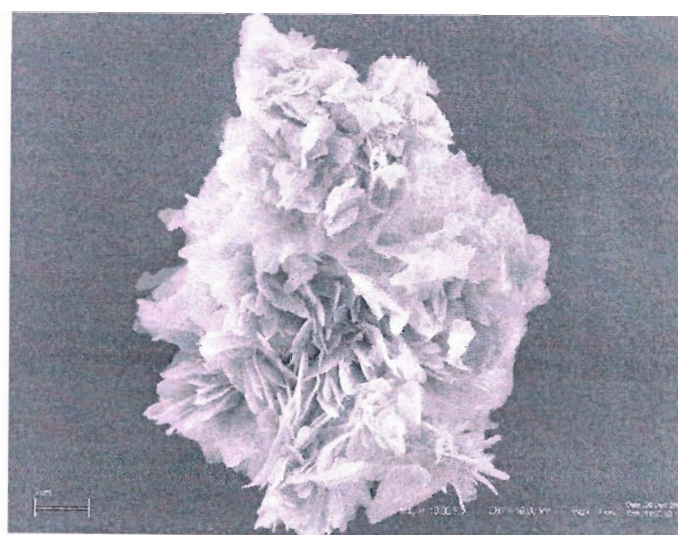
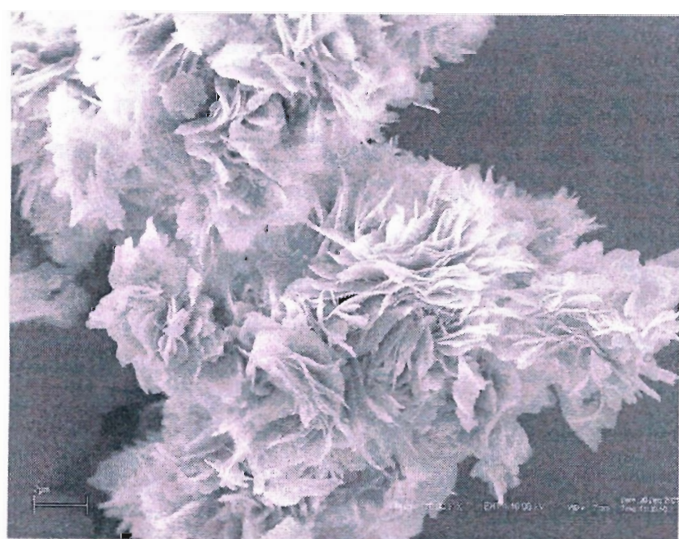
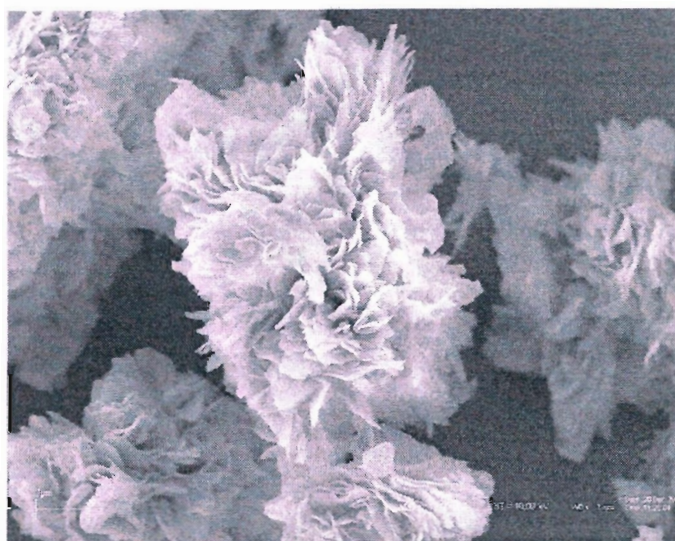


Figure 5.25: SEM images of 0.2% Ru promoted catalysts calcined



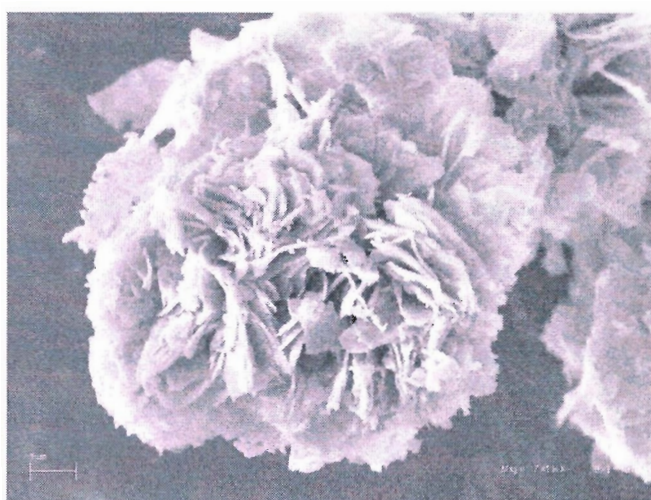
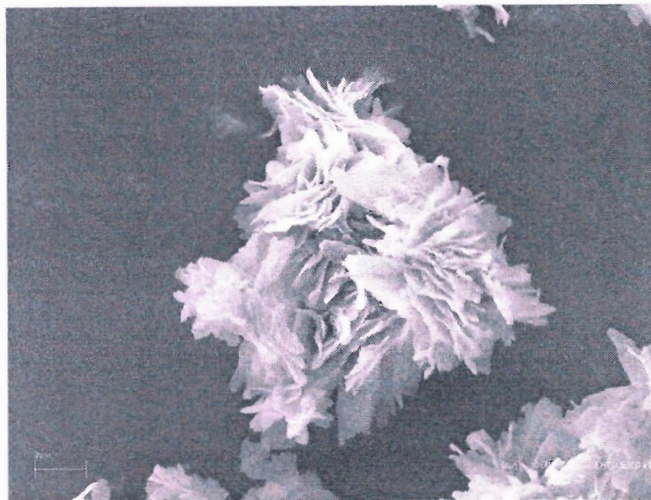
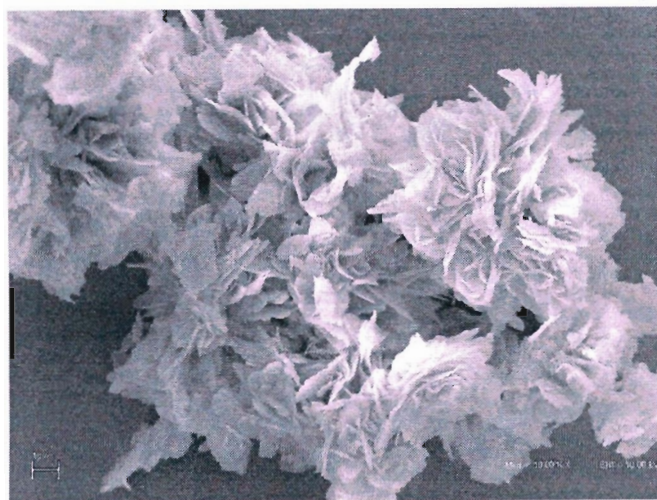


Figure 5.26: SEM images of the used 0.2% Ru promoted catalysts



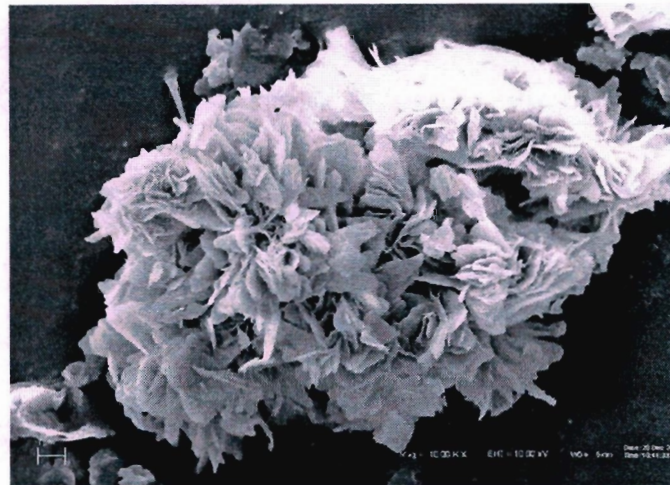
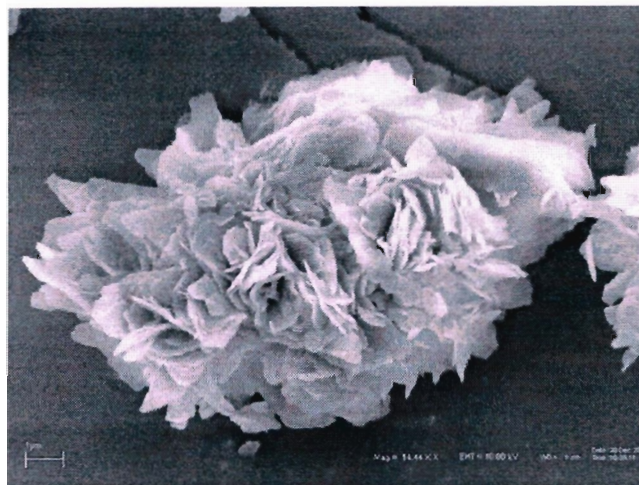
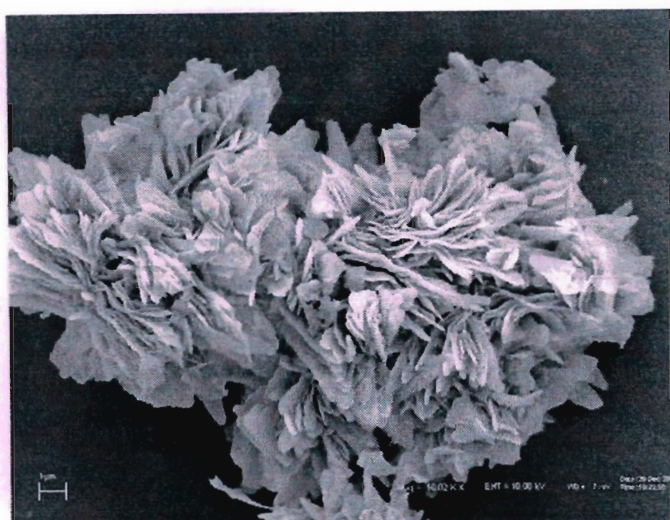
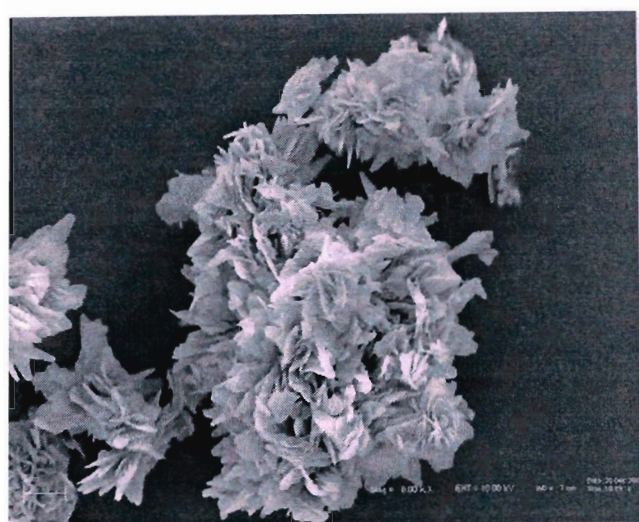


Figure 5.27: SEM images of 0.6% Ru promoted catalysts precursor



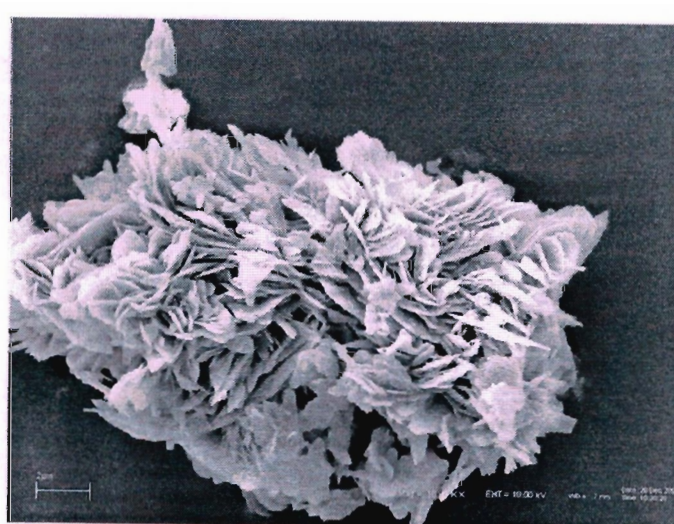
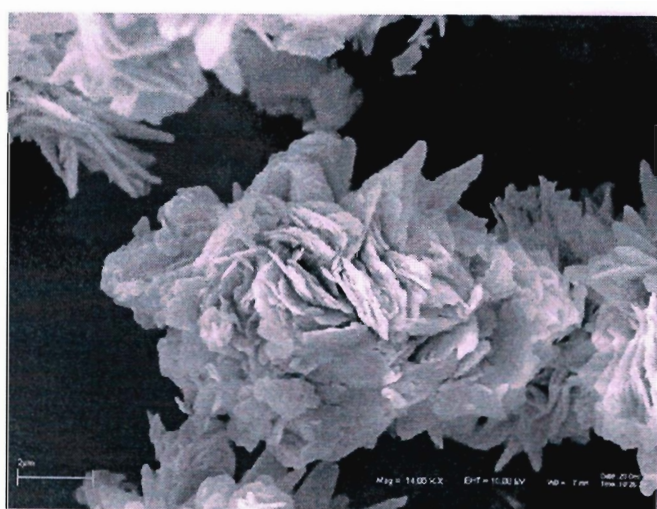
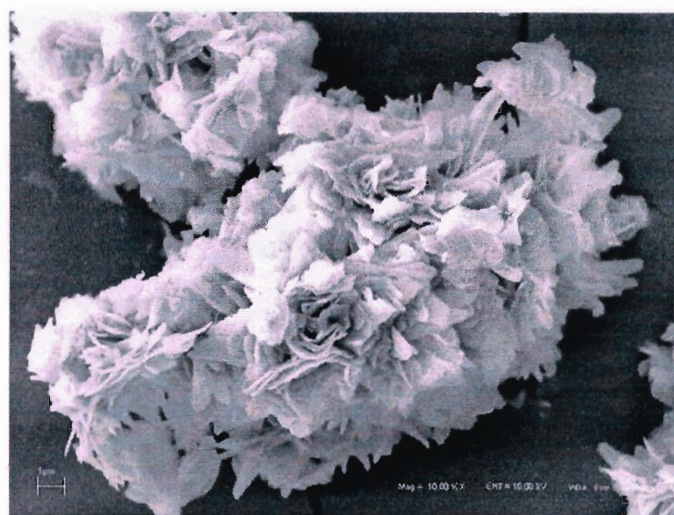
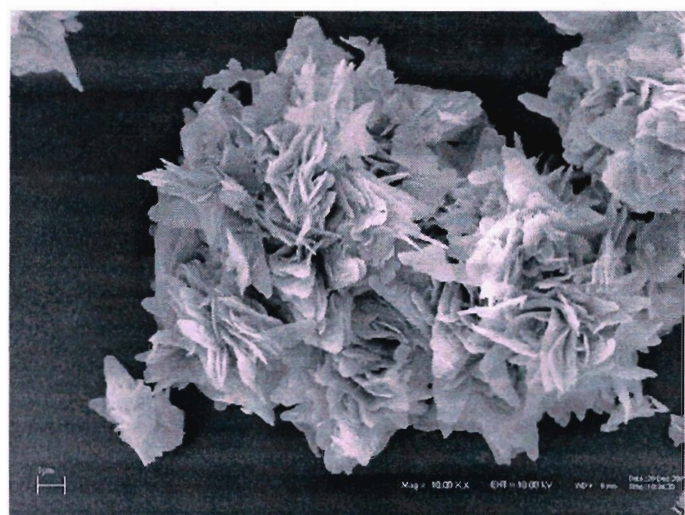


Figure 5.28: SEM images of 0.6% Ru promoted catalysts calcined



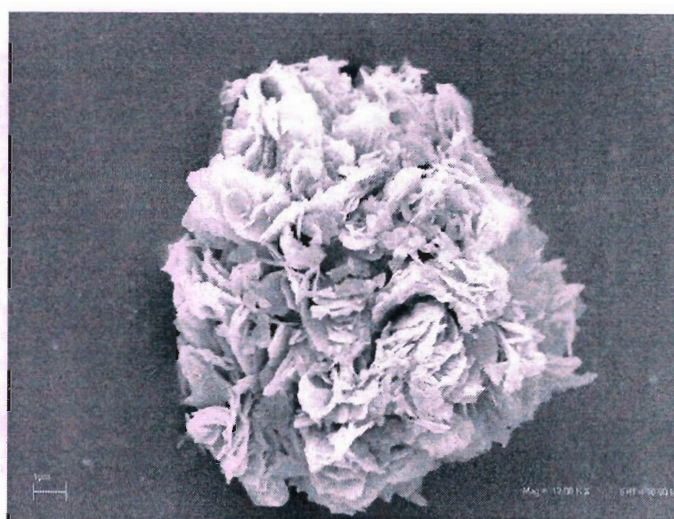
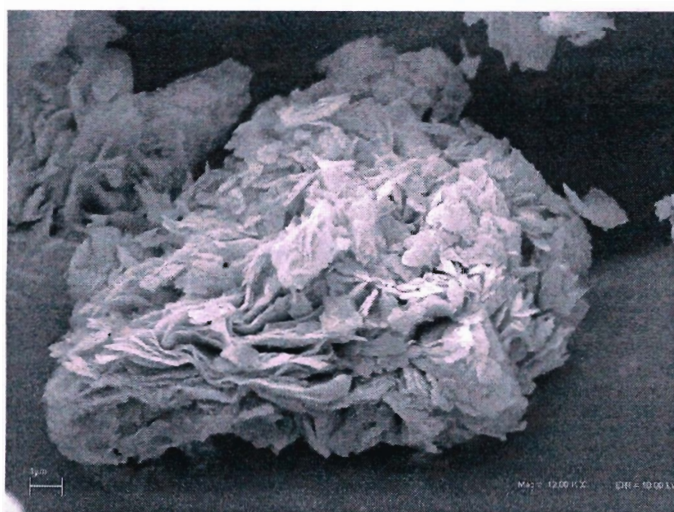
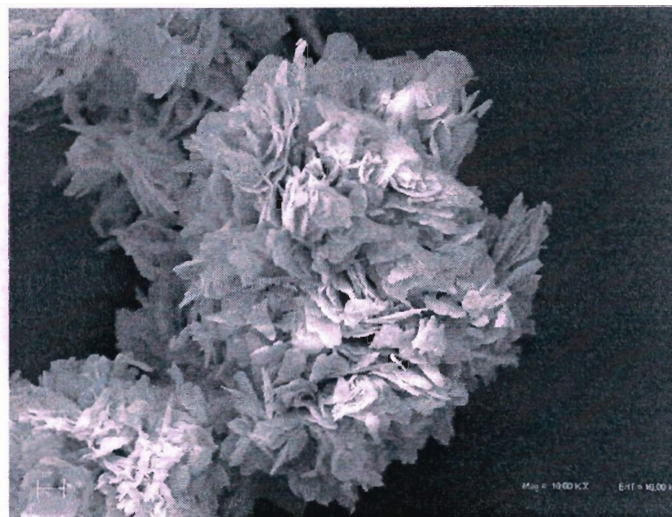
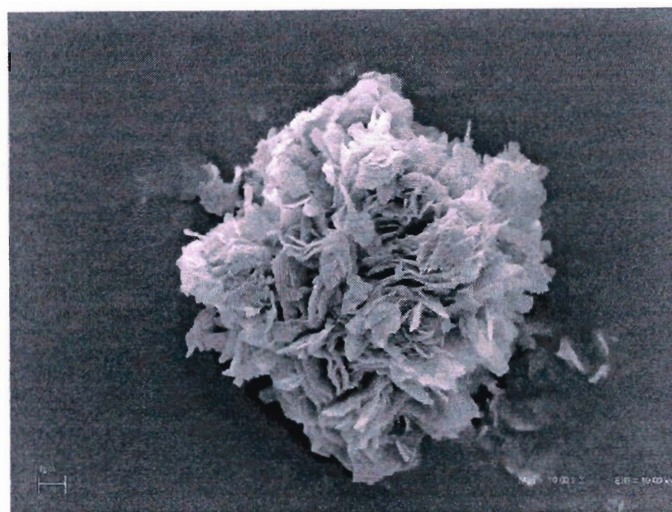


Figure 5.29: SEM images of used 0.6% Ru promoted catalyst



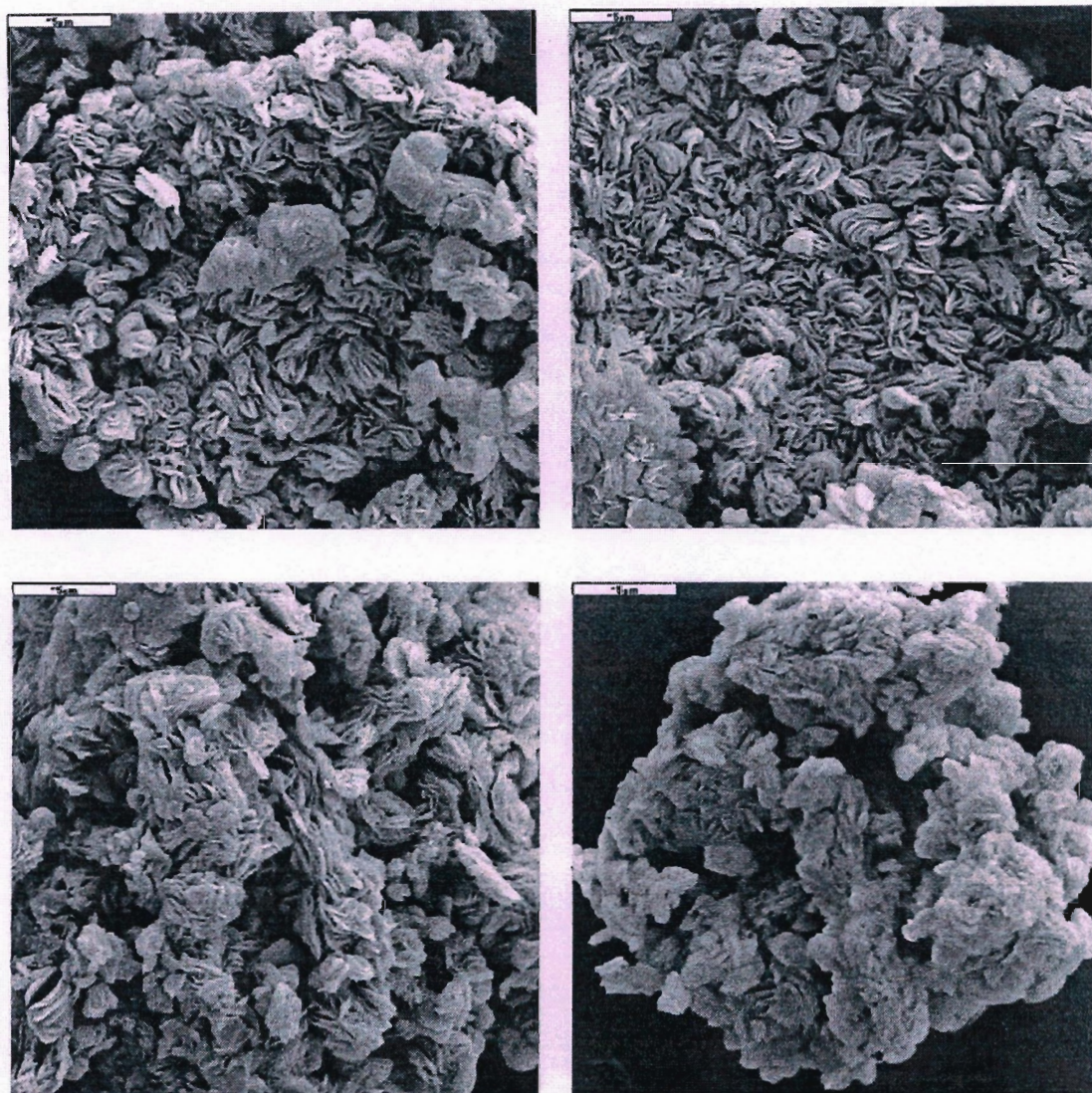


Figure 5.30: SEM images of 1% Ru promoted catalysts precursor



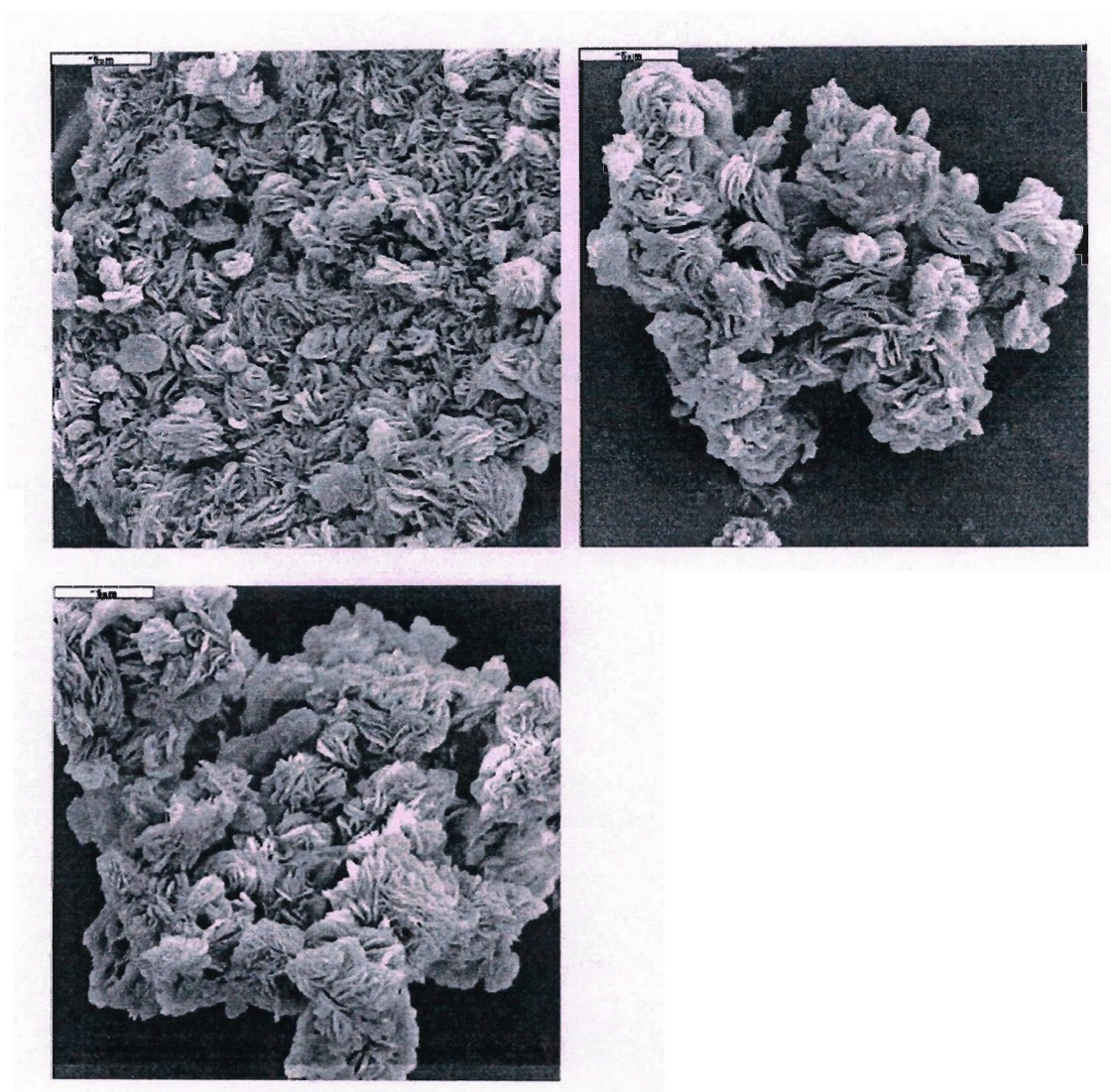


Figure 5.31: SEM images of 1% Ru promoted catalyst calcined

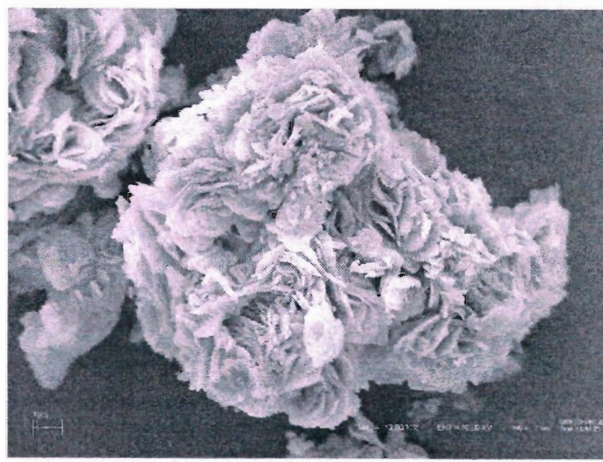
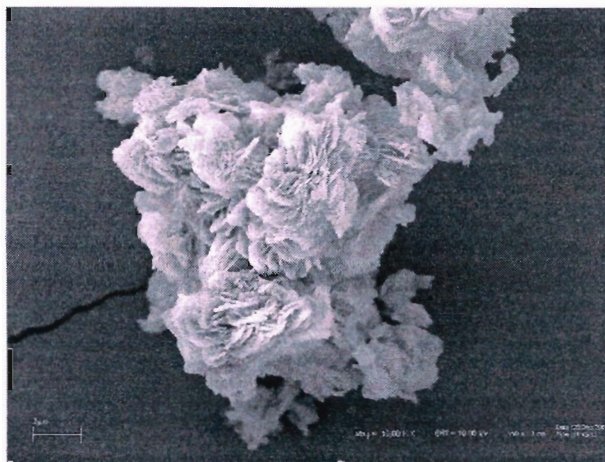
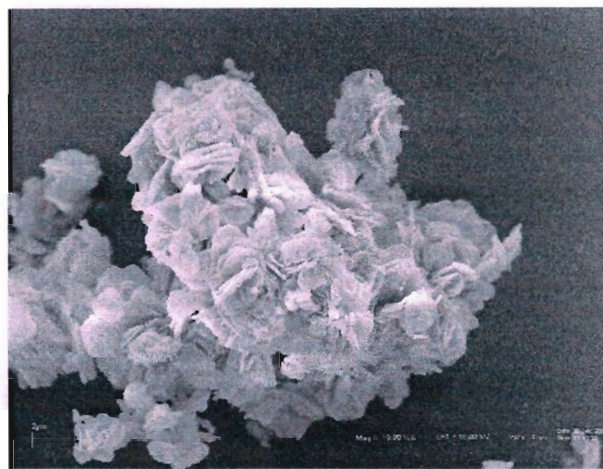
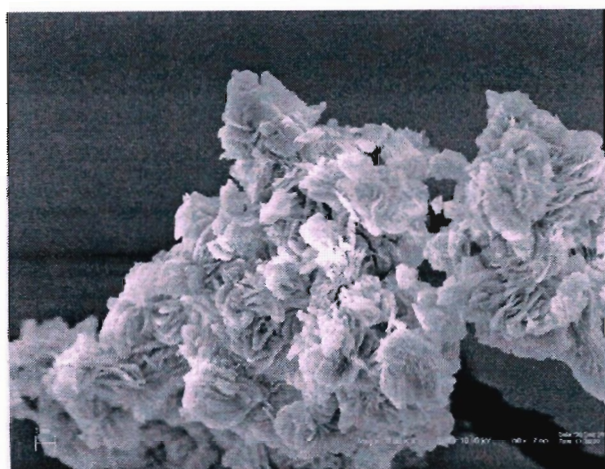


Figure 5.32: SEM images of used 1% Ru promoted catalysts.

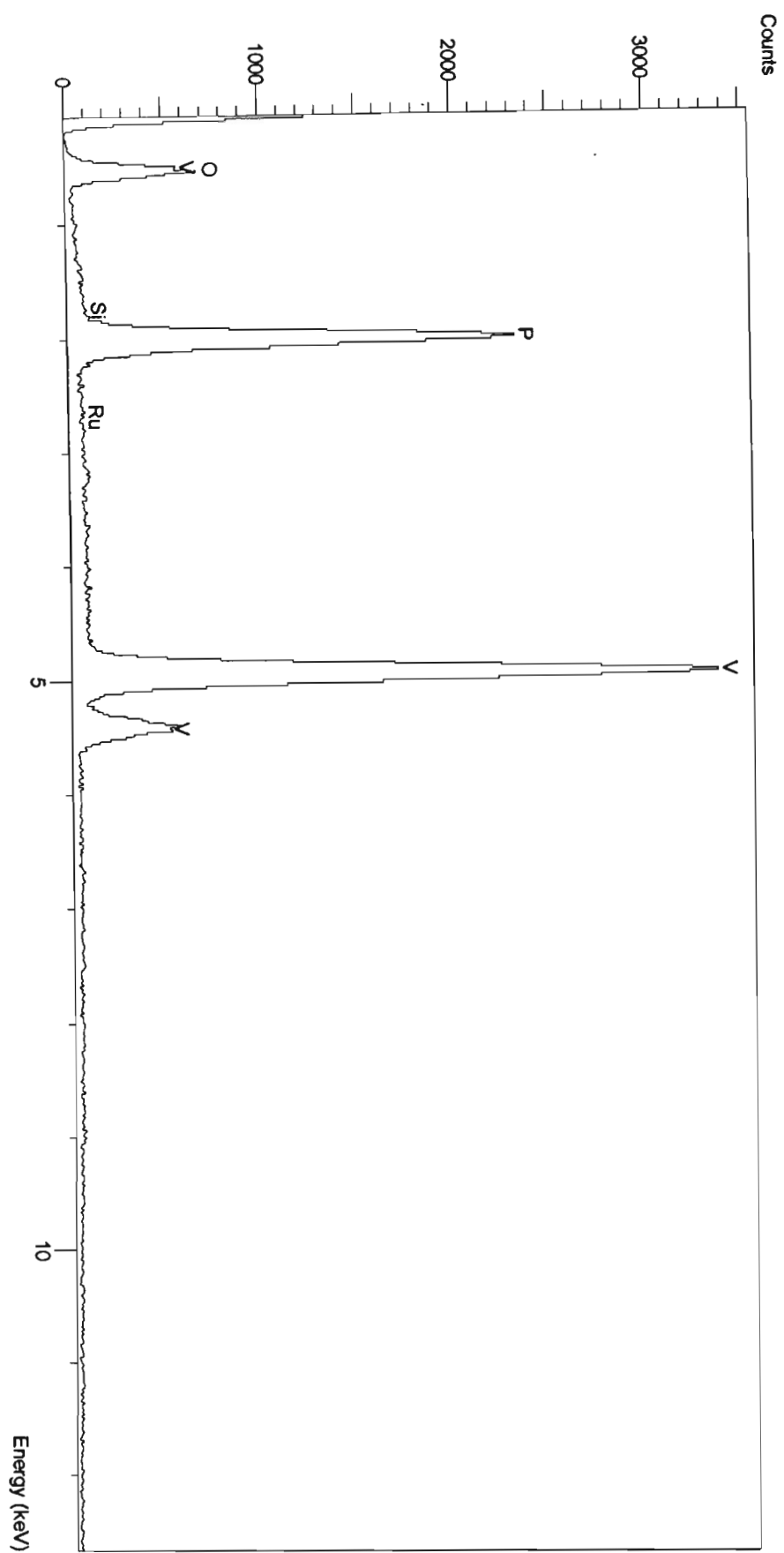
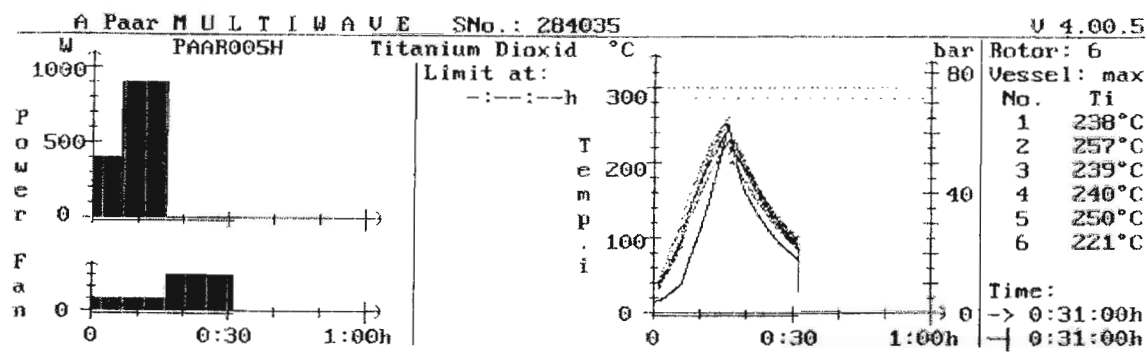


Figure 5.33: EDS spectrum of undoped catalyst precursor





Method: PAAR005H  
Note:

Sample (PAAR): Titanium Dioxid  
Note:

Ph	Power W	Time mm:ss	Power W	Fan
1	400	6:00	400	1
2	900	10:00	900	1
3	0	15:00	0	3
4	0	0:00	0	0
5	0	0:00	0	0
6	0	0:00	0	0
7	0	0:00	0	0
8	0	0:00	0	0

Ves	Weight max	Reag 1 HCl	Reag 2 H2SO4	Reag 3	Remark
1	0.200g	3.00 ml	1.00 ml	0.00 ml	
2					
3					
4					
5					
6					

Run started on 02-01-11 at 15:34

Figure 5.34: Microwave Digestion Parameters

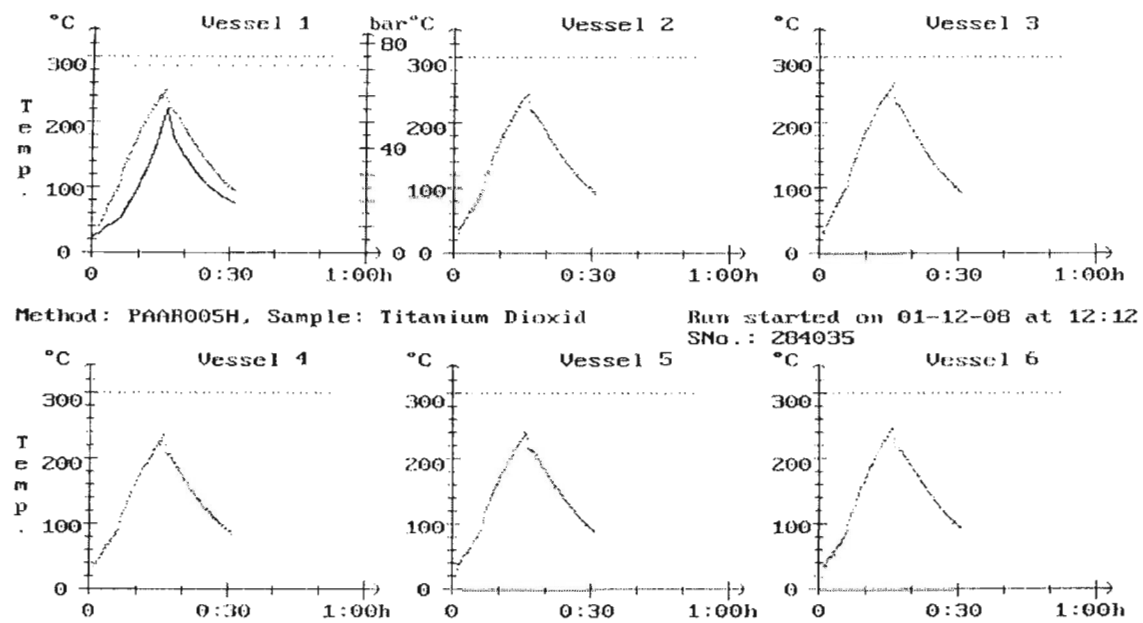


Figure 5.35: Temperature vs. time for each vessel in the Paar digester